Attachment 22:

Martell, E.A. "Iodine-131 Fallout from Underground Tests." Science. New Series, Vol. 143, No. 3602, 10 Jan. 1964. 126-129.

Iodine-131 Fallout from Underground Tests

E. A. Martell

Science, New Series, Vol. 143, No. 3602. (Jan. 10, 1964), pp. 126-129.

Stable URL:
http://links.jstor.org/sici?sici=0036-8075%28196401l0%293%3A143%3A3602%3C126%3AIFFUT%3E2.0.CO%3B2-H

Science is currently published by American Association for the Advancement of Science.

Attachment 23:

McArthur, R.D. Radionuclides in the Surface Soil at the Nevada Test Site. Desert Research Institute, DOE/NV/10845-02. Nevada Office: 1991.

DOE/NV/10845-02

DESERT RESEARCH INSTITUTE
UNIVERSITY OF NEVADA SYSTEM

RADIONUCLIDES IN SURFACE SOIL AT THE NEVADA TEST SITE

by

Richard D. McArthur

August 1991

WATER RESOURCES CENTER

Publication #45077

RADIONUCLIDES IN SURFACE SOIL AT THE NEVADA TEST SITE

by
Richard D. McArthur
Water Resources Center
Desert Research Institute
University of Nevada System
Las Vegas, Nevada

Prepared for
the U.S. Department of Energy
Field Office, Nevada
under Contract DE-AC08-90NV10845

August 1991

ABSTRACT

In 1981, the U.S. Department of Energy began the Radionuclide Inventory and Distribution Program, an attempt to assess the amount and distribution of radioactivity in surface soil at the Nevada Test Site (NTS). Over the next several years, researchers used a combination of aerial radiological surveys, soil sampling, and *in situ* measurements to study the regions of the NTS where soil radioactivity was above background levels. These regions included the ground zeros of above-ground nuclear tests, underground tests that vented, and some safety shots, as well as the sites of nuclear rocket experiments.

The results of the program were published in a series of five reports between 1983 and 1989. In this report, those results have been combined to provide an integrated picture of the current levels of soil radioactivity on the NTS. The estimated inventories of the nine most important manmade radionuclides have been reviewed (and in some cases recalculated), decay-corrected to January 1, 1990, and tabulated. New distribution maps have been prepared that show isopleths of decay-corrected radionuclide concentrations over the entire NTS. Two additional maps show the measurement locations where the gamma exposure rate exceeds 100 μR/hr and where the ^{239,240}Pu concentration exceeds 500 pCi/g.

CONTENTS

TABLES

FIGURES

RADIONUCLIDES IN SURFACE SOIL AT THE NEVADA TEST SITE

BACKGROUND

The United States began testing nuclear weapons at the Nevada Test Site (NTS) in January 1951. Since then, the NTS has become the nation's primary site for testing new nuclear weapons and studying the effects of nuclear explosions on structures and military equipment. Other nuclear energy projects at the NTS have studied safety requirements for storing and transporting nuclear weapons, explored peaceful uses of nuclear explosives,and developed nuclear rockets and ramjet engines. In all, more than 600 nuclear explosions have taken place at the NTS as part of these programs.

One result of these explosions is that the surface soil in many parts of the NTS contains measurable amounts of several long-lived radionuclides. Almost all of the 100 above-ground tests contaminated the soil near the ground zero (GZ). Several underground tests were cratering experiments that threw radioactive rock and soil hundreds of feet from the GZ, and some deeper underground tests vented radioactive material to the surface. A few safety tests, in which a nuclear device was destroyed by conventional explosives, scattered plutonium (and in some cases uranium) over the nearby ground. Finally, radioactive debris from many tests was deposited as fallout over the northern and eastern parts of the NTS.

Radiation levels at the NTS are monitored regularly, and safety officials have identified and fenced off the areas where the soil is heavily contaminated. In many other areas, radionuclide levels are not high enough to warrant closing the area but are still above background. These areas may pose a long-term risk to people working in them regularly and to people who may visit them in the future if the NTS is ever returned to the public domain. Evaluating this risk requires detailed information on the amounts of various radionuclides in the soil at different locations. Knowledge of the amount and distribution of soil radioactivity will also be important for the eventual cleanup of contaminated areas.

Several studies of radionuclide distribution were done on the NTS in the 1970s, but all were limited in scope. A series of aerial radiological surveys measured gamma-exposure rates over much of the NTS, but they did not measure individual radionuclides. The studies that did measure individual radionuclides usually focused on transuranic elements (americium and plutonium) and were limited to relatively small areas near GZs and safety shot sites. The data for those studies were obtained by collecting and analyzing large numbers of soil samples, a method too expensive and time-consuming to use for large-scale surveys.

In the mid-1970s, scientists from Lawrence Livermore National Laboratory (LLNL) and the U.S. Department of Energy's (DOE) Environmental Measurements Laboratory developed *in situ* spectrometry as a technique for measuring gamma-emitting radionuclides

in surface soil (Beck *et al.*, 1972; Anspaugh, 1976). This method was used for a survey of Frenchman Flat in 1978 and 1979, in a cleanup and treatment experiment in Area 11 in 1981, and in cleanup operations at several off-site areas in the late 1970s. It proved to be a useful method for surveying large areas much faster and cheaper than would be possible using other methods.

In 1981, the DOE began a project that would use this new technology to carry out a thorough radiological survey of the surface soil on the NTS. This project, the Radionuclide Inventory and Distribution Program (RIDP), took five years of field work and another three years of data analysis to complete. It resulted in estimates of the total amount (inventory) and the distribution of radionuclides in the soil in all parts of the NTS that had been affected by NTS operations.

The methods and results of the RIDP were published in a series of five reports:

Report #	Regions Covered	Reference
1	Galileo (Area 1)	McArthur and Kordas, 1983
2	Areas 2 and 4	McArthur and Kordas, 1985
3	rest of Yucca Flat	McArthur and Mead, 1987
4	Areas 18 and 20	McArthur and Mead, 1988
5	rest of the NTS	McArthur and Mead, 1989

The purpose of this report is to update and summarize those results, with the aim of presenting an integrated description of the current levels of radioactivity in the surface soil of the NTS.

OBJECTIVE

The objective of the RIDP was to estimate the distribution and the total inventory of the important manmade radionuclides of NTS origin in the surface soil of the NTS.

In the context of this objective, "manmade" refers to radionuclides associated with nuclear testing. Some of these radionuclides are part of the nuclear device itself; others are direct products of the nuclear reaction; still others result from activation of materials such as the device casing and nearby rock and soil by neutrons produced during the explosion. Several other radionuclides occur naturally in NTS surface soil. Although three of these, ^{40}K, ^{232}Th, and ^{238}U, were measured along with the manmade radionuclides during the RIDP, their inventory and distribution were not estimated.

Which radionuclides were "important" was not spelled out initially because it was not known which ones would be found. Most of the radionuclides produced in a nuclear explosion are relatively short-lived, with half-lives ranging from less than a second to several weeks. About 20 live long enough that they may be present in measurable amounts several years after detonation. By the end of the RIDP, 16 manmade radionuclides had been found in

measurable amounts in soil at one or more locations on the NTS (Table 1). The methods used in the project do not allow ^{239}Pu and ^{240}Pu to be measured separately; all that can be determined is the total activity of the two isotopes, denoted as $^{239,240}Pu$. The ratio of ^{239}Pu to ^{240}Pu in fallout from nuclear tests conducted at the NTS ranges from about 12 to over 6,600 (Hicks and Barr, 1984).

Finally, radionuclides "of NTS origin" are those resulting from testing on the NTS. All surface soil on the NTS contains manmade radionuclides from global fallout, that is, fallout from high-yield U.S. thermonuclear tests in the Pacific and tests conducted by other countries. (The contribution of the relatively low-yield fission tests conducted at the NTS to global fallout is small.) Regions of the NTS where the levels of radionuclides in the soil were comparable to those due to global fallout were considered areas of background activity; such areas were assumed to have no radionuclides of NTS origin in the surface soil. Levels above those attributable to global fallout were assumed to result from NTS activities.

The general areas affected by NTS activities were known before the RIDP began. The project's resources were focused on these areas, and only a few measurements were made in background areas.

TABLE 1. IMPORTANT MANMADE RADIONUCLIDES IN NTS SURFACE SOIL

Radionuclide	Half-life (y)[1]
^{60}Co	5.26
^{90}Sr	28.1
^{101}Rh	3.1
^{102m}Rh	2.9
^{125}Sb	2.7
^{133}Ba	10.7
^{134}Cs	2.05
^{137}Cs	30.2
^{152}Eu	13.
^{154}Eu	16.
^{155}Eu	1.81
^{174}Lu	3.6
^{238}Pu	86.
^{239}Pu	24,400.
^{240}Pu	6,580.
^{241}Am	458.

[1]Most values are from the *CRC Handbook of Chemistry and Physics*, 65th Edition (1984), CRC Press, Boca Raton, Florida; the value for ^{133}Ba is from the *Table of Isotopes*, 7th Edition (1978), Wiley, New York.

METHODS

The strategy developed to meet the RIDP's objective, as outlined in the project operations plan (Kordas and Anspaugh, 1982), combined the three methods used in earlier studies: aerial surveys, soil sampling, and *in situ* spectrometry. Details of how these methods were used were given in the RIDP reports, especially Report 1. The following description is only a summary.

Aerial Surveys

Between 1976 and 1984, EG&G, Inc., made a new series of aerial radiological surveys of much of the NTS:

Area	Date of Survey	Reference
Areas 25 and 26	September 1976	Tipton, 1979
Yucca Flat	August–September 1978	Fritzsche, 1982
Areas 18 and 20	October–November 1980	Feimster, 1985
Area 11	January 1982	Clark, 1983
Area 5	February 1982	unpublished
Areas 16 and 30	June 1983	Bluitt, 1986
Areas 12, 15, 17, 19	October–November 1984	Jobst, 1986

The surveys were carried out with an array of NaI(Tl) scintillation detectors mounted on a helicopter. Previous aerial surveys had been made from fixed-wing aircraft; the slower speed and greater maneuverability of the helicopter allowed wider coverage and better resolution.

The results of the aerial surveys were used to define the precise areas to be surveyed with the primary measurement technique, *in situ* spectrometry.

In Situ Spectrometry

To help coordinate the field activities, the *in situ* measurements were carried out in a series of surveys of different areas (Table 2). Most of these areas contained at least one GZ or other localized source of contamination. Such areas were usually identified by the name of a test, such as "Galileo," although the chosen name did not necessarily reflect the most important source of contamination in the area. The regions covered in the Area 15, Areas 12 and 19, Areas 17 and 18, Pahute Mesa, and Miscellaneous surveys had no GZs. Soil radioactivity in those areas was generally uniformly distributed at relatively low levels.

The portions of the NTS covered by the *in situ* surveys are shown in Figure 1. They include all the GZs of above-ground nuclear tests, the GZs of underground tests where significant amounts of radioactivity reached the surface, safety-shot sites, the rocket test facilities in Area 25, and other places where aerial surveys showed elevated levels of radioactivity. For the most part, those portions of the NTS not covered by *in situ* surveys were

TABLE 2. SUMMARY OF RIDP SURVEYS

Region	Number of *in situ* measurements	soil profiles	chemical analyses	approximate dates
Galileo	136	11	3	Aug.–Nov. 1981
Kepler	121	9	4	Dec. 1981–Apr. 1982
Whitney	173	17	7	Feb.–Apr. 1982; June 1983
Diablo	53	12	4	May 1982
Baneberry	181	15	3	May–July 1982; June 1983
Sedan, Smoky	257	25	10	Aug.–Sept. 1982
Wilson	207	23	3	Oct.–Nov. 1982
Quay	223	17	7	Dec. 1982–Feb. 1983
Hornet	376	25	12	Feb.–May 1983
Pahute Mesa	25	0	0	June 1983
Schooner	62	11	5	July 1983
Cabriolet	220	13	6	Aug.–Oct. 1983
Johnie Boy	132	14	5	Nov.–Dec. 1983
Little Feller I & II	94	18	8	Jan.–June 1984
Danny Boy	107	11	5	May–June 1984
Areas 25 & 26	181	24	5	Feb.–March 1984
Areas 17 & 18	176	15	6	Aug.–Nov. 1984 & 1985
Area 15	36	4	1	Oct.–Nov. 1984
Pinstripe, GMX	222	22	16	Jan.–Feb., May 1985
Plutonium Valley	172	22	11	Mar.–May 1985
Buggy	76	13	5	June–July 1985
Areas 12 & 19	118	24	13	June–July 1985
Oberon	30	10	5	Nov.–Dec. 1985
Frenchman Lake	291	29	6	Sept. 1985–Jan. 1986
Miscellaneous	81	15	8	Sept. 1985; Feb. 1986
Total	3,750	399	158	

known (from aerial surveys, ground–based monitoring, and the history of NTS operations) to have no contamination from NTS activities. The main exception was the mountain ranges surrounding Yucca Flat, where aerial surveys have shown above–background levels of radioactivity. These mountains were inaccessible to the survey vehicle. In addition, for safety reasons, measurements were not made in craters such as those at Sedan, Schooner, and Cabriolet.

The *in situ* measurements were made with a collimated high–purity germanium detector suspended about 7.4 m above the ground. The detector was mounted on a vehicle capable of off–road travel. Inside the vehicle were the other components of the measurement system, including an amplifier and power supply, a pulse–height analyzer, and a desktop computer. The system was maintained and operated by EG&G.

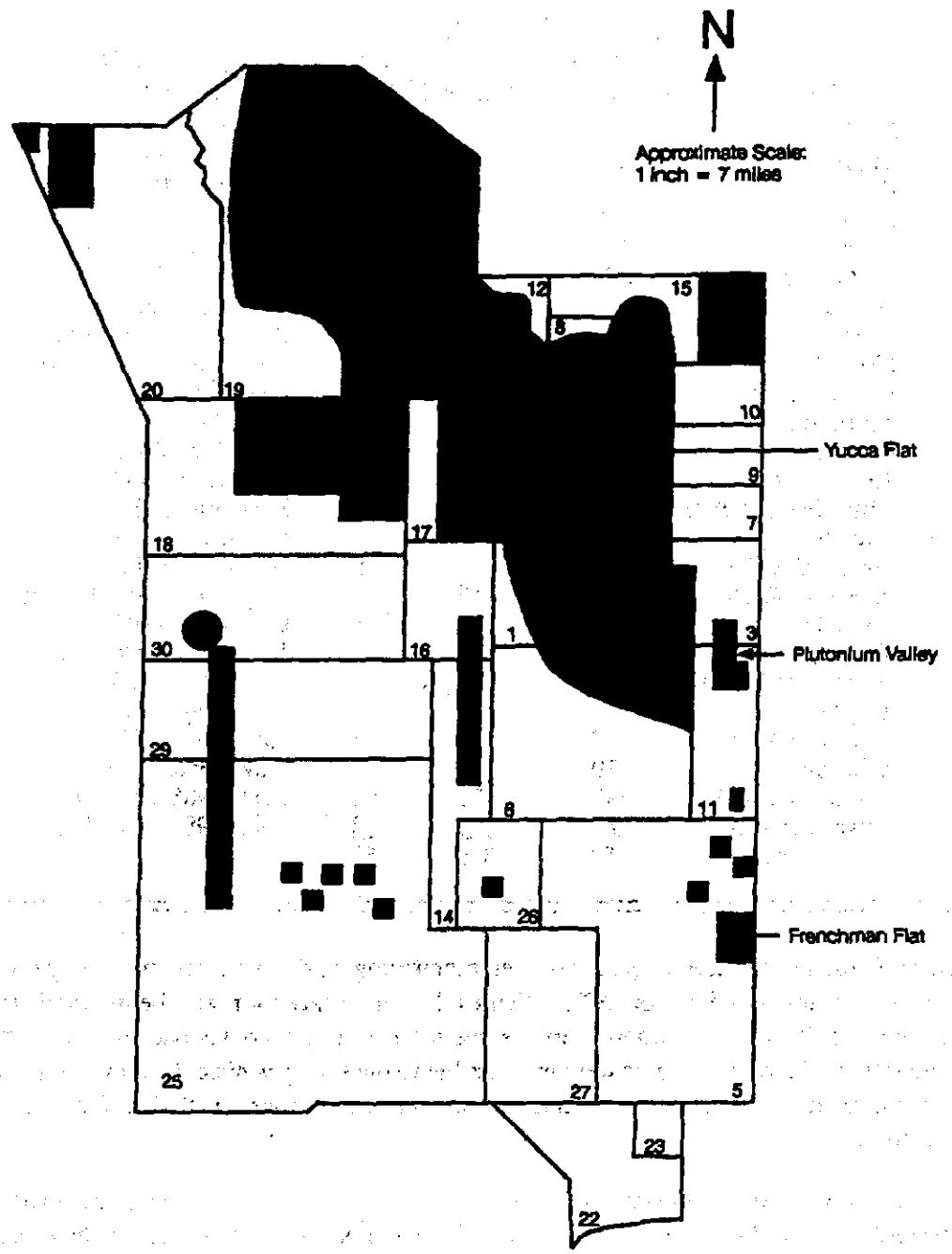

Figure 1. Portions of the NTS surveyed by the RIDP.

During each measurement, pulses from gamma rays reaching the detector were sorted into a 4096-channel energy spectrum. At the end of the 15-minute count period, the spectrum was transferred to the computer, where a spectral analysis program computed the concentrations of various radionuclides. Finally, the spectrum was transferred to magnetic tape for further analysis.

For most surveys, the locations of the *in situ* measurements were specified in advance. The basic arrangement of measurement locations was a grid of points 400 or 500 feet apart. In the early surveys, an irregular pattern of grid points was measured that reflected the isopleths of exposure rate derived from the aerial survey results. In later surveys, complete rectangular grids were measured to simplify the data analysis, though the grid spacing was often increased in areas of relatively low concentration. The measurement locations at the GZs in Area 18 were selected using importance sampling (Report 4).

The locations of most of the *in situ* measurements were determined using a microwave ranging system, with a receiver and transmitter mounted on the survey vehicle and two or more transponders positioned on remote mountaintops. In the regions that had no GZs, measurements were made primarily along roads. The locations of those measurements were determined with mileposts and odometer readings.

As each survey was completed, the spectra were sent to LLNL for analysis by a modified version of GAMANAL (Gunnink and Niday, 1971), a more sophisticated spectral analysis program than the one used in the field. The analyses were done using assumed values of 0.001204 g/cm^3 for air density, 1.5 g/cm^3 for wet soil density, and 10 percent for soil moisture. Mass attenuation coefficients for all energies of interest were obtained by interpolation from values given by Beck *et al.* (1972). Values of the inverse relaxation lengths of various radionuclides were derived from the results of analyses of soil samples as described below.

These assumptions were OK considering study was done over a wide area over many years? This analysis must not be very sensitive if that's the case.

The detectors used in the RIDP underwent an extensive series of calibrations and test measurements before being used on surveys. In addition, the energy calibration of each detector was checked three times a day during field operations. About 30 percent of the 8,550 spectra recorded during the RIDP were laboratory calibration runs to check the angular response and effective area of the detector. Another 23 percent were field calibrations.

All the RIDP spectra have been stored on magnetic tape and archived at the DOE computer center in Las Vegas. In addition, the results of the *in situ* measurements will become part of a database maintained for DOE's Basic Environmental Compliance and Monitoring Program at the NTS.

Soil Samples

Soil samples were collected and analyzed to determine the distribution of radionuclides with depth in the soil and to measure the concentrations of radionuclides that either do not emit strong gamma rays or have very low probabilities of emitting gamma rays.

The soil samples were usually collected at sites of *in situ* measurements located along two perpendicular transects through the GZ, if one was present. At most sites, a profile of four samples to a total depth of 15 cm was collected using the pit-scoop method described in Report 1. At a few sites such as Sedan, where it was suspected that radioactivity extended deeper into the soil, six increments were collected to a depth of 30 cm. The samples were dried and homogenized, then seived through a 10-mesh (1.7-mm) screen. Only the fine fraction was analyzed.

All samples were analyzed by gamma spectrometry to determine radionuclide depth distributions. The activity of each radionuclide was assumed to decrease exponentially with depth, with the rate of decrease characterized by an inverse relaxation length (α). The method for calculating inverse relaxation lengths from the gamma-spectrometry results varied during the course of the project, as described in Reports 1, 3, and 4.

Average values of the calculated inverse relaxation lengths for each radionuclide were used as parameters in the GAMANAL analysis of the *in situ* measurements. In many surveys, the depth distributions in the region near a GZ were different from those farther away. The measurements from the GZ region were therefore analyzed using a different set of inverse relaxation lengths. The inverse relaxation length values used in GAMANAL are summarized in Table 3.

A few top-increment soil samples from each survey were analyzed radiochemically for ^{90}Sr, ^{238}Pu, $^{239,240}Pu$, ^{137}Cs, and ^{241}Am. The ratios of ^{90}Sr to ^{137}Cs, ^{238}Pu to ^{241}Am, and $^{239,240}Pu$ to ^{241}Am were then calculated. Average values of these ratios, listed in Table 4, were used to estimate the inventories of ^{90}Sr, ^{238}Pu, and $^{239,240}Pu$ from the estimated inventories of ^{137}Cs and ^{241}Am.

A set of procedures for quality assurance (QA) was part of the analytical protocol for all soil samples except those from the Galileo area. These procedures, carried out under the direction of E. Essington at Los Alamos National Laboratory, included analyses of hidden replicate samples, analyses of reference blind and background samples, and interlaboratory comparisons. The results were presented in appendices to the last four RIDP reports. Two separate reports will summarize the QA procedures (Essington and Mead, in preparation) and results (Essington, in preparation).

RESULTS

Radionuclide Inventories

Table 5 gives the estimated inventories of the nine most important manmade radionuclides in surface soil in each NTS area. All inventory values except those of ^{241}Am, ^{238}Pu, and $^{239,240}Pu$ are decay-corrected to January 1, 1990.

The estimates in Table 5 are based on the inventory estimates from the individual surveys published in the previous reports. However, all of the earlier estimates were reevaluated for this report, and many of them were revised.

TABLE 3. INVERSE RELAXATION LENGTHS (1/cm) USED IN GAMANAL ANALYSES

Location		α_1	α_2	α_3	α_4	α_5
Galileo	GZ	0.6	0.4	0.4	0.05	0.6
	others	0.6	0.4	0.4	0.3	0.6
Kepler	GZ	0.6	0.4	0.4	0.05	0.6
	others	0.8	0.4	0.4	0.3	0.6
Whitney	GZ	0.8	0.1	0.4	0.05	0.6
	others	0.8	0.4	0.4	0.3	0.6
Diablo	GZ	0.8	0.4	0.4	0.05	0.6
	others	0.8	0.4	0.4	0.3	0.6
Baneberry		0.6	0.6	0.6	0.3	0.6
Smoky	GZ	0.6	0.1	0.4	0.05	0.6
	others	0.6	0.4	0.4	0.3	0.6
Sedan	GZ	0.05	0.05	0.05	0.05	0.05
	others	0.4	0.4	0.4	0.3	0.4
Oberon		0.6	0.4	0.6	0.05	0.6
Wilson	GZ	0.6	0.1	0.4	0.05	0.6
	others	0.6	0.4	0.4	0.3	0.6
Quay	GZ	1.0	0.05	1.0	0.05	1.0
	others	1.0	0.4	1.0	0.4	1.0
Hornet	GZ	0.4	0.05	0.3	0.05	0.4
	others	0.4	0.4	0.4	0.3	0.4
Pahute Mesa		0.4	0.4	0.4	0.4	0.4
Schooner	GZ	0.1	0.1	0.1	0.1	0.1
	others	0.6	0.6	0.6	0.6	0.6
Cabriolet		0.4	0.4	0.4	0.4	0.4
Johnie Boy	GZ	0.1	0.1	0.1	0.1	0.1
	others	0.4	0.4	0.4	0.4	0.4
Little Feller I	GZ	0.1	0.1	0.1	0.1	0.1
	others	0.5	0.5	0.5	0.5	0.5
Little Feller II	GZ	0.5	0.5	0.5	0.5	0.5
	other	0.1	0.1	0.1	0.1	0.1
Danny Boy	GZ	0.05	0.05	0.05	0.05	0.05
	others	0.3	0.3	0.3	0.3	0.3
Areas 25 & 26		0.3	0.05	0.3	0.05	0.3
Area 15		0.6	0.6	0.6	0.6	0.6
Buggy	GZ	0.2	0.2	0.2	0.2	0.2
	others	0.5	0.5	0.5	0.5	0.5
Areas 17 & 18		0.4	0.4	0.4	0.4	0.4
Areas 12 & 19		0.1	0.1	0.1	0.1	0.1
Plutonium Valley		0.6	0.6	0.6	0.6	0.6
Pinstripe & GMX		0.5	0.05	0.5	0.05	0.5
Frenchman Lake	GZ	0.1	0.05	0.1	0.05	0.1
	others	0.4	0.05	0.4	0.05	0.4

Note: α_1 used for ^{241}Am, ^{238}Pu, $^{239,240}Pu$
α_2 used for ^{60}Co, ^{101}Rh, ^{102m}Rh, ^{125}Sb
α_3 used for ^{137}Cs
α_4 used for ^{133}Ba, ^{134}Cs, ^{152}Eu, ^{154}Eu
α_5 used for ^{155}Eu, ^{174}Lu

TABLE 4. AVERAGE RADIONUCLIDE RATIOS

Location	$^{90}Sr/^{137}Cs$	$^{238}Pu/^{241}Am$	$^{239,240}Pu/^{241}Am$
Galileo	1.5	not reported	5.0
Kepler	1.3	2.0	6.0
Whitney	2.7	3.2	9.9
Diablo	2.0	2.7	5.6
Baneberry	0.25	0.69	3.9
Smoky	2.5	0.72	7.2
Sedan	0.82	1.0	5.5
Oberon	1.6	0.13	6.7
Wilson	1.9	0.52	21.
Quay	2.2	0.26	7.5
Hornet	3.3	0.70	8.1
Schooner	0.95	1.7	0.69
Cabriolet	1.0	1.95	0.90
Palanquin	0.93	0.93	2.6
Johnie Boy	5.2	1.9	11.
Little Feller I & II	2.0	0.12	5.7
Danny Boy	0.63	0.12	4.0
Areas 25 & 26	0.84	0.20	6.5
Area 15	1.4	1.3	6.8
Buggy	0.97	1.4	4.4
Areas 17 & 18	1.5	1.6	6.3
Areas 12 & 19	0.97	1.5	6.8
Plutonium Valley	0.58	0.14	5.9
Pinstripe	0.88	1.04	5.8
GMX	0.56	0.14	7.2
Kay Blockhouse	0.86	0.39	9.2
RWMS	0.68	0.29	7.9
Frenchman Lake	2.6	0.31	8.2

One reason for revising the estimates was the inconsistent treatment in previous reports of upper limit values (ULVs). If the GAMANAL program was unable to find the peaks associated with a particular radionuclide, it calculated a ULV from the integrated background counts in the energy window where the peak should have been. In many regions far from a GZ, most of the measurement results were ULVs. Such regions obviously had low concentrations, but they often covered a large area and so could contain a substantial part of the total inventory.

In some of the previous reports, inventories were not estimated at all for regions where most of the results were ULVs, leading to an underestimate of the total inventory. In the others, the ULVs were treated as actual measurements, leading to an overestimate. To make the treatment of ULVs consistent and more accurate, the following rules were applied in estimating the inventory in these regions:

TABLE 5. ESTIMATED INVENTORIES OF MAJOR MANMADE RADIONUCLIDES IN NTS SURFACE SOIL AS OF JANUARY 1, 1990

	Radionuclide Inventory (Ci)								
Area	^{241}Am	^{238}Pu	$^{239,240}Pu$	^{60}Co	^{137}Cs	^{90}Sr	^{152}Eu	^{154}Eu	^{155}Eu
1	4.2	6.5	24.	1.1	8.8	15.	15.	0.1	0.5
2	2.9	8.6	22.	1.2	24.	46.	14.	0.	0.4
3	4.6	3.1	37.	1.0	12.	33.	18.	0.1	0.5
4	6.6	13.	40.	1.6	12.	13.	9.1	0.	0.2
5	0.6	0.1	4.8	0.6	0.4	0.9	10.	0.2	0.
6	1.7	3.3	8.4	0.2	2.8	3.5	0.	0.	0.
7	2.2	0.6	16.	1.0	5.2	9.2	22.	0.2	0.3
8	17.	8.0	110.	5.7	42.	25.	4.4	0.	0.6
9	4.2	2.2	89.	0.7	8.7	13.	23.	0.2	0.3
10	19.	19.	110.	9.7	84.	55.	2.2	0.3	5.0
11	3.3	0.5	29.	0.	0.5	0.3	0.	0.	0.
12	5.7	8.5	39.	1.2	20.	17.	0.	0.	0.
15	8.0	7.8	63.	0.3	19.	22.	0.	0.	0.
16	0.7	1.5	3.7	0.1	2.9	3.7	0.	0.	0.
17	2.8	4.5	18.	1.0	15.	19.	0.	0.	0.
18	19.	5.6	100.	0.7	10.	17.	1.1	0.1	0.8
19	21.	32.	140.	1.1	36.	31.	0.	0.	0.
20	23.	30.	41.	7.9	5.5	4.3	13.	1.6	4.8
25	0.	0.	0.	0.	0.2	0.1	0.4	0.	0.
26	0.	0.	0.	0.	0.	0.	0.	0.	0.
30	3.2	4.5	14.	0.8	1.5	1.3	0.7	0.1	0.2
Total	150.	160.	910.	35.	310.	330.	130.	2.8	14.

1. ^{137}Cs was almost always present in measurable amounts, so the few ULVs were treated as valid data.

2. ^{241}Am and ^{60}Co were assumed to be present at one–half the ULV, as determined by inspection of the data. For example, if the ^{241}Am values in a region tended to be ULVs in the 25 to 35 nCi/m^2 range, a value of 15 nCi/m^2 was assumed.

3. The three europium isotopes were found only relatively close to a GZ. They were assumed not to be present at all in regions where only ULVs were reported. Some previous inventory estimates for these radionuclides were therefore not used in making Table 5.

Inventories of the plutonium isotopes and ^{90}Sr were estimated from ^{241}Am and ^{137}Cs inventories using the radionuclide ratios from the nearest GZ area.

Additional recalculation was necessary for Yucca Flat because the original estimates in Reports 1, 2, and 3 were not made for separate NTS areas.

The values in Table 5 also incorporate estimates for the unsurveyed parts of the NTS areas containing the mountains around Yucca Flat that were inaccessible to the RIDP vehicles. The unsurveyed parts of other areas (Areas 5, 6, 11, 16, 18, 20, 25, 26, and 30) are assumed to have negligible amounts of soil contamination from NTS activities, as are the areas not listed in Table 5 (Areas 14, 22, 23, 27, and 29). The total area for which inventories are estimated is about 500 square miles, roughly 40 percent of the total area of the NTS.

Appendix A describes in detail how the estimates in Table 5 were calculated. Several errors in the previously reported results for Areas 8 and 18 are corrected in Appendix C.

Most of the radionuclides listed in Table 1 are not found in global fallout at levels high enough to be measured with the methods used in the RIDP. All occurrences of these radionuclides on the NTS are therefore assumed to result from NTS activities. An exception is ^{137}Cs, which was present in surface soil southwest of the NTS (upwind) at levels of 30 to 60 nCi/m^2 in the early 1980s (McArthur and Miller, 1989). If the average concentration of ^{137}Cs on the NTS due to global fallout is 35 nCi/m^2 as of January 1, 1990, then about 46 Ci of the 310 Ci of ^{137}Cs reported in Table 5 is from global fallout. The fraction of ^{90}Sr due to global fallout is probably similar.

What is the sensitivity level of this technique if it can't detect global fallout?

In addition to the nine radionuclides listed in Table 5, six other manmade radionuclides were found at a few sites:

- ^{133}Ba was present at 23 points near the Johnie Boy GZ. It was also found at four Wilson points, two Hornet points, and one Cabriolet point. The current total inventory is estimated to be less than 0.1 Ci.

- ^{134}Cs was present at Baneberry and at two Cabriolet points. The estimated inventory was 0.4 Ci, which has since decayed to less than 0.1 Ci.

- ^{101}Rh was present at Sedan (3.9 Ci) and at four points near the Palanquin GZ. The decay–corrected inventory is 1.0 Ci.

- ^{102m}Rh was found at relatively high levels at Sedan (29 Ci) and in lesser amounts at Smoky (1.7 Ci), Cabriolet (1.4 Ci), and in Area 15 north of Sedan (0.4 Ci). The current inventory is estimated to be 6.4 Ci.

- ^{174}Lu was found at Sedan and Smoky (25 Ci total) and was measured at one Schooner point. The current inventory is estimated to be 4.9 Ci.

Radionuclide Distributions

The distributions of the nine most important radionuclides are shown in Figures 2 through 10 . Each of these figures was produced by first plotting all the decay–corrected values that exceeded 100 nCi/m^2 on a map of the NTS, then drawing concentration isopleths on the map by hand.

Why didn't they look at the additional six also

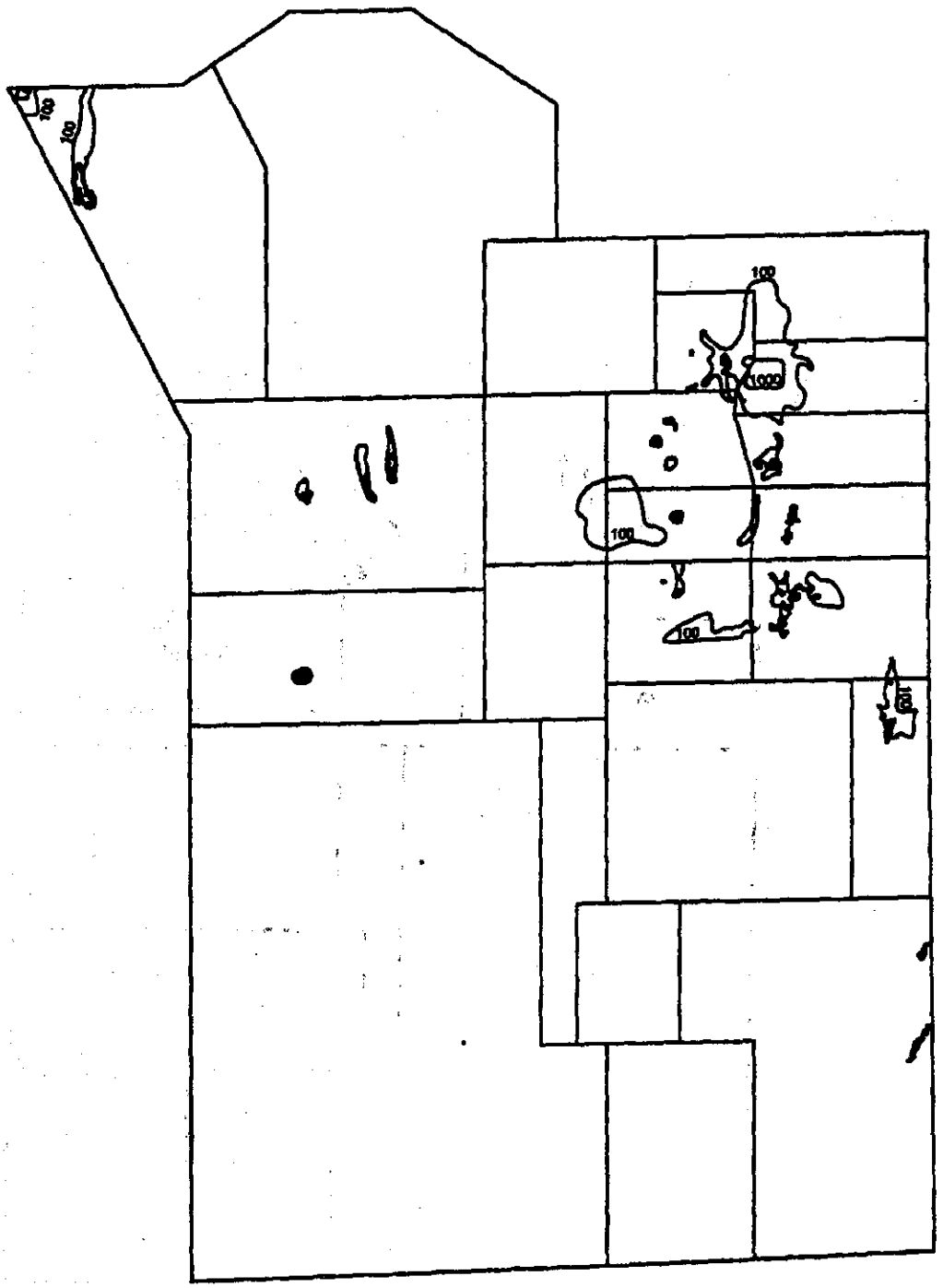

Figure 2. Distribution of ^{241}Am on the NTS as of January 1, 1990. Isopleth levels are 100, 1,000, and 10,000 nCi/m^2.

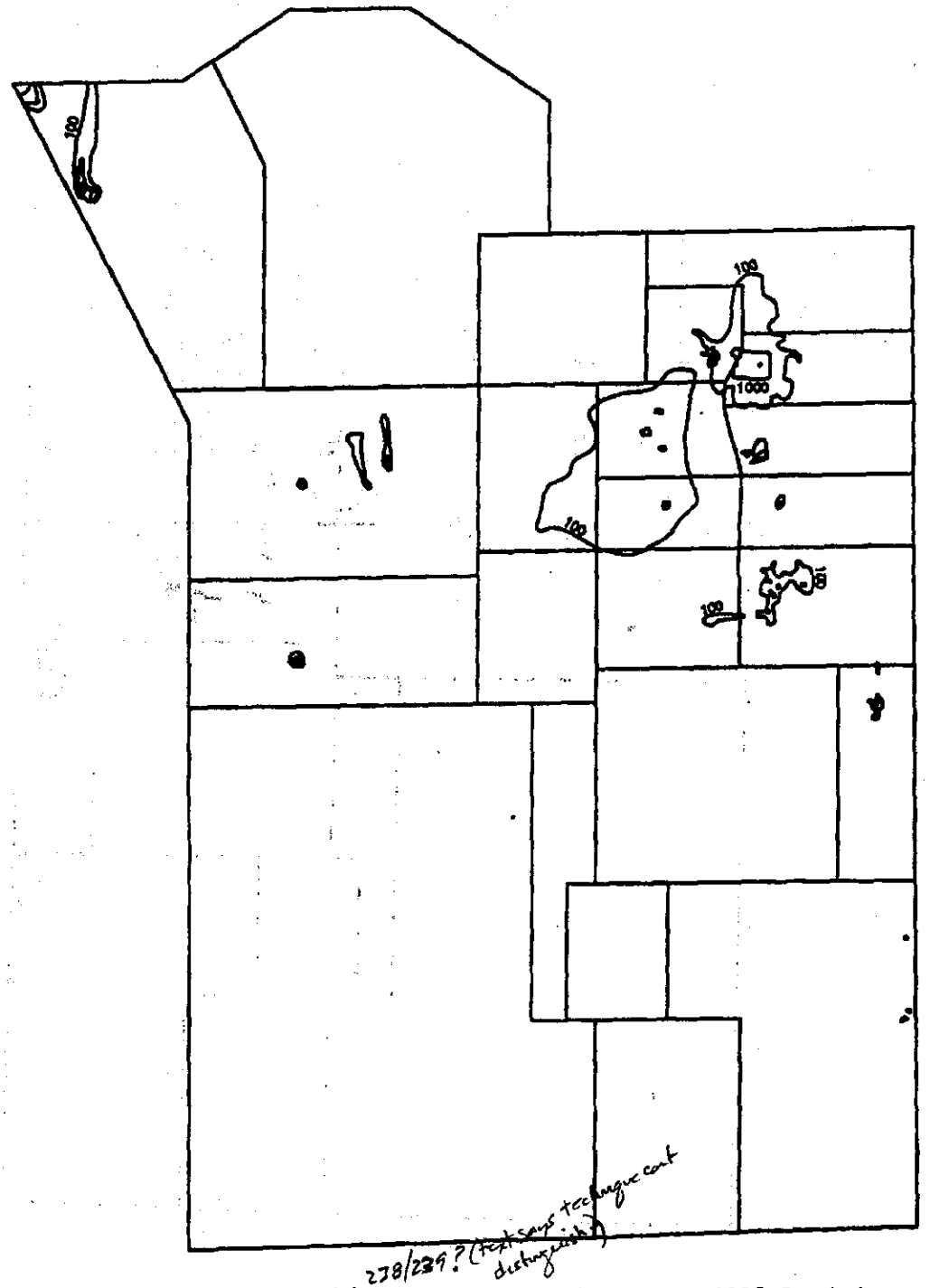

Figure 3. Distribution of ^{238}Pu on the NTS as of January 1, 1990. Isopleth levels are 100, 1,000, and 10,000 nCi/m^2. No measurements of ^{238}Pu were made in the Galileo area in Area 1.

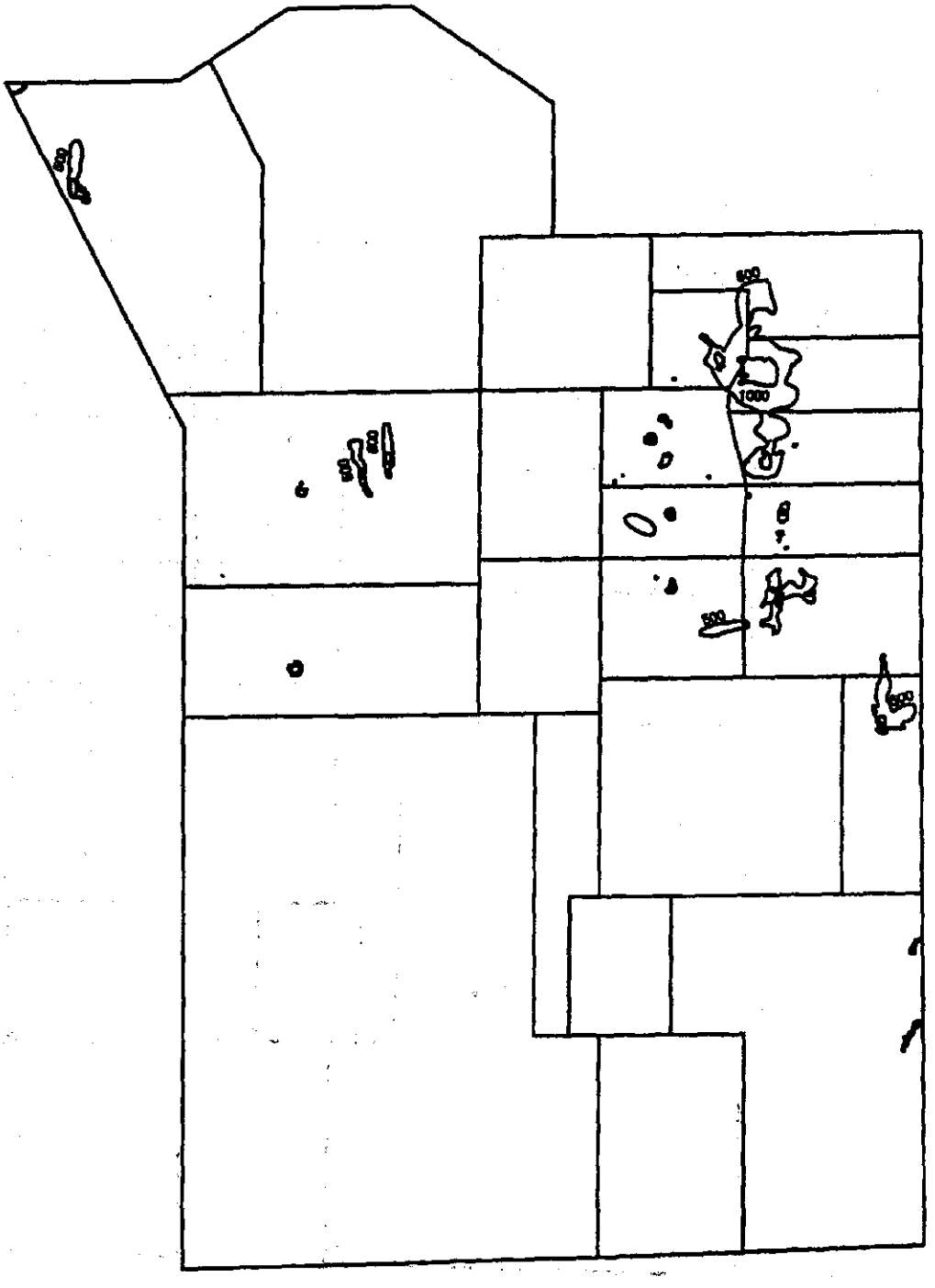

Figure 4. Distribution of $^{239,240}Pu$ on the NTS as of January 1, 1990. Isopleth levels are 500, 1,000, and 10,000 nCi/m^2.

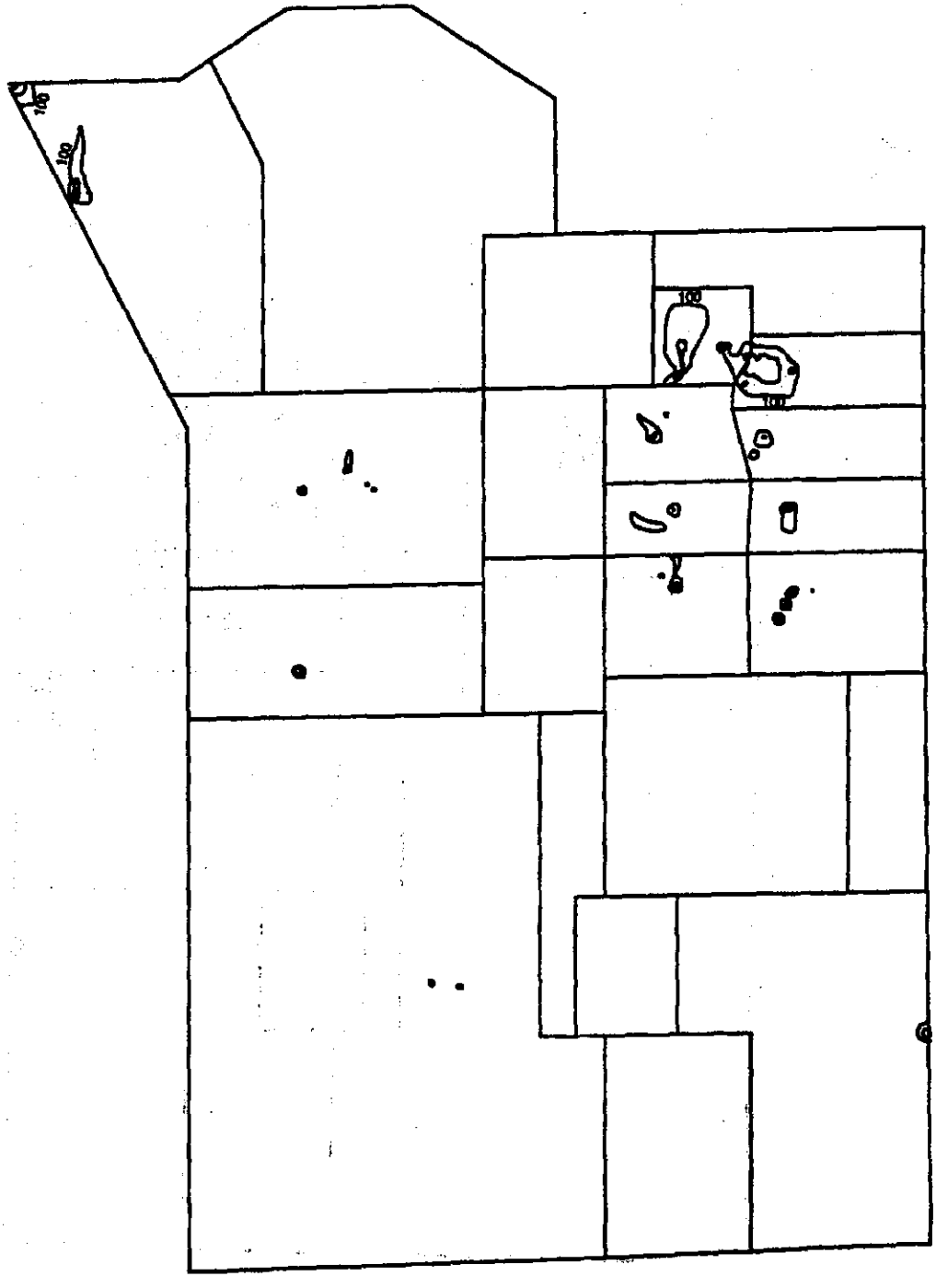

Figure 5. Distribution of ^{60}Co on the NTS as of January 1, 1990. Isopleth levels are 100, 1,000, and 10,000 nCi/m^2.

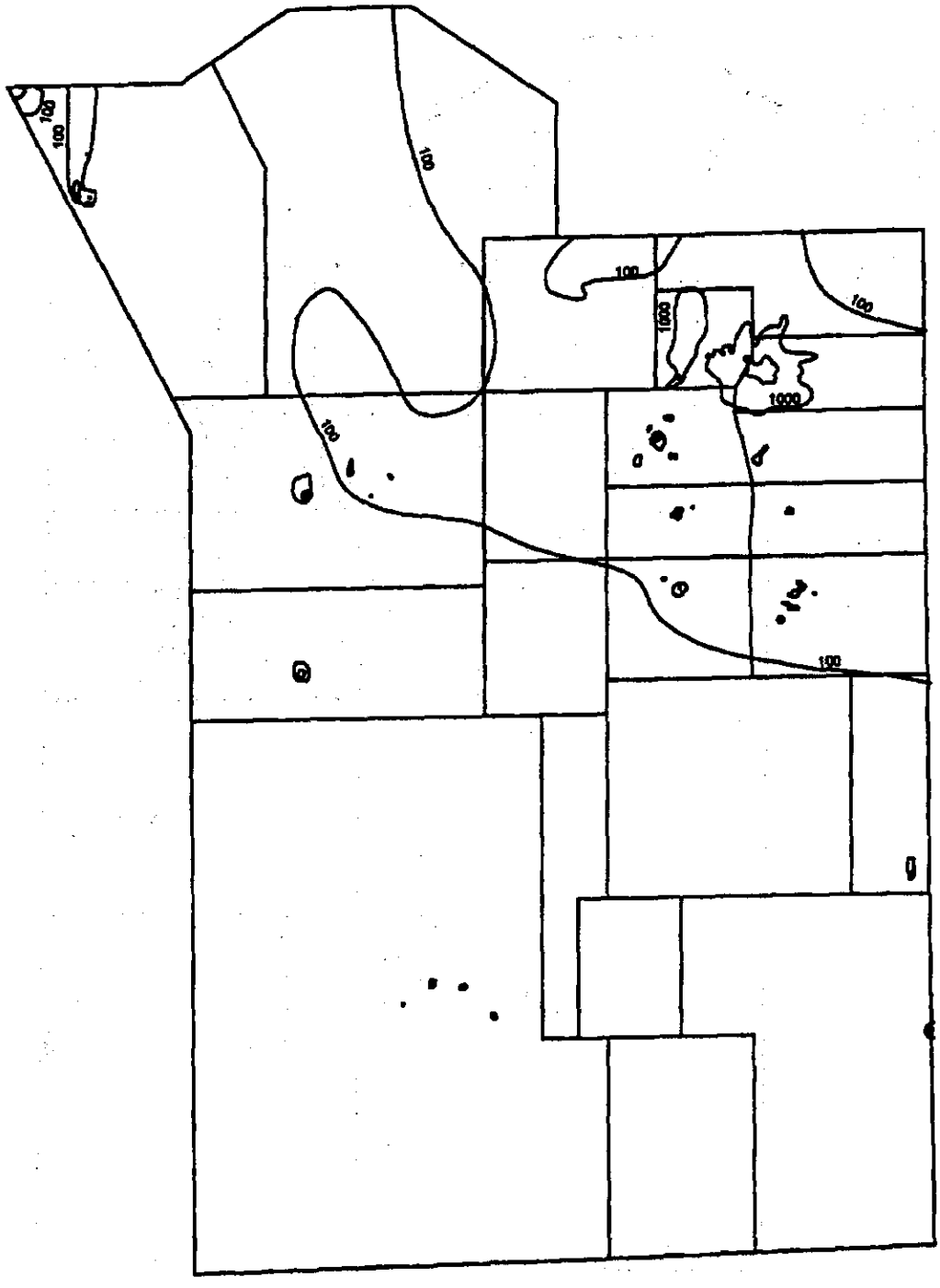

Figure 6. Distribution of ^{137}Cs on the NTS as of January 1, 1990. Isopleth levels are 100, 1,000, and 10,000 nCi/m^2.

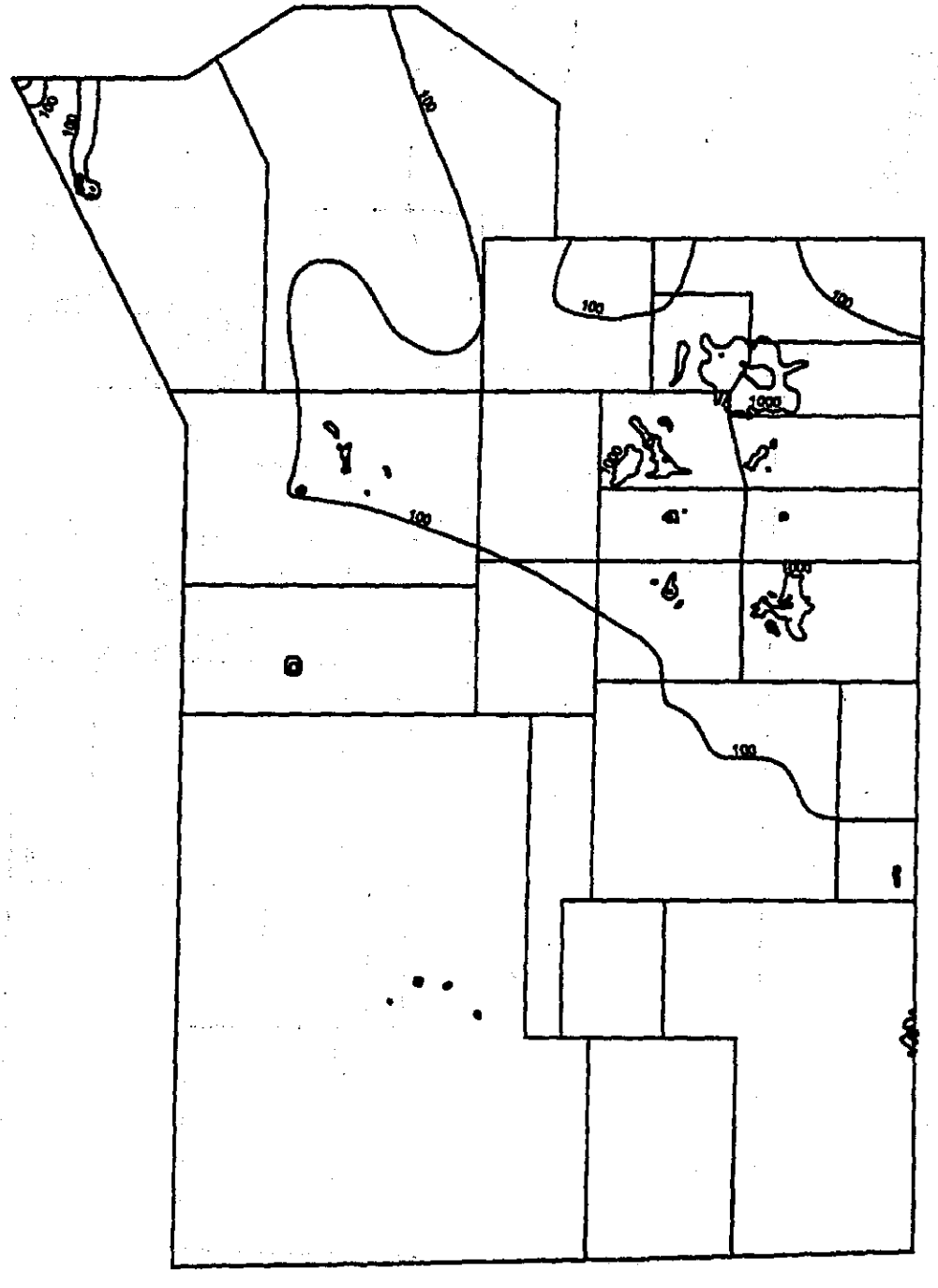

Figure 7. Distribution of ^{90}Sr on the NTS as of January 1, 1990. Isopleth levels are 100, 1,000, and 10,000 nCi/m^2.

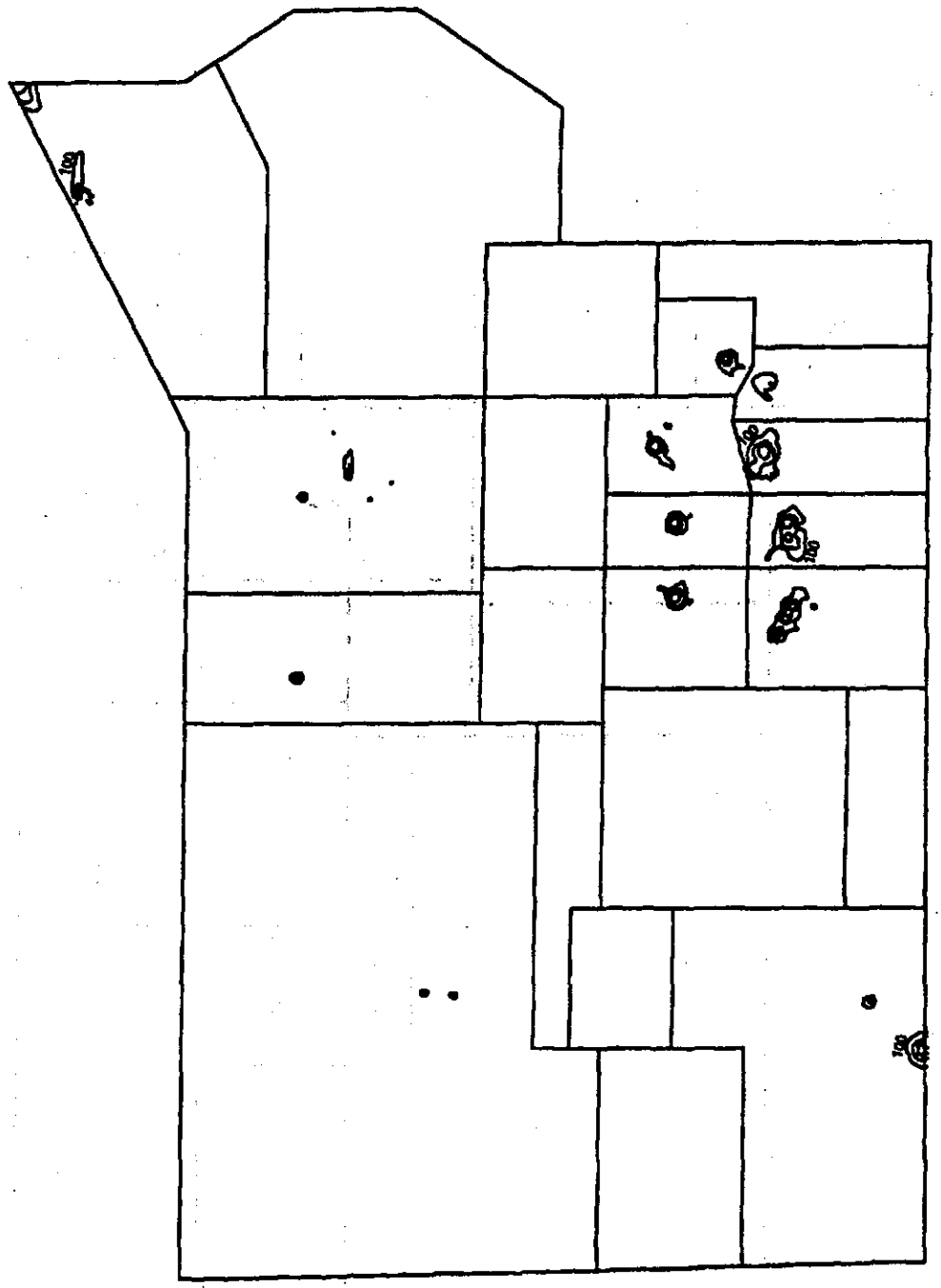

Figure 8. Distribution of ^{152}Eu on the NTS as of January 1, 1990. Isopleth levels are 100, 1,000, and 10,000 nCi/m^2.

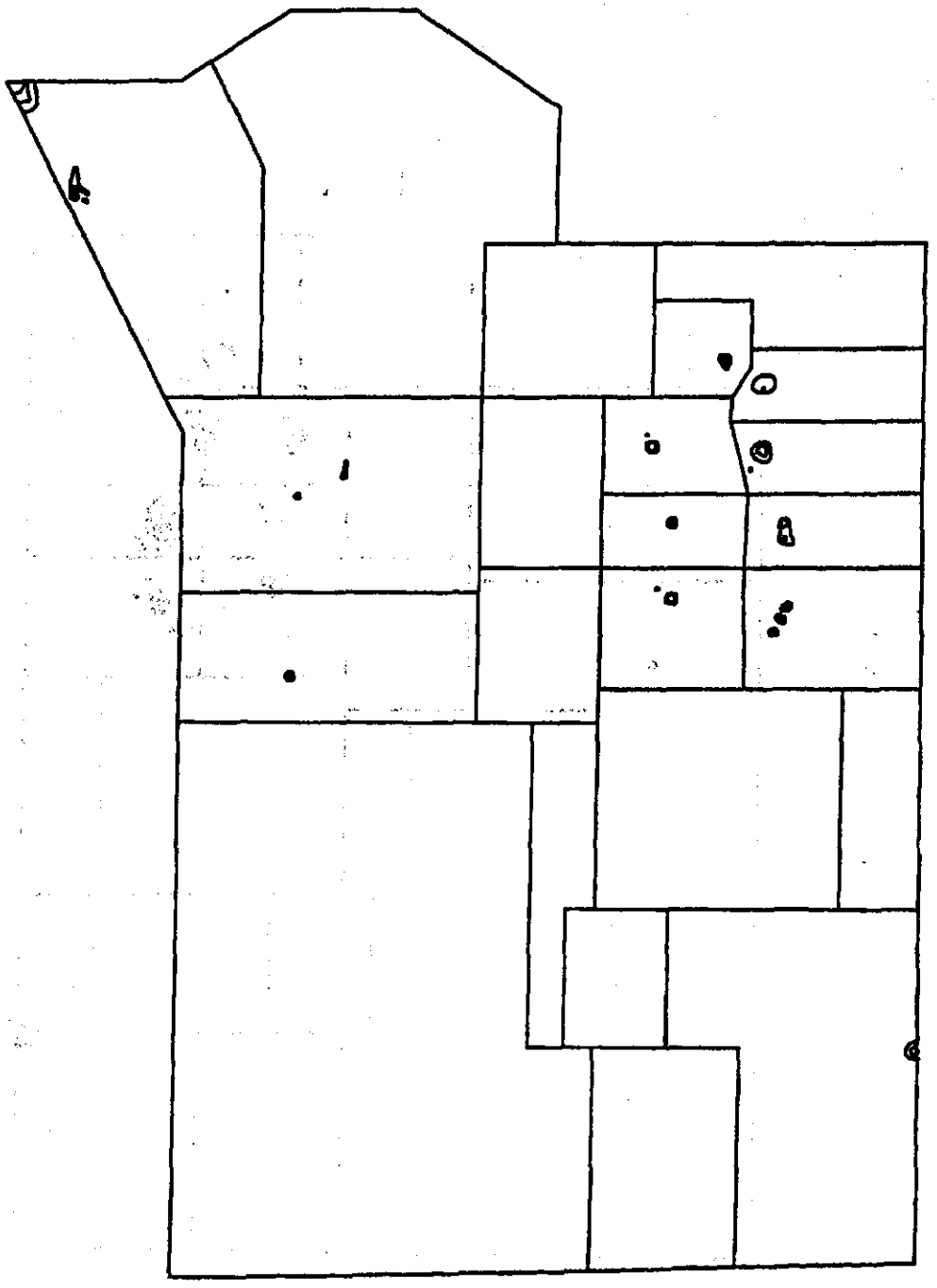

Figure 9. Distribution of ^{154}Eu on the NTS as of January 1, 1990. Isopleth levels are 100, 1,000, and 10,000 nCi/m^2.

Cs, Sr, Co, Pu
Seem to be most
mobile (widespread)

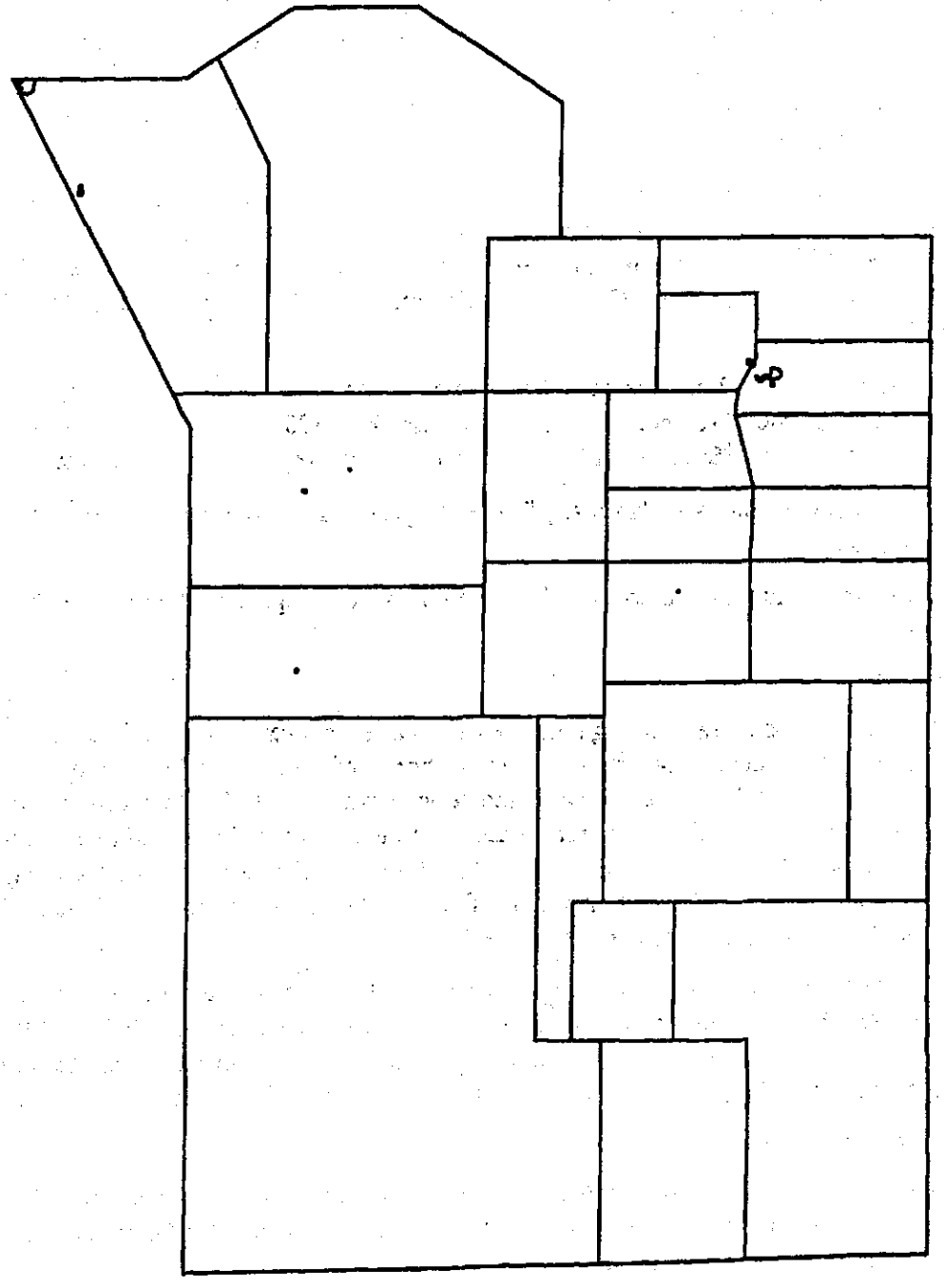

Figure 10. Distribution of ^{155}Eu on the NTS as of January 1, 1990. Isopleth levels are 100, 1,000, and 10,000 nCi/m^2.

Figures 2 through 10 are only intended to give a general picture of the overall distribution of soil radioactivity on the NTS. The small size of most contaminated areas relative to the size of the NTS makes it impossible to label most of the isopleths without obscuring this picture. The values of any unlabeled isopleth can be inferred by using the following guidelines:

- Isopleths are drawn for 100 nCi/m^2, 1,000 nCi/m^2, and 10,000 nCi/m^2 for all radionuclides except ^{239,240}Pu, where a 500 nCi/m^2 isopleth replaces the 100 nCi/m^2 one. (Because the ^{239,240}Pu to ^{241}Am ratio exceeds 5 in most areas and the smallest ^{241}Am measurements are around 40 nCi/m^2, few calculated ^{239,240}Pu values are less than 200 nCi/m^2.)

- The general distribution pattern is the same for all radionuclides. In the southern and western parts of the NTS, concentrations are less than 100 nCi/m^2 except in isolated areas. Only ^{137}Cs and ^{90}Sr exceed 100 nCi/m^2 over a broad region in the northeast corner.

- All isopleths behave "normally," with larger-valued isopleths contained within smaller-valued ones.

Larger-scale, more detailed maps for any contaminated region can be found in the five RIDP reports.

Exposure Rate

The total exposure rate from gamma radiation at each location was calculated by first multiplying the decay-corrected concentration of each radionuclide by a radionuclide-specific factor that converts the concentration in nCi/m^2 to exposure rate in μR/h. The exposure rates due to the individual radionuclides were then added to give a total for each location. The procedures for determining the conversion factors and calculating the exposure rates were provided by L. Anspaugh (LLNL), the Scientific Director of the RIDP. Appendix B describes the calculations in detail.

Figure 11 is a map showing the 96 measurement locations where the exposure rate exceeds 100 μR/h. At only 10 locations does the exposure rate exceed 500 μR/h. All 10 are in Area 20, two near the Schooner GZ and 8 near the Palanquin GZ. Four Palanquin locations exceed 1,000 μR/h, with the maximum value being 1,600 μR/h.

^{239,240}Pu Concentration

The value of 500 pCi/g of ^{239,240}Pu in soil is currently being considered as a criterion for fencing off contaminated areas at the NTS. Measurements of ^{239,240}Pu in nCi/m^2 are converted to pCi/g by the formula

$$\text{pCi/g} = 0.1 \times (\text{nCi/m}^2) \times \alpha/1.5,$$

where 1.5 is the soil density in g/cm^3. Thus for $\alpha = 0.05$/cm, 500 pCi/g is equivalent to 150,000 nCi/m^2; for $\alpha = 1.0$, the value is 7,500 nCi/m^2.

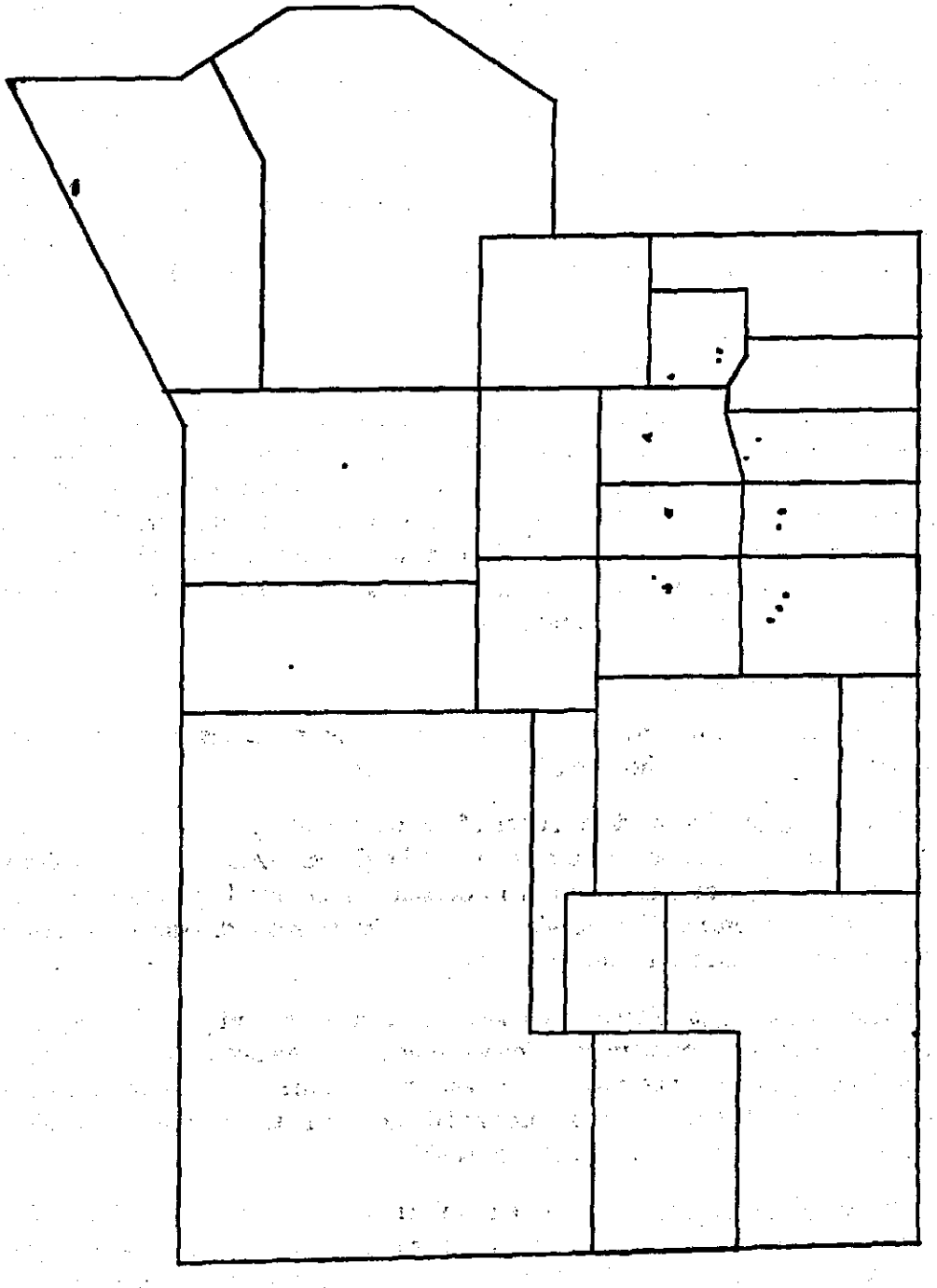

Figure 11. Locations of *in situ* measurements where the exposure rate exceeds 100 μR/h.

Figure 12 shows the 133 locations of *in situ* measurements where the $^{239,240}Pu$ concentration exceeds 500 pCi/g. The highest values are near the Oberon GZ in Area 8, where two measurements exceed 100,000 pCi/g (the maximum is 320,000 pCi/g). Four other points at Oberon, one at Wilson, one at Quay, and four at Little Feller II exceed 10,000 pCi/g.

The highest concentration calculated for a Plutonium Valley location was 3,000 pCi/g. However, concentrations are undoubtedly much higher in the immediate vicinities of the four blast centers. Also, substantial amounts of plutonium are known to be present in the soil in regions outside the NTS boundary at Frenchman Lake (Area 5) and the Schooner site (Area 20).

UNCERTAINTY OF THE RESULTS

The project operations plan (Kordas and Anspaugh, 1982) specified an overall goal of providing "a final inventory that is known with 95% confidence within at least a factor of two." The project scientists feel that this level of precision has been attained, but this assessment derives more from their expert judgment than from any numerical analysis. The process by which the inventory estimates are produced is complex, and uncertainty enters it at a number of points. A thorough evaluation of how these uncertainties interact to affect the precision of the final results is not currently practicable.

Bottom line there is a lot of uncertainty in these #'s from a lot of Sources.

Sources of Uncertainty

Listed below are the major sources of uncertainty in the inventory estimates and distribution maps and an indication of their importance.

Counting error. The random nature of radioactive decay is an intrinsic source of variation in any measurement of radioactivity. The GAMANAL program calculates the counting error as a percentage of the activity of each radionuclide. Reported values typically range from 3 to 40 percent. High activities are usually measured with a smaller percent error (but larger absolute error) than low activities.

Physical parameters. GAMANAL takes into account air density, soil density, and soil moisture content when calculating radionuclide activities. As noted on page 7, the same values of these parameters were used for the analysis of the *in situ* measurements from every survey. Differences between the values used and the actual values for a given area could cause an error of a few percent in the calculated activities.

Inverse relaxation lengths. The inverse relaxation lengths used in GAMANAL were averages of several values calculated from soil profiles. The calculated inverse relaxation lengths are usually quite variable, so choosing a single representative value entails a high degree of uncertainty. The computed conversion factors are extremely sensitive to the value of the inverse relaxation length, especially at low energies (see Report 1, p. 20).

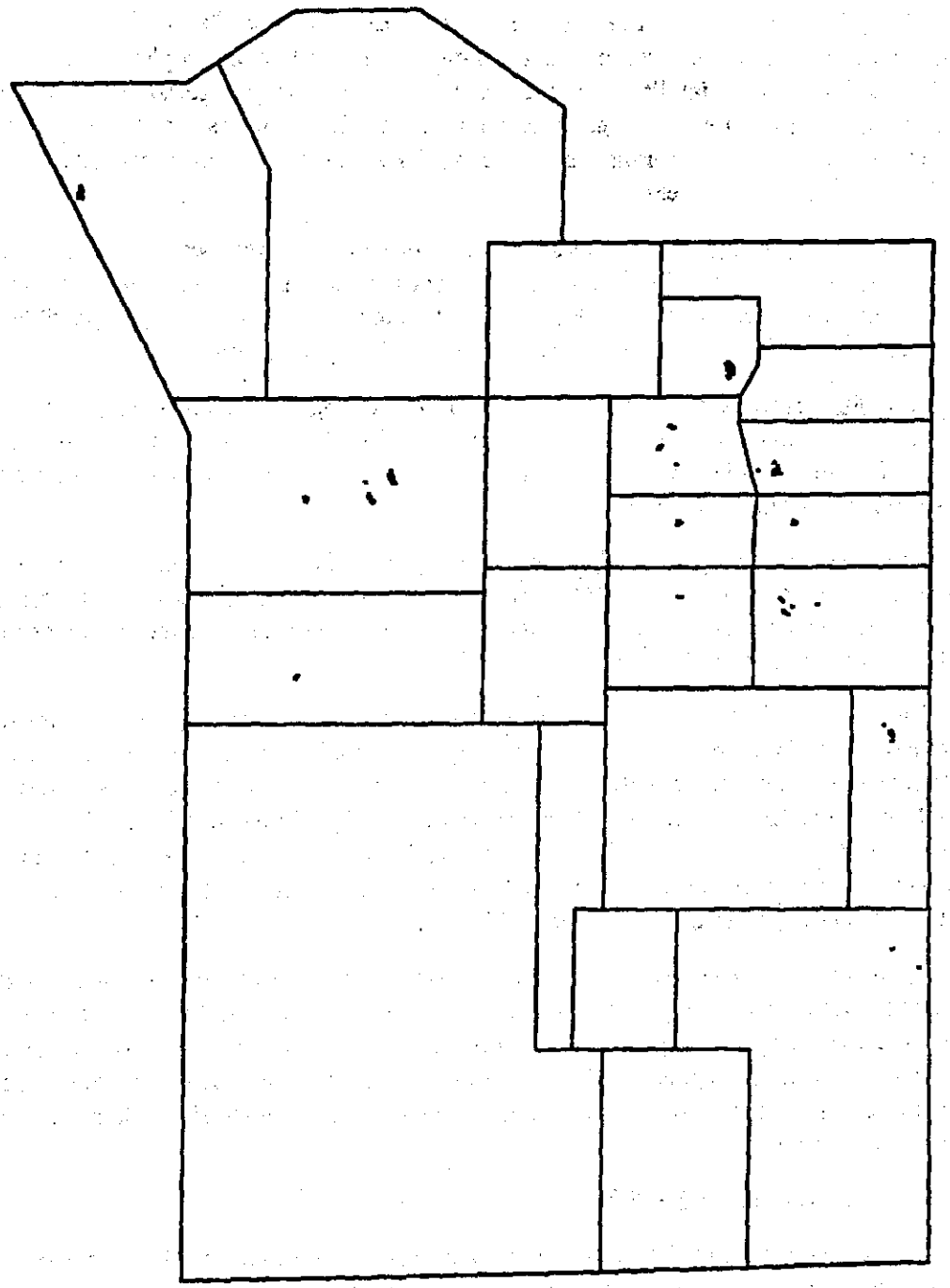

Figure 12. Locations of *in situ* measurements where the $^{239,240}Pu$ level exceeds 500 pCi/g.

Radionuclide ratios. The ratios used to estimate inventories of ^{238}Pu, $^{239,240}Pu$, and ^{90}Sr were averages of values measured in soil samples. The number of samples involved was usually small, and the variability in the measured ratios was usually large, so the values used to estimate inventories have a high uncertainty. Errors in the ratios affect the inventory estimates directly, so if the average ratio is too high by 50 percent, the inventory estimate will also be too high by 50 percent.

Upper Limit Values. When ULVs were used in a data set, they were treated as valid measurements, so the resulting estimates are larger than they should be. The areas within which inventories were estimated were usually set up to include as few ULVs as possible, so the error involved in the total inventory figures is probably negligible.

Sampling error. Sampling error results from estimating the total inventory in an area from measurements at relatively few locations. The size of the sampling error depends on the distribution of radioactivity in the area, the number of measurements, and how the measurement locations are chosen.

The only RIDP study areas where the sampling variability can be estimated directly are the four GZs in Area 18, where importance sampling was used to select the measurement locations (Report 4). The sampling standard deviation at these sites ranged from 5 percent to 40 percent of the total inventory.

Most of the other GZ areas were sampled on a regular grid, with 400-foot or 500-foot grids being used in the regions of highest activity. The sampling variability of the grid design at Frenchman Lake was estimated to be about 20 percent (Report 5, pp. 46–48), and the variability at similar GZ areas is probably comparable. The sampling variability is probably somewhat larger at safety shot sites like those in Plutonium Valley, where contamination occurs in discrete particles that are typically not as uniformly distributed around the GZ as is the radioactivity from a fission explosion.

Location. The locations of the *in situ* measurements were usually determined with a microwave ranging system. The errors in the computed locations can be anywhere from 10 feet to 250 feet or more, depending primarily on the relative positions of the location and the two microwave transponders. The effect of such errors on the inventory estimates and distribution maps is hard to determine, but it is believed to be relatively small compared to other uncertainties.

Comparison with Earlier Studies

During the course of the RIDP, surveys were made of four regions that had previously been studied by researchers from the Nevada Applied Ecology Group (NAEG). The estimates of $^{239,240}Pu$ inventory obtained by both groups for these regions are shown in Table 6. While the estimates are not entirely comparable because of differences in the areas surveyed, the comparison is still of some interest.

TABLE 6. RIDP AND NAEG ESTIMATES OF ^{239,240}PU INVENTORY

Region	Size of Region (km^2)		Inventory (Ci)	
	RIDP	NAEG	RIDP	NAEG
GMX	0.97	0.13	1.4	1.5
Plutonium Valley	8.7	4.8	29	36
Palanquin/Cabriolet	12	~3.4	48*	13*
Little Feller II	0.87	1.1	27	25 to 31

*Includes ^{241}Am inventory

References: RIDP Reports 4 and 5; Gilbert, 1977; Gilbert *et al.*, 1985.

GMX. The NAEG estimate was based on the analysis of 111 soil samples. Of the 65 RIDP *in situ* measurements at GMX, 8 were within the NAEG study area. Using the average of these eight measurements and a ^{239,240}Pu/^{241}Am ratio of 7.2 (the average from three RIDP soil samples) leads to an estimate of 1.1 Ci of ^{239,240}Pu in the NAEG area. If the NAEG's Pu/Am ratio of 10.3 (based on 89 samples) is used instead, the estimated inventory for the NAEG study area is 1.4 Ci, in good agreement with the NAEG estimate.

Plutonium Valley. The area surveyed by the RIDP includes all but the southern edge of the NAEG study area. The RIDP found a substantial amount of ^{239,240}Pu, about 7 Ci, north and east of the NAEG area. Consequently, the RIDP estimate for the NAEG area is about 22 Ci, somewhat less than the NAEG estimate. The NAEG estimate was based on 205 soil samples, while the RIDP estimate was based on 128 *in situ* measurements.

Palanquin/Cabriolet. The area surveyed by the RIDP was twice as large as that surveyed by the NAEG, which partly explains the difference in inventory estimates. In addition, the NAEG did not include the regions within 500 feet of the GZs in its survey. On the other hand, the NAEG was able to sample in the rocky area near the two GZs where the RIDP vehicle could not go. The difference in regions surveyed makes a detailed comparison of the data difficult.

Little Feller II. The original RIDP estimate in Report 4 was three times the NAEG estimate. Investigation of the discrepancy led to discovery of a major error in the calculations; see Appendix C for details. The corrected RIDP estimate (based on 54 *in situ* measurements) agrees closely with the NAEG estimate (based on analyses of 712 soil samples).

The results of these comparisons thus tend to confirm the accuracy of the *in situ* method as used in the RIDP.

REFERENCES

Anspaugh, L.R. 1976. *In situ* methods for quantifying specific radionuclides. IEEE Transactions on Nuclear Science NS-23, 1190.

Beck, H. L., J. Decampo, and C. Gogolak. 1972. *In situ* Ge(Li) and Na(Tl) gamma-ray spectrometry. HASL-258, Health and Safety Laboratory, Atomic Energy Commission, New York, N.Y.

Bluitt, C. M. 1986. An aerial radiological survey of Areas 16 and 30, Nevada Test Site (Date of survey: June 1983). EGG-10282-1118, EG&G Energy Measurements, Inc., Las Vegas, Nevada.

Clark, H. W. 1983. An aerial radiological survey of Area 11, Nevada Test Site (Date of survey: January 1982). EGG-10282-1004, EG&G Energy Measurements Group, Las Vegas, Nevada.

Essington, E.H. Reliability of analytical results for the Radionuclide Inventory and Distribution Program. (In preparation)

Essington, E.H. and S.W. Mead. Quality assurance procedures for the Nevada Test Site Radionuclide Inventory and Distribution Program. (In preparation)

Feimster, E. L. 1985. An aerial radiological survey of Areas 18 and 20, Nevada Test Site (Date of survey: October - November 1980). EGG-10282-1093, EG&G Energy Measurements, Inc., Las Vegas, Nevada.

Fritzsche, A. E. 1982. An aerial radiological survey of Areas 1, 2, 3, 4, 6,7, 8, 9, 10, 12, 15, and 17, Yucca Flat, Nevada Test Site (Date of survey: 8 August - 2 September 1978). EGG-1183-1808, EG&G Energy Measurements Group, Las Vegas, Nevada.

Gilbert, R. O. 1977. Revised total amounts of $^{239,240}Pu$ in surface soil at safety-shot sites. In White, M. G., P. B. Dunaway, and D. L. Wireman, eds., *Transuranics in Desert Ecosystems*. NVO-181, U.S. Department of Energy, Las Vegas, Nevada, pp. 423-429.

Gilbert, R. O., J. C. Simpson, D. W. Engel, and R. R. Kinnison. 1985. Estimating isotopic ratios, spatial distribution, and inventory of radionuclides at Nuclear Sites 201, 219, and 221. In Howard, W. A., and R.G. Fuller, eds., *The Dynamics of Transuranics and Other Radionuclides in Natural Environments*. NVO-272, U.S. Department of Energy, Las Vegas, Nevada, pp. 381-429.

Gunnink, R., and J. B. Niday. 1971. Computerized quantitative analysis by gamma-ray spectrometry. Vol. 1-5, UCRL-51061, Lawrence Livermore National Laboratory, Livermore, California.

Hicks, H. G., and D. W. Barr. 1984. Nevada Test Site Fallout Atom Ratios: $^{240}Pu/^{239}Pu$ and $^{241}Pu/^{239}Pu$. UCRL–53499–1, Lawrence Livermore National Laboratory, Livermore, California.

Jobst, J. E. 1986. An aerial radiological survey of Areas 12, 15, 17 and 19, Nevada Test Site (Date of survey: October – November 1984). EGG–10282–1113, EG&G Energy Measurements, Inc., Las Vegas, Nevada.

Kordas, J. F., and L. R. Anspaugh. 1982. Nevada Test Site Radionuclide Inventory and Distribution — Project Operations Plan. UCID–19413, Lawrence Livermore National Laboratory, Livermore, California.

McArthur, R. D., and J. F. Kordas. 1983. Radionuclide Inventory and Distribution Program: The Galileo Area. DOE/NV/10162–14, Publication #45035, Water Resources Center, Desert Research Institute, University of Nevada System, Las Vegas.

McArthur, R. D., and J. F. Kordas. 1985. Nevada Test Site Radionuclide Inventory and Distribution Program: Report #2. Areas 2 and 4. DOE/NV/10162–20, Publication #45041, Water Resources Center, Desert Research Institute, University of Nevada System, Las Vegas.

McArthur, R. D., and S. W. Mead. 1987. Nevada Test Site Radionuclide Inventory and Distribution Program: Report #3. Areas 3, 7, 8, 9, and 10. DOE/NV/10384–15, Publication #45056, Water Resources Center, Desert Research Institute, University of Nevada System, Las Vegas.

McArthur, R. D., and S. W. Mead. 1988. Nevada Test Site Radionuclide Inventory and Distribution Program: Report #4. Areas 18 and 20. DOE/NV/10384–22, Publication #45063, Water Resources Center, Desert Research Institute, University of Nevada System, Las Vegas.

McArthur, R. D., and S. W. Mead. 1989. Nevada Test Site Radionuclide Inventory and Distribution Program: Report #5. Areas 5, 11, 12, 15, 17, 18, 19, 25, 26, and 30. DOE/NV/10384–26, Publication #45067, Water Resources Center, Desert Research Institute, University of Nevada System, Las Vegas.

McArthur, R. D., and F. L. Miller, Jr. 1989. Off–Site Radiation Exposure Review Project: Phase II Soils Program. DOE/NV/10384–23 Rev., Publication #45064, Water Resources Center, Desert Research Institute, University of Nevada System, Las Vegas.

Tipton, W. J. 1979. An aerial radiological survey of Areas 25 and 26, Nevada Test Site (Date of survey: September 1976). EGG–1183–1745, EG&G Energy Measurements Group, Las Vegas, Nevada.

APPENDIX A
CALCULATION OF TOTAL RADIONUCLIDE INVENTORIES

Table 5 gives the total estimated inventories of nine radionuclides in each NTS area where contamination from NTS activities occurs. This appendix gives the details of how those numbers were obtained.

TABULATION OF RESULTS

The first step was to tabulate the inventory estimates on an area-by-area basis. About one-third of the estimates were obtained directly from tables in the earlier RIDP reports. Many others were modified from earlier results to make the treatment of upper limit values consistent. Also, the estimates for parts of Yucca Flat had to be recalculated to give estimates for the individual NTS areas.

In addition, inventory estimates were calculated for regions which could not be surveyed because of the terrain, but which were known to have some contamination from NTS activities. The average radionuclide concentrations assumed for these regions are listed in Table A-1.

TABLE A-1. AVERAGE RADIONUCLIDE CONCENTRATIONS ASSUMED FOR UNSURVEYED REGIONS

Region	Radionuclide Concentration (nCi/m^2)		
	^{241}Am	^{60}Co	^{137}Cs
West of Yucca Flat			
Area 1	30	4	50
Area 4	150	200	450
Area 2	75	100	400
East of Yucca Flat			
Areas 3, 7, 9	20	8	100
Area 10	30	20	500
North of Yucca Flat			
Area 8	30	300	700
Area 15	100	4	200
West side of Area 17	20	10	150

The tabulated inventory estimates are shown in Table A-2. The following notes give details of how these estimates were derived. Much of the discussion is in terms of average

concentrations of a radionuclide in a region. Inventories are estimated from the average and the area of the region by the formula:

$$I = \text{average activity } (nCi/m^2) \times \text{area } (mi^2) \times 0.0026,$$

where the .0026 factor converts nCi/m^2 to Ci/mi^2.

Area 1: The Galileo results are from the polygons of influence method using all the data, ULVs included (Table 9, Report 1). The Hornet region includes parts of regions HO–6 and QU–6 from Figure 3, Report 3; the calculations used the HO–6 averages. The South Yucca estimates used the average of the five grid points in Area 1. The same values were assumed for the unsurveyed part of Area 1 except that ^{241}Am was given a value of 30 nCi/m^2 instead of 60 because one South Yucca grid point had high ^{241}Am. No $^{238}Pu/^{241}Am$ ratio was reported for Galileo, so the Kepler value of 2.0 was used. The ratios used for the Galileo area were also used for South Yucca and the unsurveyed area.

Area 2: The Whitney, Shasta, and Diablo results are from Table 6 of Report 2, except that europium was assumed to be zero in the background regions. The remaining surveyed region includes parts of regions BA–3, SE–3, and WI–2 (Report 3); the average values were determined by inspection of the data. The values for the unsurveyed west side of Area 2 were derived from the Area 17 plots in Report 5. The average of the radionuclide ratios in 11 samples from the Whitney, Shasta, and Diablo areas (Table 3, Report 2) was used for the other two regions.

Area 3: The Hornet results are the combined inventories in regions HO–1 through HO–5 (Table 9, Report 3) plus contributions from regions QU–5, QU–6, and HO–6 determined by inspection of the data. The South Yucca values were based on the three Area 3 points. The averages of eight measurements east of the Hornet and Quay grids (Figure 2, Report 3) were used to estimate the inventories in the unsurveyed eastern parts of Areas 3, 7, and 9.

Area 4: The Kepler results are from Table 6 in Report 2; the ^{137}Cs value in Table A–2 is 0.2 Ci less than the value in Report 2 because a small part of the Kepler area is in Area 1. Europium was assumed to be absent from the background regions, but the ^{152}Eu inventory was rounded upward to reflect a small area of contamination east of the GZ area (Figure 7, Report 2). The Quay results are based on averages in the QU–6 region. The unsurveyed region was estimated from the four points on the western edge of the Kepler area.

Area 5: Results are from Tables 10 and 13 of Report 5.

TABLE A-2. ESTIMATED RADIONUCLIDE INVENTORIES

Area	Region	Area (sq mi)	Radionuclide inventory (Ci)								
			^{241}Am	^{239}Pu	$^{239,240}Pu$	^{60}Co	^{137}Cs	^{90}Sr	^{152}Eu	^{154}Eu	^{155}Eu
1	Galileo	4.8	1.0	2.0	5.0	2.8	4.8	7.2	21.3	2.2	0.6
	Hornet	5.7	1.3	0.9	10.2	0.1	3.5	11.7	0	0	0
	S. Yucca	7.6	1.2	2.3	5.9	0.1	1.0	1.5	0	0	0
	unsurveyed	8.4	0.7	1.3	3.3	0.1	1.1	1.6	0	0	0
		26.5	4.2	6.5	24.4	3.1	10.4	22.0	21.3	2.2	0.6
2	Whitney	2.7	0.4	1.4	4.8	1.6	4.0	11.2	19.4	0.7	0.1
	Shasta	4.9	0.7	2.1	5.3	0.7	10.4	27.0	0.3	0	0.3
	Diablo	4.0	1.0	2.7	5.6	0.4	9.0	18.0	0.4	0	0.1
	Sedan	6.1	0.4	1.2	3.3	0.2	3.2	7.9	0	0	0
	unsurveyed	2.0	0.4	1.2	3.2	0.5	2.1	5.2	0	0	0
		19.7	2.9	8.6	22.2	3.4	28.7	69.3	20.1	0.7	0.3
3	Hornet	8.5	3.4	2.3	27.1	1.8	8.5	28.1	24.4	1.1	0.6
	S. Yucca	4.6	0.2	0.1	1.5	0.1	0.6	2.0	0	0	0
	unsurveyed	19.2	1.0	0.7	8.1	0.4	5.0	16.4	0	0	0
		32.3	4.6	3.1	36.7	2.3	14.1	46.5	24.4	1.1	0.6
4	Kepler	9.7	5.8	11.6	34.8	3.9	10.8	14.0	13.0	0.9	0.2
	Quay	5.2	0.4	0.1	3.0	0.1	2.0	4.4	0	0	0
	unsurveyed	1.1	0.4	0.8	2.5	0.6	1.3	1.6	0	0	0
		16.0	6.6	12.5	40.3	4.6	14.1	20.0	13.0	0.9	0.2
5	Frenchman Lake	2.2	0.4	0.1	3.4	1.0	0.4	1.1	12.1	0.8	0
	GMX, etc.	0.7	0.2	0.0	1.4	0.0	0.0	0.0	0.2	0	0
		2.9	0.6	0.1	4.8	1.0	0.4	1.1	12.3	0.8	0
6	S. Yucca	32.3	1.7	3.3	8.4	0.4	3.3	5.0	0	0	0
7	Quay	6.7	1.5	0.4	11.2	2.1	2.8	6.1	29.9	2.4	0.4
	unsurveyed	12.6	0.7	0.2	4.9	0.3	3.3	7.2	0	0	0
		19.3	2.2	0.6	16.1	2.4	6.1	13.3	29.9	2.4	0.4
8	Bansberry	5.2	0.9	0.7	3.6	8.9	26.4	6.6	0	0	0
	Smoky	3.3	15.6	7.0	106.7	2.1	13.4	17.1	6.0	0.4	0.7
	unsurveyed	5.4	0.4	0.3	2.3	4.2	9.8	13.8	0	0	0
		13.9	16.9	8.0	112.6	15.2	49.6	37.5	6.0	0.4	0.7
9	Wilson	7.5	3.6	1.9	75.6	1.5	7.0	13.3	31.0	2.9	0.4
	unsurveyed	12.5	0.6	0.3	13.6	0.3	3.2	6.2	0	0	0
		20.0	4.2	2.2	89.2	1.8	10.2	19.5	31.0	2.9	0.4
10	Sedan	7.7	18.4	18.4	101.1	24.7	83.7	68.4	3.0	4.2	6.0
	unsurveyed	12.3	1.0	1.0	5.3	0.6	16.0	13.1	0	0	0
		20.0	19.4	19.4	106.4	25.3	99.7	81.5	3.0	4.2	6.0
11	Pu Valley	3.4	3.3	0.5	29.0	0.0	0.4	0.2	0	0	0
	Pinstripe	0.6	0.0	0.0	0.0	0.0	0.2	0.2	0	0	0
		4.0	3.3	0.5	29.0	0.0	0.6	0.4	0	0	0
12		39.6	5.7	8.5	38.5	2.2	22.0	21.0	0	0	0
15	Yucca Flat	4.3	2.5	2.1	21.3	0.3	8.8	12.1	0	0	0
	E side	12.2	0.6	0.8	4.3	0.0	2.2	3.1	0	0	0
	unsurveyed	18.8	4.9	4.9	37.2	0.2	9.8	13.7	0	0	0
		35.3	8.0	7.8	62.8	0.5	20.8	28.9	0	0	0
16	east half	14.3	0.7	1.5	3.7	0.1	3.2	4.7	0	0	0
17	Yucca Flat	11.2	1.8	2.8	11.3	1.4	9.2	14.0	0	0	0
	unsurveyed	20.2	1.0	1.7	6.6	0.5	7.3	11.0	0	0	0
		31.4	2.8	4.5	17.9	1.9	16.5	25.0	0	0	0
18	Little Feller I	0.6	6.0	0.7	33.6	0.3	0.3	0.5	0	0	0.1
	Little Feller II	0.3	4.7	0.6	27.0	0.0	0.3	0.6	0.1	0	0.1
	Johnie Boy	4.0	1.0	1.9	10.6	0.8	2.1	10.9	0.8	0.4	0.4
	Danny Boy	0.9	6.6	0.8	26.0	0.2	2.3	1.4	0.5	0.1	0.3
	NE corner	21.5	1.0	1.6	6.3	0.1	6.2	9.4	0	0	0
		27.3	19.3	5.6	103.5	1.4	11.2	22.8	1.4	0.5	0.9
19		148.3	21.2	31.8	144.2	1.9	39.9	38.7	0	0	0
20	Schooner	1.7	9.4	16.0	6.4	9.7	1.5	1.5	14.0	17.0	5.2
	Cabriolet	4.5	14.0	14.0	35.0	8.5	4.9	4.5	2.6	1.0	0.4
		6.2	23.4	30.0	41.4	18.2	6.4	6.0	16.6	18.0	5.6
25	NRDS	0.9	0.0	0.0	0.0	0.1	0.2	0.2	0.5	0	0
26	bunker	0.2	0.0	0.0	0.0	0.0	0.0	0.0	0	0	0
30	Buggy	0.3	3.2	4.5	14.1	1.4	1.7	1.6	0.9	0.4	0.2

Note: One decimal place was retained in these tabulated values to reduce rounding errors in later calculations. None of the estimates should be considered accurate to more than two significant figures.

Area 6: The estimates were made from 25 South Yucca measurements and the radionuclide ratios used for the Galileo area in Area 1.

Area 7: The Quay values include the inventories in regions QU–1 through QU–4 and contributions from WI–2, QU–5, and QU–6 (Table 9, Report 3). Inventories in the unsurveyed region were estimated as in Area 3.

Area 8: The Baneberry results include regions BA–1, BA–2, and 80 percent of BA–3, while the Smoky results include regions SM–1, SM–2, and 23 percent of SE–3 (Table 5, Report 3). Contamination from both ^{60}Co and ^{137}Cs extends north of the surveyed area at Baneberry, so relatively high levels were assumed for the unsurveyed region.

Area 9: The Wilson inventories are the sum of the reported inventories for region WI–1 and the portion of region WI–2 that is in Area 9 (Table 9, Report 3). Inventories in the unsurveyed region were estimated as in Area 3.

Area 10: The Sedan estimates are the sum of the estimates for regions SE–1 and SE–2 and 65 percent of the estimates for SE–3 (Table 5, Report 3). Averages in the unsurveyed region were estimated from the four easternmost Sedan points.

Area 11: Results are from Tables 7 and 13 in Report 5.

Area 12: Results for ^{60}Co, ^{137}Cs, and ^{90}Sr are from Report 5. The other estimates were calculated from an assumed level of 55 nCi/m^2 of ^{241}Am (see Table 19, Report 5).

Area 15: The results for Yucca Flat are from Report 5, as are most of the results from the east side. The ^{241}Am inventory for the east side is based on an assumed average level of 20 nCi/m^2. Elevated levels of radioactivity extend into the unsurveyed region north of Yucca Flat, so relatively high averages were used for that region.

Area 16: The aerial survey showed ^{137}Cs contamination in most of the eastern half of Area 16, so the average of the six ^{137}Cs measurements along the Mid–Valley Road (85 nCi/m^2) was used for the entire region. Assumed levels of 20 nCi/m^2 of ^{241}Am and 3 nCi/m^2 of ^{60}Co were used along with the ratios from the west side of Area 1 to estimate the other inventories.

Area 17: The Yucca Flat results are from Report 5. Contamination extends west of the surveyed area, so above–background levels were used for the unsurveyed area.

Area 18: Most of the estimates for the four GZ regions are from Table C–1 on page 43. All three europium isotopes are assumed to be absent from the regions north of the Little

Feller I and Johnie Boy GZs; ^{154}Eu is also assumed to be absent from the Littler Feller I and Little Feller II GZ areas. The estimates for ^{137}Cs and ^{90}Sr in the northeast corner of Area 18 are from Report 5. The remaining estimates were computed using assumed values of 18 nCi/m^2 of ^{241}Am and 2 nCi/m^2 of ^{60}Co and the ratios in Table 16 of Report 5.

Area 19: The ^{137}Cs and ^{90}Sr values are from Report 5. The other estimates were computed from assumed values of 55 nCi/m^2 of ^{241}Am and 5 nCi/m^2 of ^{60}Co and the average radionuclide ratios in Table 18, Report 5.

Area 20: Results are from Table 4 in Report 4.

Areas 25 and 26: Results are from Table 2 in Report 5. Because of the extensive cleanup of the contaminated sites in these areas, the inventories of ^{241}Am and plutonium were assumed to be insignificant.

Area 30: Results are from Table 4 in Report 5.

DECAY CORRECTION

After the inventory estimates had been tabulated, the totals for each area were decay–corrected to give the final estimates for Table 5. The formula for calculating the decay–corrected inventory I_c is

$$I_c = I_o \exp[-0.693t/t_h]$$

where I_o is the uncorrected inventory estimate, t is the time in years between the survey date and January 1, 1990, and t_h is the half–life of the radionuclide from Table 1. The survey date used for each area was the approximate date of the highest *in situ* measurements:

Survey	Date	Survey	Date
Galileo	12/01/81	Danny Boy	06/22/84
Kepler	10/08/81	Area 25	03/23/84
Whitney/Shasta	02/16/82	Area 26	03/28/84
Diablo	05/12/82	Area 17	11/20/84
Baneberry	06/29/82	Area 18	08/22/85
Smoky	10/04/82	Area 15 (Yucca)	10/23/84
Sedan	09/16/82	Area 15 (E side)	11/18/84
Wilson	12/02/82	GMX, RWMS,	
Quay	02/16/83	Kay blockhouse	02/01/85
Hornet	05/04/83	Pinstripe	02/01/85
South Yucca	06/01/83	Pu Valley	05/15/85
Schooner	10/05/83	Buggy	06/27/85
Cabriolet	08/24/83	Area 12	07/09/85
Johnie Boy	12/12/83	Area 19	07/30/85
Little Feller I	06/26/84	Area 16	09/17/85
Little Feller II	01/17/84	Frenchman Lake	10/22/85

Unsurveyed regions were given the date of the major survey in a given area. For example, the unsurveyed part of Area 3 was assigned the same date as the Hornet survey, May 4, 1983.

APPENDIX B
CALCULATION OF EXPOSURE RATE

The gamma–exposure rate at each location of an *in situ* measurement was calculated from the formula

$$\text{exposure rate} = \sum_{i=1}^{14} a_i X_i,$$

where X_i is the concentration (nCi/m^2) of radionuclide i and a_i is the factor for converting nCi/m^2 of radionuclide i to $\mu R/h$. The formula includes only 14 radionuclides because ^{90}Sr gives off no gamma radiation as it decays.

Conversion Factors

The conversion factor for a given radionuclide depends on the energy of the gamma rays it emits and its depth distribution in the soil, as characterized by the inverse relaxation length α. Table B–1 gives the conversion factors for the 14 radionuclides at the 9 different α values used in analyzing the *in situ* measurements.

TABLE B–1. CONVERSION FACTORS ($\mu R/h$ per nCi/m^2)

	Inverse relaxation length (1/cm)								
Nuclide	0.05	0.1	0.2	0.3	0.4	0.5	0.6	0.8	1.0
^{241}Am	0.000035	0.000075	0.00011	0.00013	0.00015	0.00016	0.00017	0.00019	0.00021
^{133}Ba	0.0012	0.0015	0.0021	0.0028	0.0031	0.0034	0.0035	0.0039	0.0042
^{60}Co	0.0096	0.010	0.015	0.018	0.020	0.021	0.022	0.024	0.025
^{134}Cs	0.0030	0.0065	0.010	0.012	0.013	0.014	0.015	0.016	0.017
^{137}Cs	0.0012	0.0024	0.0035	0.0042	0.0047	0.0050	0.0053	0.0058	0.0062
^{152}Eu	0.0026	0.0048	0.0069	0.0080	0.0090	0.0098	0.0104	0.011	0.012
^{154}Eu	0.0026	0.0050	0.0075	0.0089	0.0099	0.0106	0.0113	0.0122	0.013
^{155}Eu	0.0001	0.00021	0.00032	0.00040	0.00044	0.00048	0.00051	0.00055	0.00059
^{174}Lu	0.00023	0.00043	0.00064	0.00075	0.00084	0.00090	0.00095	0.00103	0.00110
^{101}Rh	0.00055	0.00105	0.00174	0.00208	0.00235	0.00256	0.00273	0.0030	0.0032
^{102m}Rh	0.00083	0.0016	0.0023	0.0027	0.0030	0.0032	0.0036	0.0038	0.0040
^{125}Sb	0.00090	0.0018	0.0027	0.0032	0.0035	0.0038	0.0040	0.0044	0.0047
^{238}Pu	7.0×10^{-8}	9.0×10^{-8}	1.1×10^{-7}	1.4×10^{-7}	1.5×10^{-7}	1.7×10^{-7}	1.8×10^{-7}	2.1×10^{-7}	2.4×10^{-7}
$^{239,240}Pu$	1.6×10^{-7}	2.0×10^{-7}	2.7×10^{-7}	3.5×10^{-7}	4.0×10^{-7}	4.4×10^{-7}	4.6×10^{-7}	5.1×10^{-7}	5.6×10^{-7}

The factors for 11 radionuclides in Table B–1 were obtained from those given in Tables 1 and 2 of Beck (1980) and reproduced in Table B–2. Beck calculated conversion factors for various values of the relaxation length in g/cm^2; these values were converted into inverse relaxation lengths by dividing them into the soil density ρ, assumed to be 1.5 g/cm^3. Plots of conversion factor versus log α are nearly linear over the range of α values in Table B–2. Values of the conversion factors for the nine α values in Table B–1 were therefore obtained by interpolating and extrapolating from such plots.

TABLE B–2. CONVERSION FACTORS (μR/h per nCi/m²) FROM BECK (1980)

Nuclide	relaxation length (g/cm²) [inverse relaxation length (1/cm)][1] 1.6 [0.9375]	4.8 [0.3125]	16 [0.09375]
^{241}Am	0.000197	0.000136	0.0000710
^{60}Co	0.0254	0.0179	0.00992
^{134}Cs	0.0168	0.0118	0.00636
^{137}Cs	0.00615	0.00432	0.00231
^{152}Eu	0.0117	0.00817	0.00446
^{154}Eu	0.0127	0.00896	0.00488
^{155}Eu	0.000581	0.000397	0.000203
^{174}Lu	0.00109	0.000767	0.000416
^{101}Rh	0.00316	0.00212	0.00108
^{102m}Rh	0.00395	0.00272	0.00146
^{125}Sb	0.00461	0.00317	0.00169

[1]Calculated assuming a soil density of 1.5 g/cm³.

Conversion factors for ^{133}Ba and plutonium are not given in Beck (1980). These factors were calculated as follows.

1. The energy and branching intensity of the gamma rays given off during the decay of each radionuclide were obtained from ICRP Publication 38 (International Commission on Radiological Protection, 1983). These values are shown in Table B–3. The gamma rays emitted by ^{240}Pu and other gamma rays of lower energy or branching intensity emitted by ^{239}Pu were judged to be insignificant and were omitted from the calculations.

2. Table 7 of Beck *et al.* (1972) gives exposure rates for various values of α/ρ and source energy, for a source strength of 1 gamma ray/cm²–sec. The α/ρ values used in that table were multiplied by $\rho = 1.5$ g/cm³ to give α values. The exposure rate was then plotted as a function of source energy for each of four values of α (Figure B–1).

3. For the energy of each gamma ray listed in Table B–3, linear interpolation and extrapolation from Figure B–1 were used to find the exposure rate at the four values of α. Figure B–2 shows a plot of the resulting values for ^{238}Pu. The exposure rates for the nine α values of interest were then obtained by linear interpolation and extrapolation from these four values. For example, at $\alpha = 0.5$/cm, the 43–keV gamma ray gives an exposure rate of 0.073 μR/hr, while the 100–keV gamma ray gives 0.22 μR/hr.

TABLE B–3. ENERGY AND BRANCHING INTENSITY OF GAMMA RAYS

Nuclide	Energy (keV)	Branching Intensity (1/Bq•sec)
^{133}Ba	53.15	0.0217
	79.62	0.0256
	81.00	0.338
	160.6	0.00615
	223.2	0.00460
	276.4	0.0709
	302.9	0.184
	356.0	0.621
	383.9	0.0891
^{238}Pu	43.48	0.000389
	99.86	0.0000747
^{239}Pu	38.69	0.0000586
	51.62	0.000208
	98.81	0.0000130
	129.3	0.0000620
	203.5	0.00000560
	332.8	0.00000505
	345.0	0.00000561
	375.0	0.0000158
	380.2	0.00000307
	382.7	0.00000260
	393.1	0.00000444
	413.7	0.0000151
	451.4	0.00000192

4. For each value of α, the conversion factor for each gamma ray was computed from the exposure rate and the branching intensity B by the formula

   conversion factor = exposure rate x B x 3.7×10^{-3}.

   The constant 3.7×10^{-3} has units of Bq•m^2•sec/nCi, so the conversion factor has units of (μR/hr)/(nCi/m^2).

5. The conversion factor for each radionuclide was obtained by adding the factors for the individual gamma rays. Thus for ^{238}Pu with α = 0.5/cm,

$$\begin{aligned} \text{43keV:} \quad & 0.073 \times .000389 \times 3.7\times10^{-3} && = 1.05 \times 10^{-7} \\ \text{100 keV:} \quad & 0.22 \times .0000747 \times 3.7\times10^{-3} && = \underline{0.61 \times 10^{-7}} \\ & && \text{Total} = 1.66 \times 10^{-7} \end{aligned}$$

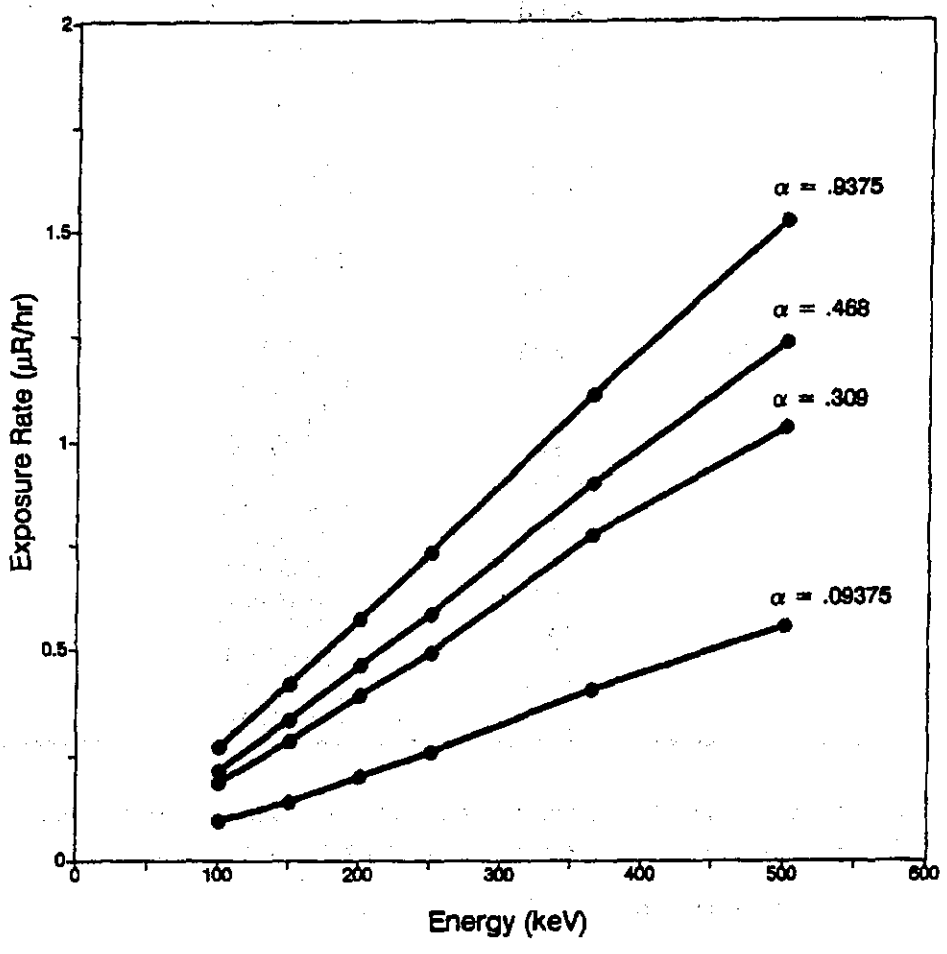

Figure B–1. Exposure rate as a function of energy for different depth distributions (data from Beck *et al.*, 1972).

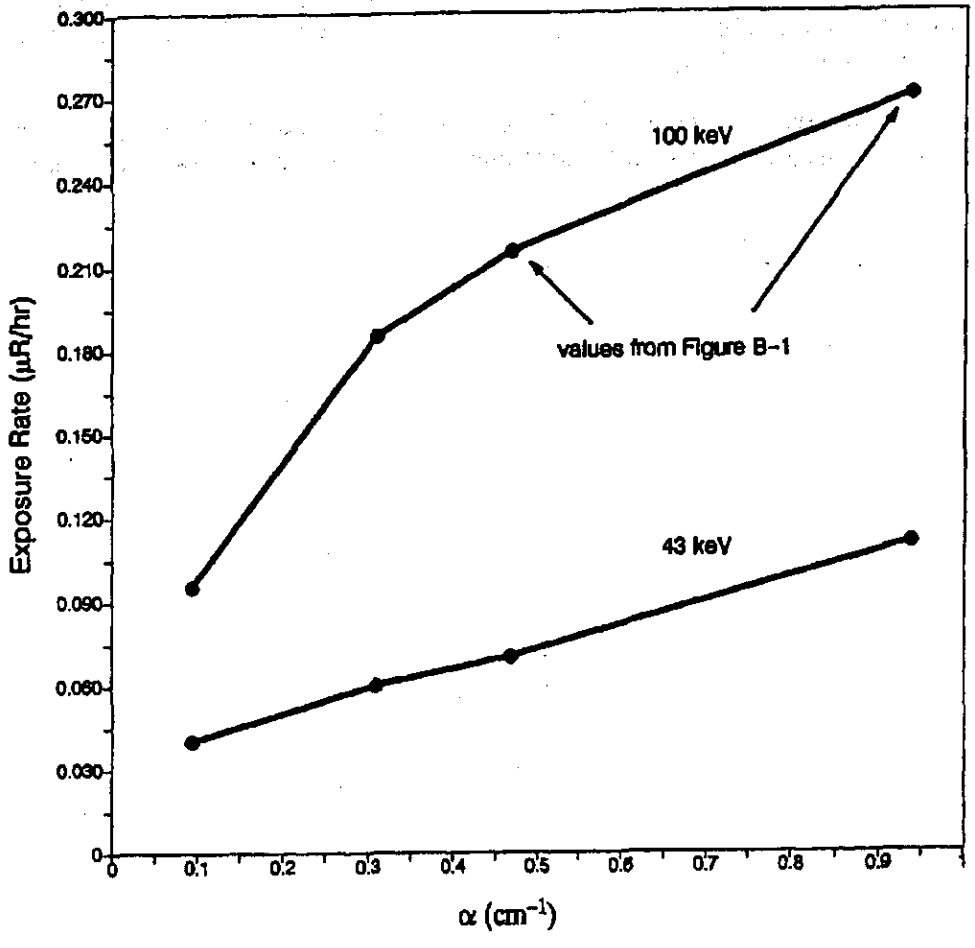

Figure B–2. Exposure rate as a function of α for ^{238}Pu gamma rays.

REFERENCES

Beck, H. L. 1980. Exposure rate conversion factors for radionuclides deposited on the ground. EML-378, Environmental Measurements Laboratory, U.S. Department of Energy, New York, N.Y.

Beck, H. L., J. Decampo, and C. Gogolak. 1972. *In situ* Ge(Li) and NaI(Tl) gamma-ray spectrometry. HASL-258, Health and Safety Laboratory, U.S. Atomic Energy Commission, New York, N.Y.

International Commission on Radiological Protection. 1983. *Radionuclide Transformations: Energy and Intensity of Emissions.* ICRP Publication 38, Pergamon Press, New York.

APPENDIX C
CORRECTIONS TO PREVIOUS REPORTS

Report 3

In Table 5 on p. 21, the inventory of ^{90}Sr in Region BA-2 (Baneberry) was given incorrectly as 0.4 Ci. The correct value is 4.0 Ci.

Report 4

a. The labels on the Johnie Boy results in Table 7, p. 43, were switched. Table C-1 below is a corrected version of Table 7.

b. In Appendix A, the Nevada Grid Coordinates of the soil samples at the Little Feller II site are wrong. The right values, as obtained from the NAEG database, are given below.

	Coordinates	
Point	East	North
43	606117	862204
44	606342	862329
45	606167	862509
46	606042	862664
47	605941	862581
48	605852	862769
49	605867	862819
50	605667	862939
51	605797	863169

Earlier results for these samples were reported in Essington (1985).

Figure C-1 shows the true locations of the soil samples and the *in situ* measurements at Little Feller II. This figure is a revision of part of Figure 33 in Report 4.

Use of incorrect locations for the soil profiles resulted in inappropriate values of the inverse relaxation length being chosen for the GAMANAL analysis of the *in situ* measurements. Figure C-1 shows that seven of the nine profiles were from inside the GZ region and two were from outside. The averages of the calculated inverse relaxation lengths (from Table 5, Report 4) for the two most important radionuclides in each region are as follows:

	^{241}Am	^{137}Cs
inside GZ region	0.51/cm	0.55/cm
outside GZ region	0.11/cm	0.05/cm

The values used in the GAMANAL analysis were just the opposite: 0.1/cm for points in the GZ region and 0.5/cm for points outside.

Therefore, the concentrations of ^{241}Am and ^{137}Cs were recalculated using inverse relaxation lengths of 0.5/cm for the GZ region and 0.1/cm for the outside region. The general effect of this correction was to decrease the computed concentrations in the GZ region and increase those outside. The corrected values are plotted along with hand-drawn concentration isopleths in Figures C-2 and C-3.

Corrected inventory estimates are included in Table C-1, a revision of Table 7 in Report 4. The estimated ^{137}Cs inventory is essentially unchanged; the estimated ^{241}Am inventory, however, decreases by about a factor of three.

REFERENCES

Essington, E.H. 1985. Progress of soil radionuclide distribution studies for the Nevada Applied Ecology Group. In Howard, W.A., P.B. Dunaway, and R.G. Fuller, eds., *The Radioecology of Transuranics and Other Radionuclides in Desert Ecosystems*. NVO-224, U.S. Department of Energy, Nevada Operations Office, Las Vegas, pp. 145-184.

TABLE C–1. INVENTORY ESTIMATES FOR AREA 18

Region	Area ($ft^2 \times 10^6$)	Radionuclide Inventory ± Sampling S.D. (CI)			
		^{241}Am	^{238}Pu	$^{239,240}Pu$	^{60}Co
Little Feller I					
GZ area	5.76	5.2 ± 1.9	.57 ± .21	29. ± 11.	.29 ± .16*
N of GZ	10.	.83	.091	4.6	.011*
Little Feller II	9.36	4.7 ± 1.4	.56 ± .17	27. ± 8.1	.034 ± .0027*
Johnie Boy					
GZ area	32.	.35 ± .025*	.67 ± .048	3.9 ± .28	.50 ± .092
N of GZ	79.	.61 ± .029*	1.2 ± .055	6.7 ± .32	.26 ± .015*
Danny Boy	24.64	6.6 ± 1.3	.79 ± .16	26. ± 5.2	.20 ± .037
Total	160.76	18. ± 2.7	3.9 ± .32	97. ± 15.	1.3 ± .19

TABLE C–1. INVENTORY ESTIMATES FOR AREA 18–Continued

Region	Radionuclide Inventory ± Sampling S.D. (CI)				
	^{137}Cs	^{90}Sr	^{152}Eu	^{154}Eu	^{155}Eu
Little Feller I					
GZ area	.12 ± .018	.22 ± .032	.039 ± .0041*	.024 ± .0026*	.058 ± .0066*
N of GZ	.15	.27	.046*	.033*	.079*
Little Feller II	.29 ± .030	.58 ± .060	.10 ± .0078*	.10 ± .0088*	.11 ± .0077*
Johnie Boy					
GZ area	1.0 ± .10	5.2 ± .52	.78 ± .091	.41 ± .027	.35 ± .020
N of GZ	1.1 ± .071	5.7 ± .37	.60 ± .036*	.64 ± .035*	.58 ± .024*
Danny Boy	2.3 ± .29	1.4 ± .18	.53 ± .073	.13 ± .010	.27 ± .019*
Total	5.0 ± .32	13. ± .67	2.1 ± .12	1.3 ± .046	1.4 ± .038

*These estimates are based largely on upper limit values.

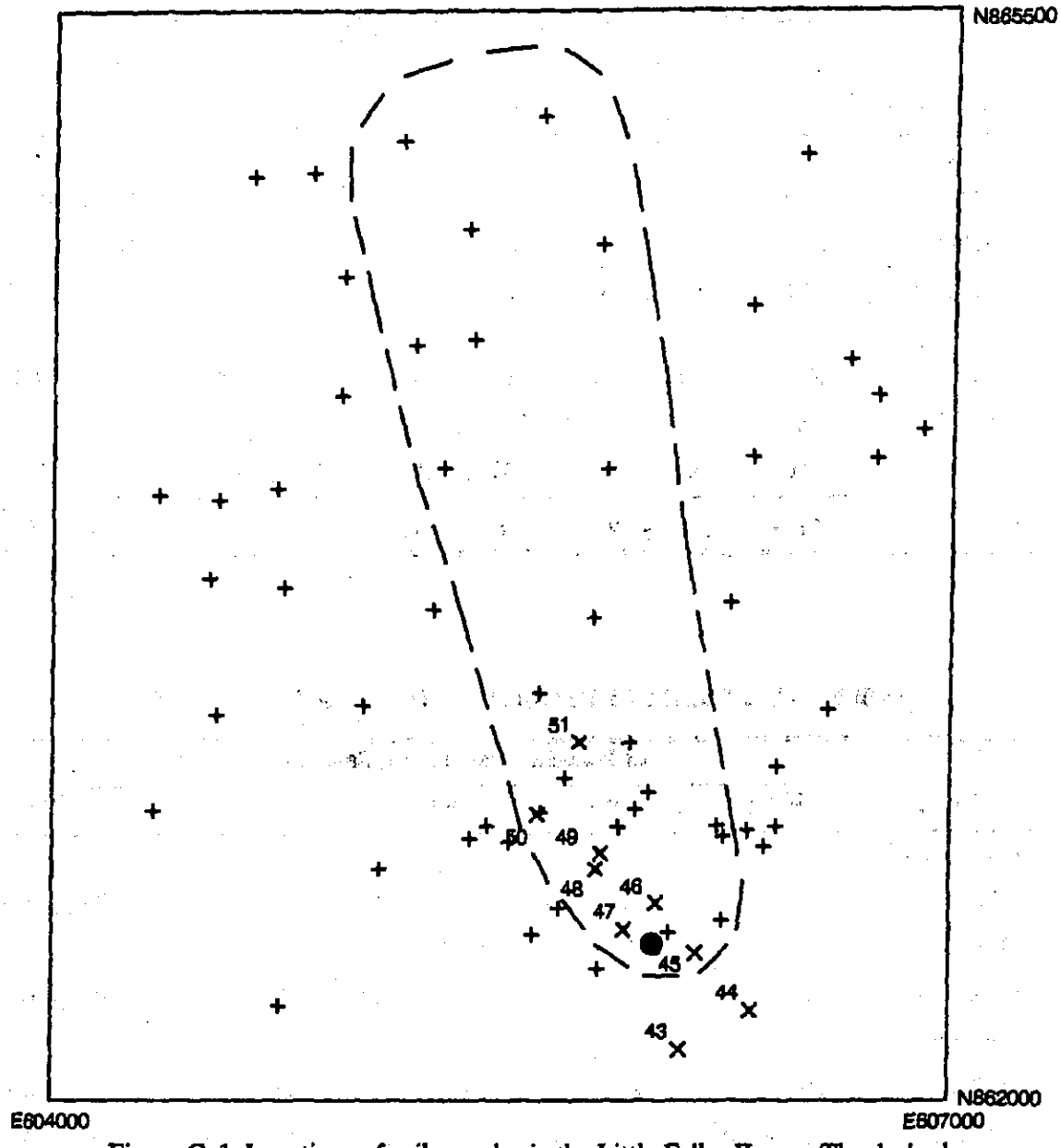

Figure C–1. Locations of soil samples in the Little Feller II area. The dashed line encloses the GZ region defined for choosing inverse relaxation lengths.

+ location of *in situ* measurement

× location of soil sample

● ground zero

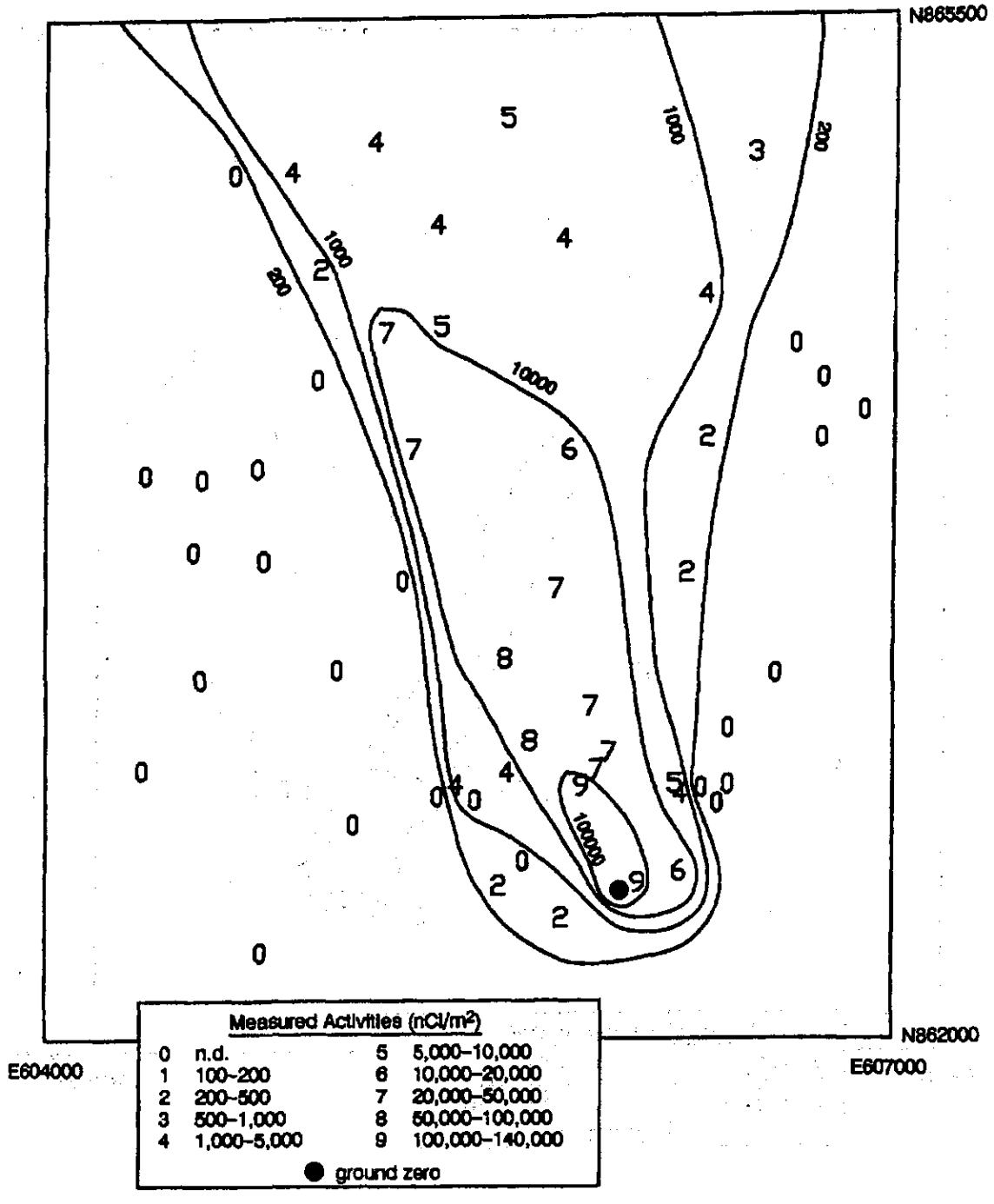

Figure C-2. Activity of ^{241}Am in the Little Feller II area.

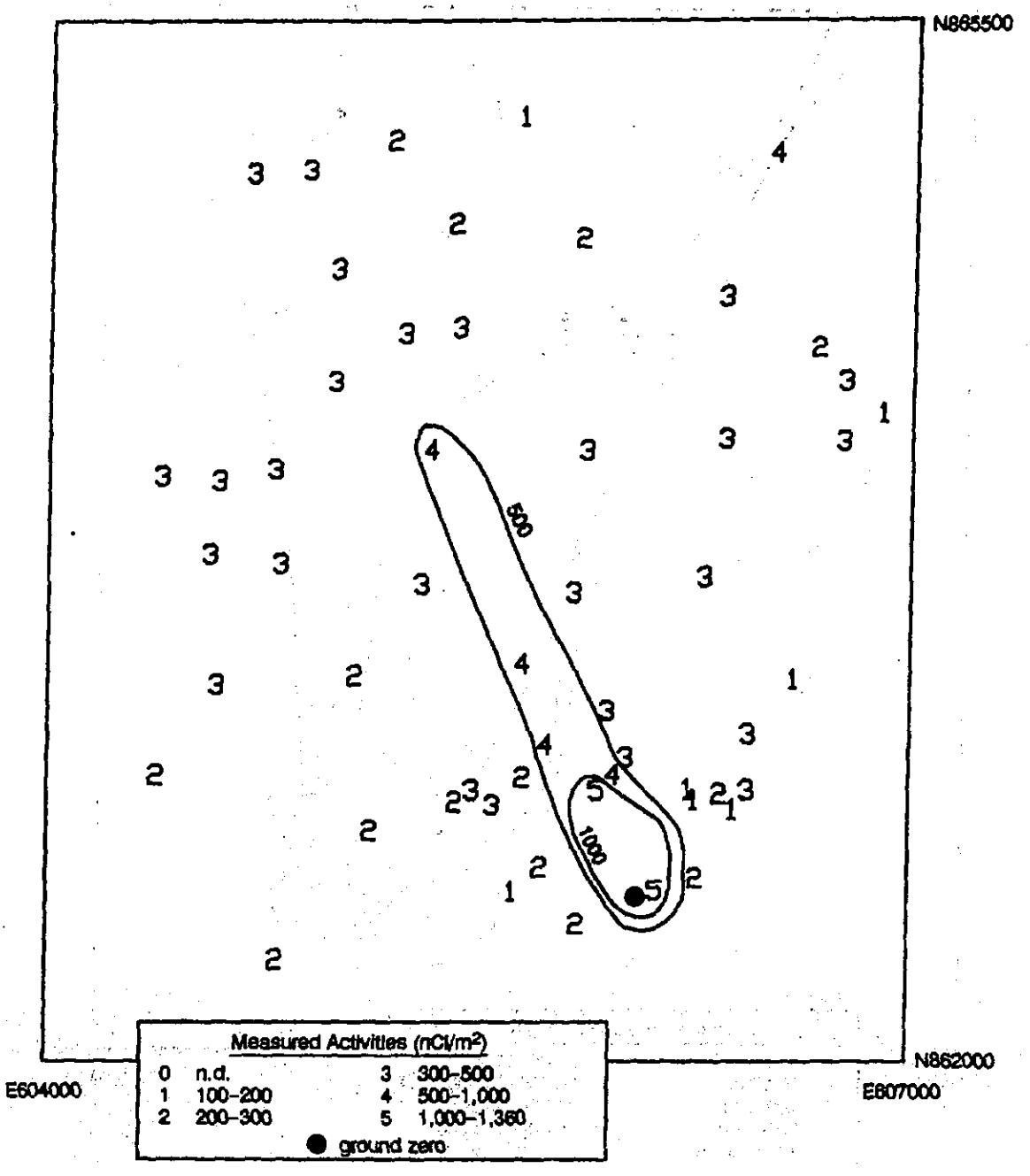

Figure C–3. Activity of ^{137}Cs in the Little Feller II area.

Data Capture
Document Discovery

(This form will be used in recording information in the Site Research Database after the document is scanned)

Reviewers – fill out all information that applies to the document then place list in front of the document

Name: Gene Rollin

Site/Facility of Data Capture: NTS Date: 11/06/03

Site/Facility Box Number: NA Accession Number: NA

Site That Document Applies To:

DOE Site(s) √

Name(s): Nevada Test Site

AWE Site(s) ☐

Name(s):_____

_____

Other: _____

_____

☐ Use document title clearly written on document

√ Document Title & Comments:_

Radionuclides in Surface Soil at the NTS

Document Type:

☐ **Diagnostic X-rays/Medical Information** (i.e. occupational medical dose, exam frequencies, equipment performance characteristics)

√ **Environmental Data** (i.e. ambient radiation, in-site releases, on-site radionuclide concentrations)

☐ **Facilities/Processes** (i.e.; source terms, contamination surveys, general area/breathing zone air sampling, area radiation surveys, radon/thoron monitoring, fixed location dosimeters, missed dose information, radiological control limits, Radiation Work Permits, incidents/accidents))

☐ **External Dosimetry** (i.e.; Thermoluminescent Dosimeters (TLDs), film badges, Pocket Ion Chambers, analytical methods, exchange frequency, detection limits, record keeping practices, codes, performance characteristics)

☐ **Internal Dosimetry** (i.e.; urinalysis, fecal, In-Vivo, breath sampling, radon/thoron, nasal smears, analytical methods, exchange frequency, detection limits, record keeping practices, codes, performance characteristics)

☐ **Claimant Specific Document**

Keyword(s): *Check the Key Words on the Back of this Form*

Rev. 02

Site Database/Data Capture
Key Words List

☐ **External Dosimetry**
- ☐ criticality beta dose
- ☐ detection limit
- ☐ exchange frequency
- ☐ film badge
- ☐ personnel information
- ☐ pocket ionization chamber (PIC)
- ☐ TLD

☐ **Medical X-rays**
- ☐ photofluorography
- ☐ X-ray

☐ **Internal Dosimetry**
- ☐ bioassay
- ☐ detection limit
- ☐ intake
- ☐ in vitro
- ☐ urinalysis
- ☐ whole body count (WBC)
- ☐ fecal

☐ **Incident/Accident Reports**
- ☐ criticality

☐ **Workplace Monitoring Data**
- ☐ Radiological Survey

Radionuclide(s)
- √ Americium
- ☐ Californium
- √ Cesium
- √ Cobalt
- ☐ Iodine
- ☐ Radon
- ☐ Radium
- ☐ Strontium
- ☐ Plutonium
- ☐ Technetium
- ☐ Thorium
- ☐ Tritium (H-3)
- ☐ Uranium
- ☐ _____
- ☐ _____
- ☐ _____

Other Key Words
- ☐ containment
- ☐ dose
- ☐ lower limit of detection (LLD)
- ☐ minimum detectable activity (MDA)
- ☐ photon
- ☐ remediation
- ☐ solubility
- ☐ uncertainty analysis

√ **Environmental Monitoring**
- ☐ dispersion model
- ☐ dust sample

Attachment 24:

Rodgers, John, et. al. Performance Evaluation of LANL Environmental Radiological Air Monitoring Inlets at High Wind Velocities Associated with Resuspension. Los Alamos National Laboratory, LA-UR-00-3091.

LA-UR-00-3091

Approved for public release; distribution is unlimited.

Title: **Performance Evaluation of LANL Environmental Radiological Air Monitoring Inlets At High Wind Velocities Associated with Resuspension**

Author(s): John Rodgers (PI), Piotr Wasiolek, Jeff Whicker, ESH-4
Craig Eberhart, ESH-17
Keith Saxton, David Chandler, Washington State University/USDA, Pullman, WA

Submitted to: FINAL REPORT for TDEA committee

Los Alamos
NATIONAL LABORATORY

I. Introduction

Environmental air monitoring for radioactive particles is a vital component of radiation workers protection during certain contaminated site remediation activities, and in similar circumstances such as may occur in nuclear accident response in the environment. Air monitoring is also an indispensable component of site perimeter monitoring for demonstrating compliance with the Clean Air Act regulations, and related concerns for spread on contamination by wind of federal facilities sites such as LANL.

Assessment of health risks associated with airborne aerosols implies that measurements be made defining the aerosol characteristics, concentrations and exposures that contribute to, or simply correlate with, adverse health effects. The application of sampling and analytical systems for aerosols must recognize that particles exist modally as size distributions generated by distinctively different source categories and having distinctly different chemistries. Two important reasons for making size-specific aerosol measurements are (a) to relate the in-situ aerosol size characteristics to the potential lung deposition sites, and thus toxicity, and (b) separation of the size distribution modes to identify sources, transformation processes or aerosol chemistry.

Environmental air monitors contain some combination of a sampling inlet through which an aerosol sample must be drawn, and an aerosol particle-collecting device inside of the monitor (e.g., air filter). The sampling inlet design, which may vary considerably depending on the air monitor application, determines the aerosol sampling efficiency. The inlet effectiveness (sampling efficiency) of a sampler, E_s, is defined as the ratio of the aerosol concentration for given particle size determined by sampling with the inlet under defined test condition, C_s, to the aerosol concentration determined with an isokinetic probe sampling the same test aerosol conditions (assumed to be the true aerosol concentration), C_0 (McFarland and Ortiz, 1982):

$$E_s = \frac{C_s}{C_0}, \qquad (1)$$

For example, the PM_{10} (particles with an aerodynamic diameter less than or equal to a nominal 10 micrometers) air quality standard for particulate matter is defined by the U.S. EPA (EPA 1999a) as 50 micrograms per cubic meter ($\mu g\ m^{-3}$) annual arithmetic mean concentration, and 150 $\mu g\ m^{-3}$ 24-hour average concentration measured in the ambient air. Only inlets fulfilling the performance parameters of PM_{10} samplers prescribed in EPA (1999b) in terms of their sampling efficiency can be used for measurements to demonstrate compliance with the standard. One such performance parameter is the particle size transmission characteristic (i.e., sampler effectiveness) of the sampler inlet for particles in the PM_{10} size range. Of particular importance is the particle size at which the sampler effectiveness is 50% (i.e., the DP_{50} particle size cutpoint). Another variable of sampler inlet performance is its collection efficiency as a function of wind speed. Wind speed can greatly influence collection of larger size particles, and deposition losses on inlet surfaces. For example, collection efficiency for the Andersen 321A PM_{10} inlet is shown in Figure 1 based on data by McFarland *et al.* (1984).

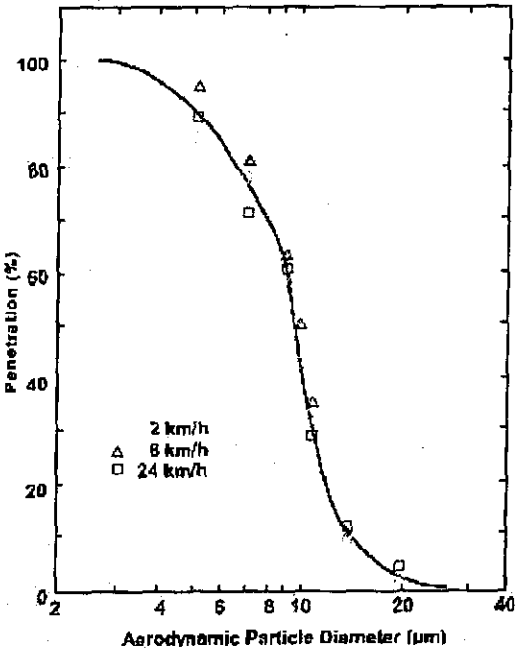

Figure 1. Collection performance (%penetration) versus aerodynamic diameter illustrating the influence of wind speed for the Andersen 321A PM_{10} inlet (adapted from McFarland et al. 1984).

In light of the dependency of inlet performance on particle size and wind speed, the sampling inlet is a critical element in every aerosol measuring system. Inlets must be designed with care, and their performance characteristics under ambient conditions understood. An ideal inlet should be designed such that all particles of interest (including toxic components that might be present), enter and arrive at the collecting zone, while excluding precipitation (rain and snow), insects, plant matter, and other debris (Liu and Pui, 1981). And most importantly, the desired performance characteristics (DP_{50} cut point, internal losses, etc.) of the inlet should be unaffected by wind speed up to the

design limit. Unfortunately, there can be a conflict between the need to protect sampler components from rain and debris, and the need to obtain a representative sample of the aerosol of interest under environmental wind conditions. This can lead to design compromises that balance component protection against sampling performance. Examples of inlet designs found in ambient air monitoring instruments include the simple weatherproof louvered housing design used in typical hi- vol monitoring stations such as the AIRNET stations operated on and off-site at LANL, a modified flat plate University of Minnesota Inhalable Particulate Matter (UM IPM) air sampling inlet design used with and without such protective housings for resuspension studies by ESH-4, and the more elaborate size-selective inlet design developed for the LANL/Canberra alpha Environmental Continuous Air Monitor (alpha-ECAM) to be deployed by the Accident Response Group (ARG). For a given inlet design, inlet efficiency E_s will be a function of particle size, wind speed, and sampling flow rate, and sometimes the orientation of the inlet with respect to the wind direction. High efficiency is easily achieved for particles having a small aerodynamic diameter (AD<2.5 μm). For larger particles and high wind speeds, good inlet efficiency can only be obtained by careful design (Liu and Pui, 1981).

The matter of what constitutes acceptable performance depends on the goals of the air monitoring application. The alpha-ECAM for ARG applications, for example, is designed to provide worker respiratory protection information on resuspended Pu contaminated soil particles during recovery operations. Thus its inlet is designed to have good performance for inhalable particles (AD≈15 μm) under a wide range of wind speeds. For resuspension monitors, the aim is to measure environmental levels of airborne radionuclides associated with wind-blown soil particles. These data can be used not only for detecting elevated air concentrations, but also to identify and control sources of migrating contaminants such as contaminated soil at the waste disposal sites. In the case of contaminant migration, particulate radioactivity that can be transported by wind is typically associated with soil particles having aerodynamic diameters (AD) ranging from sub-micron size up to 15 μm or 30 μm. Since particulate resuspension is a threshold phenomenon, not arising until wind speeds of 5–10 m s^{-1} have been achieved, the assessment of environmental inlet efficiency should be carried out under wind speed conditions in the range 5-15 m s^{-1} so that the combination of particle size and inlet

velocity conditions can be evaluated. Generating such test conditions is particularly challenging and not easily done in small wind tunnels. That may be why data on inlet efficiency of these types of environmental monitoring inlets at high wind speed is practically non-existent. The requirements for aerosol inlets performance evaluation, and basic factors that should be considered for such tests were analyzed by Mark *et al.* (1992). Their recommendation combined with the EPA procedures (EPA 1999b) were the basis for the test program of the commonly used inlets in the LANL under ambient air conditions. It was determined that a high-velocity, large cross-section aerosol wind tunnel was needed to meet the objectives of the test program.

II. Inlets' tested in the study

1. Open-face-inverted Inlet

Open-face-inverted inlets for atmospheric sampling consist of a simple filter holder operating face down, as shown in Fig. 2. These two particular filter holders (HI-Q model RVPH-102 or RVPH-25)[1], are for filters of 102-mm and 47-mm diameter, respectively. Both open-face inlets are operated at a flow rate of 113 L min^{-1}. Inverted inlets have been previously tested by the Southern Research Institute (SRI) (Bird *et al.*, 1973). Their DP_{50} efficiencies were found to be 39%, 30% and 20% for 5 μm AD particles at wind speeds of 2.6, 12.8 and 18.9 m s^{-1}, respectively. For 12-μm AD particles the DP_{50} efficiencies were 35%, 12%, and 35% at the same wind speeds. In this project the inverted inlets were used to established baseline performance in field test with uncharacterized ambient aerosols.

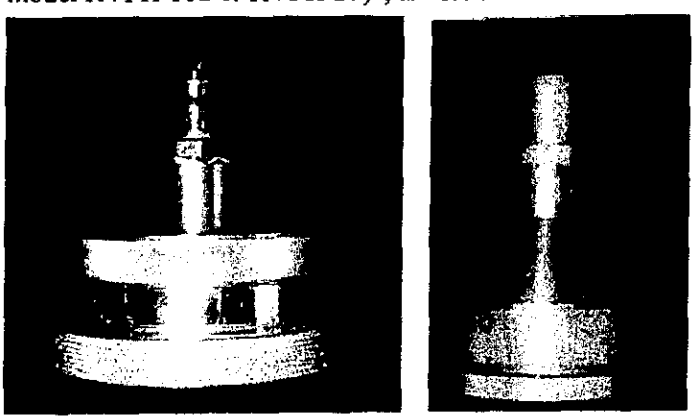

Figure 2. 102-mm and 47-mm filter holders as inverted open-face atmospheric aerosol samplers.

2. University of Minnesota (UM) IPM Inlet

To correct the deficiency of open-face inverted inlets in terms of their aspiration efficiency, Liu and Pui (1981) proposed a new, modified inlet capable of better performance under high wind conditions. This new Inhalable Particulate Matter (IPM) inlet has a flange (2.4-cm wide) surrounding the filter holder, and circular top to keep out rain and snow. This inlet was evaluated in a wind tunnel at various wind speeds up to 2.5 m s^{-1}. The aspiration efficiency of the inlet for 8.5- and 11-μm AD particles was about 100±10%. However, it was less (about 80%) for 13.4 μm AD particles at higher wind speed.

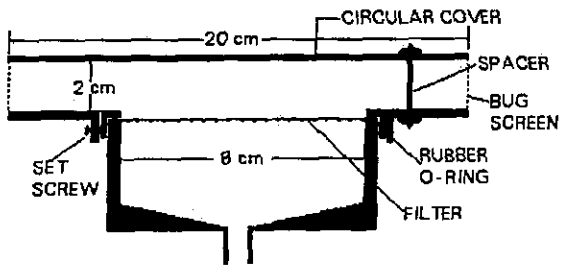

Figure 3. Schematic diagram of the LANL/CSU inlet based on design by Liu and Pui (1981)

The modified UM IPM filter was reproduced for the LANL/Colorado State University (CSU) collaborative project on airborne transport of contaminated soils via resuspension. The LANL/CSU inlet diagram and physical realization are presented in Figs. 3 and 4. The inlet uses a commercial 102-mm diameter filter holder (Hi-Q Model RVPH-102) with custom-made parallel plate flanges. The inlet slot is protected with a coarse metal anti-bug screen. The typical airflow rate use for this inlet is 113 L min^{-1}.

Figure 4. LANL/CSU inlet based on design by Lui and Pui (1981).

[1] HI-Q Environmental Products Company, 7386 Trade St, San Diego, CA 92121

3. AIRNET Air Sampling Station

For compliance purposes the LANL Air Quality Group (ESH-17) operates network of more than 50 environmental air stations (called AIRNET) to sample radionuclides in ambient air. A typical station is shown in Fig. 5 with its housing open for sample changeout. Each sampler is equipped with a pump and sample collectors located inside a 122-cm high x 61-cm deep x 76-cm wide (48"x 24"x30") weather housing with dual louvered openings on all four sides of the enclosure[2]. A polypropylene filter mounted in a filter holder is used to collect a particulate matter sample (for gross alpha/beta counting, gamma spectroscopy and radiochemical determinations). A silica gel cartridge in parallel with the filter is used to collect a water vapor sample for tritium determination. The oil-less pump generates a sample flow rate of about 113 L min^{-1} through the filter and 0.2 L min^{-1} through the cartridge inside the housing, which therefore is the inlet of this sampler (Fig 6). Instrumentation within the housing records the total time the pump ran during the sample period and the flow in the particle and the tritium sampling trains. With the recent heightened interest in the health effects of beryllium, some AIRNET filter samples are being analyzed for this contaminant as well as radioactivity.

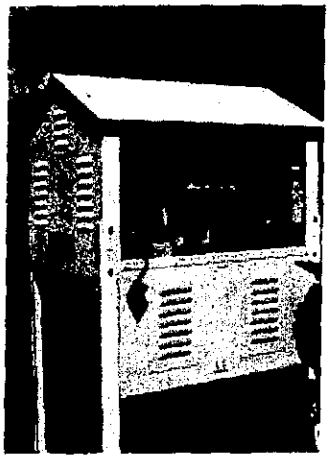

Figure 5. AIRNET Station

Figure 6. Interior of AIRNET station (visible filter holder, tritium cartridge and pump)

[2] SAIC RADeCO Model 210B; SAIC, Safety and Security Instruments 16701 West Bernardo Drive, San Diego, CA 92127

4. PM_{10} Graseby-Andersen Inlet

The PM_{10} Graseby-Andersen (G-A) inlet (Figs. 7 and 8) is part of the Graseby PM_{10} Medium Flow Air Sampler[3]. The sampler is designed and optimized to collect representative samples of particulates for gravimetric analysis. The sampler operates at a nominal flow rate of 113 L min^{-1}. Suspended particles in ambient air enter the inlet and then are accelerated through multiple impactor nozzles. Particles larger than 10 μm AD are separated from the rest by inertial effects as the accelerated jets are deflected in the lower plenum. The combine airflow flows down the vent tube to the filter, a 102-mm fiber-glass filter. The Graseby-Andersen (G-A) PM_{10} inlet was tested by McFarland and Ortiz (1982) in a large aerosol wind tunnel at Texas A&M University, with the results presented in Fig. 9. The G-A PM_{10} inlet design does meet the EPA PM_{10} cutpoint D_{50} of 10.0±0.5μm. The G-A PM_{10} inlet provides a useful reference-sampling inlet for the PM_{10} component in ambient air samples, and was used for that purpose in this project.

Figure 7. G-A PM10 inlet

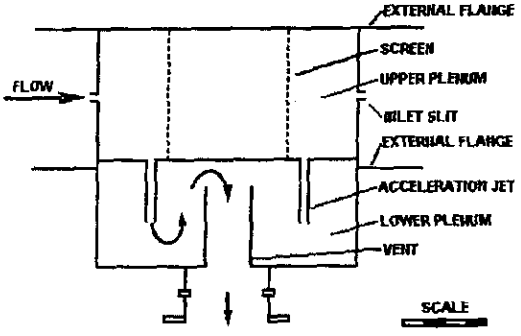

Figure 8. Schematic diagram of the G-A PM10 inlet

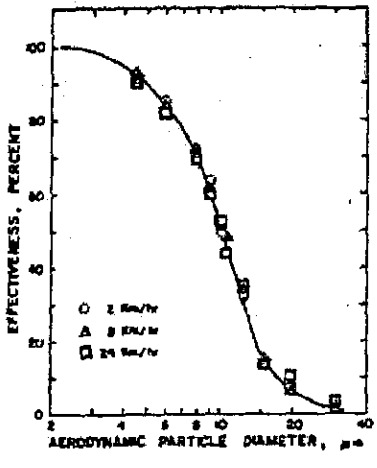

Figure 9. Effectiveness vs particle AD as a function of wind speed for the G-A PM10 inlet. Adapoted fromMcFarland and Ortiz (1982).

[3] Andersen Instruments, 500 Technology Court, Smyrna, GA 30082

5. ECAM Inlet

The Los Alamos Accident Response Group (ARG) program has, over the past several years, sponsored development of a new environmental continuous air monitor (ECAM) to provide radiological air monitoring for accident responders at the scene of an

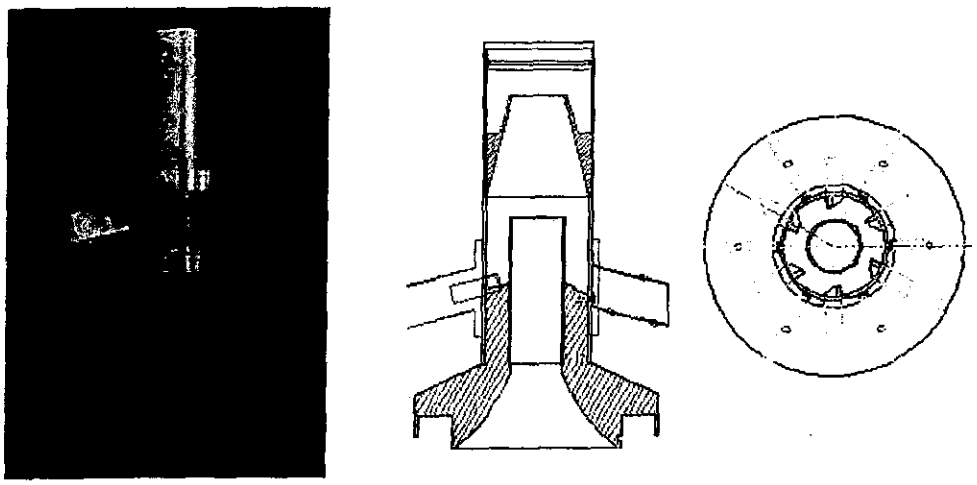

Figure 10. ECAM inlet

accident involving a nuclear weapon, no matter what the ambient conditions might be. The instrument design is based on the Laboratory-designed plutonium alpha-CAM (Canberra Industries Alpha Sentry CAM), with the addition of a special inlet, and on-board vacuum blower and data communication capabilities. The special inlet has been designed to meet several objectives: first, the inlet must be capable of maintaining excellent aerosol collection performance in high wind conditions; second, the inlet must be protected from precipitation to prevent damage to the detector and the filter; and third, the inlet should provide size-selective separation of particles in the sample such that the large particle components of ambient dusts are removed to help prevent sample burial and interference with the alpha-radiation detection process. To achieve good inlet performance in high wind as well as calm, the design must decelerate the airflow as it enters the inlet without at the same time introducing distortions in the particle size distribution present in the free stream. This is accomplished by and omni-directional array of six modified shrouded probes making up the inlet. As seen in Figure 10, the nozzles of the probes are recessed inside shroud cells, which provide the needed

deceleration as airflow impinges on the inlet, and also provides protection from rain. The shrouded probe concept has been shown to provide excellent aerosol transmission efficiency regardless of velocity and particle size. Each of the six nozzles discharges into the base of an inverted cyclone. The cyclone design parameters as such that the 50% transmission cut point is at 10-μm aerodynamic diameter. Note in the cross-section drawing that there is a small conical trap at the top of the cyclone that is meant to capture large particles removed from the sample by the induced cyclonic flow. The exact configuration of the trap was still under development at the time of these tests, and a temporary design was installed for evaluation. The output of the inlet passes out of the base through the cyclone outlet tube down into the CAM head attached below.

III. Methods

A. Field Testing

The initial filed test of relative collection efficiencies of selected inlets was performed in the vicinity of the 46-m meteorological tower at the LANL TA-54 site.

Site Description

The TA-54 station is located in a clearing just off the eastern tip of Mesita del Buey on the Pajarito Plateau at longitude of 106° 13' 22.1", latitude 35° 49' 32.8" and elevation of 1996.3 m (6548 ft) above sea level. The terrain drops 15 m into Canada del Buey to the north and drops 10 m into Pajarito Canyon to the south. To the east-southeast, the terrain drops gently about 75 m to the eastern edge of White Rock Canyon. The station is shown in Fig. 12 looking southeast toward the residential area of White Rock. The eastern escarpment of White Rock Canyon can be seen near the top of the photo. The photograph presents the site during construction of the meteorological tower. Since then,

Figure 12. Bird view of the TA-54 site.

the natural vegetation has returned to the area around the tower. Beyond the clearing, pinion and juniper trees of several meters height cover a most of the surrounding area. The plateau tilts at about 1.5 degrees to the east-southeast in the vicinity of this station.

During the test period (March 2

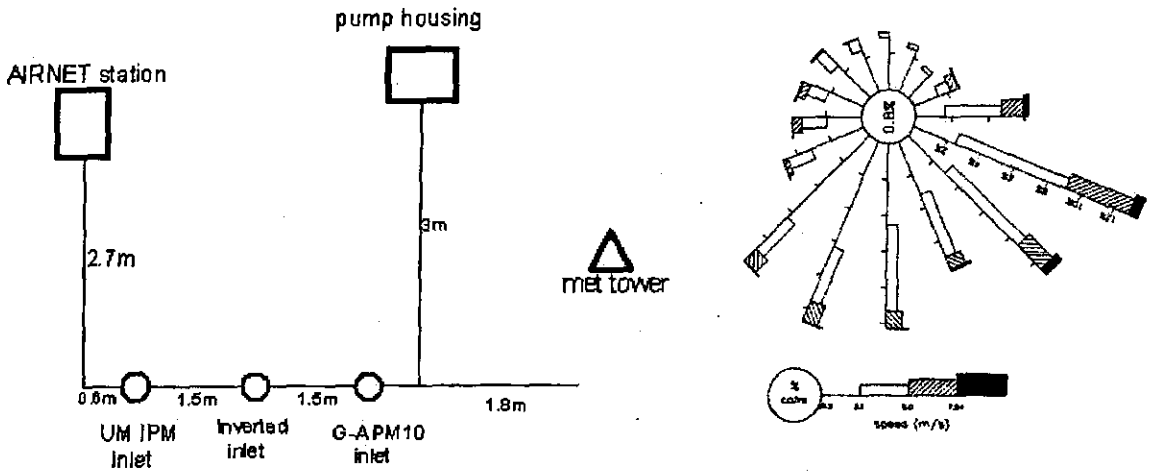

Figure 13. Plain view of the test site and the wind rose for test period

- May 4, 2000) the average wind speed at the site was 3 m s^{-1} with gusts up to 17 m s^{-1}, and total precipitation 43.2 mm. The wind conditions during each test are listed in Table 3 and Fig 13. The schematic diagram of the site is presented in Fig. 13 and actual view of the test site in Fig. 14.

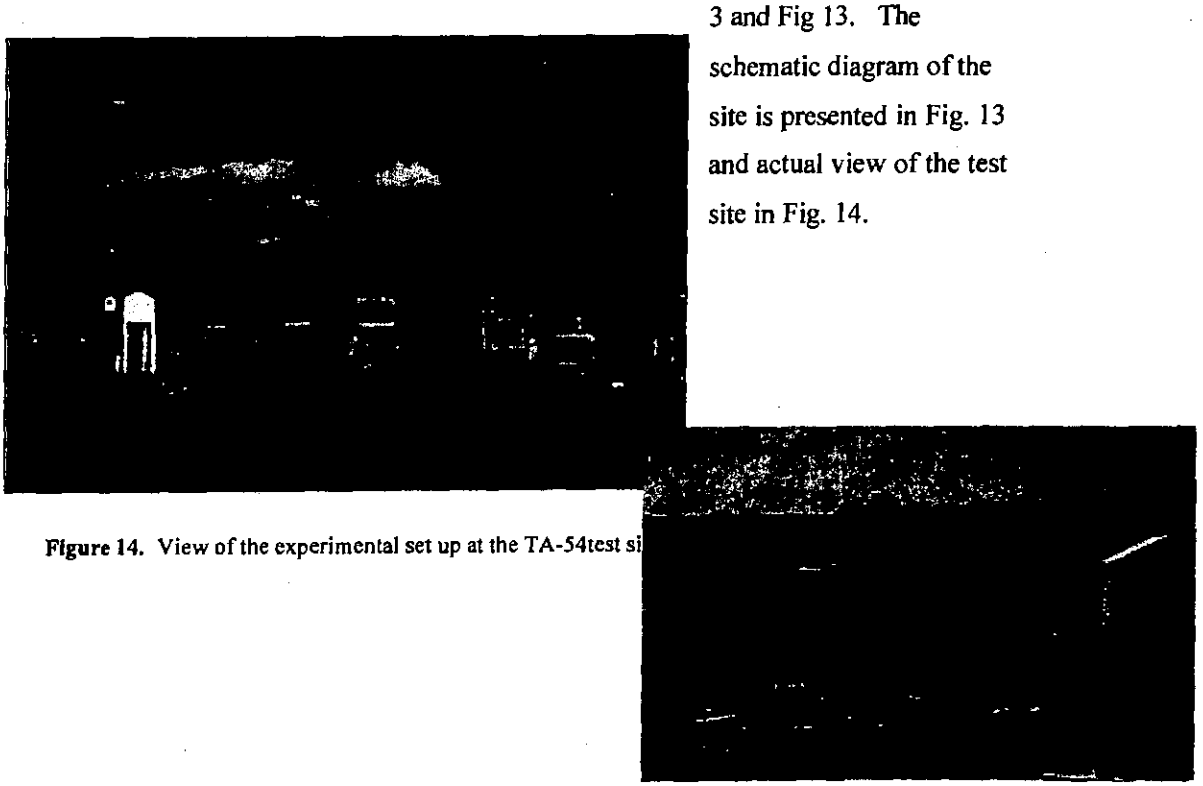

Figure 14. View of the experimental set up at the TA-54test si

designed to compare inlet efficiencies of the several types for ambient aerosols relative to each other. No reference sample was collected as a basis for comparison. Several configurations of inlets were tested for three one-week-long sampling periods. The first arrangement consisted of the UM IPM, the inverted 102-mm and AIRNE-station inlets (Fig. 15). In the next configuration the 102-mm inverted inlet was replaced with a 47-mm inverted inlet equipped with the filter type routinely used by ESH-17 in the AIRNET-station (Fig 16). To establish comparison against the PM_{10} standard, the G-A PM_{10} inlet replaced the inverted one (Fig. 17). The UM IPM and G-A inlets were operated using 102-mm Gelman A/E filters. The filters were collected weekly using methodology specific for individual inlet.

A summary of operational parameters of all tested inlets are presented in Table 1.

Figure 17. G-A, UM IPM and AIRNET inlets

Table 1. Operational parameters of tested inlets

Inlet	Filter type	Nominal Flowrate L min^{-1} (cfm)
UM IPM	102-mm Gelman[4] A/E (glass fiber)	113 (4)
102-mm Inverted	102-mm Gelman A/E	113 (4)
47-mm Inverted	47-mm Gelman A/E & Dynatech polypropylene	85 (3)
G-A inlet	102-mm Gelman A/E	113 (4)
AIRNET station	47-mm Dynatech polypropylene	113 (4)

Airflow to any two of the inverted, UM IPM, and G-A inlets, when operational, was provided from a single high capacity oil-less vacuum pump located in a separate housing (see Fig.14). AIRNET-station airflow was provided from a built-in oil-less pump with exhaust to the outside. For consistency and to avoid additional biases, the actual flow rate to all samplers was measured at the beginning and at the end of sampling period with the same, calibrated flow meter[5]. After approximately 170 h of sampling and after 24-h delay for humidity equilibration, filters were analyzed gravimetrically on calibrated balances with precision of 0.001g. AIRNET-type filters were analyzed by New Mexico Department of Health Scientific Laboratory Division Air & Heavy Metals Section. Filters from UM IPM, Inverted, and G-A inlets were analyzed in LANL ESH-4 HPAL facilities using ANSI traceable Mettler Precision Balance PM1200[6]. Duration of sampling in hours was taken from a timer built into AIRNET station. Meteorological conditions: average wind speed, maximum gust, and soil moisture for the test, were obtained from an automatic data logging station operated by ESH-17. The average weekly mass concentration C, was calculated as,

$$C\ (\mu g\ m^{-3}) = \frac{(Wg - Wt)}{V_a \times \Delta Time}, \qquad (2)$$

where, Wt and Wg is the tare and gross weight of the filter in grams, V_a is the actual volumetric flow rate in $m^3\ min^{-1}$ calculated as an average of the flow rates measured at the beginning and at the end of sampling, and ?Time is elapsed time in minutes.

[4] Gelman Sciences, 600 South Wagner Road, Ann Arbor, MI 48103
[5] SAIC RADeCO Model C-828 S/N 1909
[6] Mettler-Toledo, Inc. 1900 Polaris Parkway Columbus, Ohio 43240

B. High Velocity Aerosol Wind Tunnel Testing

Wind tunnel setup

A high velocity portable wind tunnel (Fig 18) was used in the study for inlet testing. The tunnel was designed and built at the USDA/ARS Palouse Conservation Field Station near Pullman, WA (Pietersma *et al.*, 1996) as part of a soil erosion project. It is 13.4 m long and has a working section 7.3 m long, 1.2 m high and 1.0 m wide. Power is supplied by a 33-kW gasoline industrial gas engine, which drives a 1.4-m industrial axial vane fan (Joy Series 1000 Model 54-26) (Fig 19). Variable-pitch blades and variable engine speed allow the wind speed to be set manually. Using 13 available engine speeds, the velocity can be adjusted from <2 to 20 m s^{-1}. There is a transition from the fan inlet height to the ground level (Fig. 20). Intensive flow conditioning is an option in this wind tunnel. Fan-induced turbulence and swirl can be eliminated using 2 perforated plates, a honeycomb and a small mesh screen spaced over a distance of about 2 m. For these tests however, flow conditioning was limited in orders to achieve the highest wind speeds.

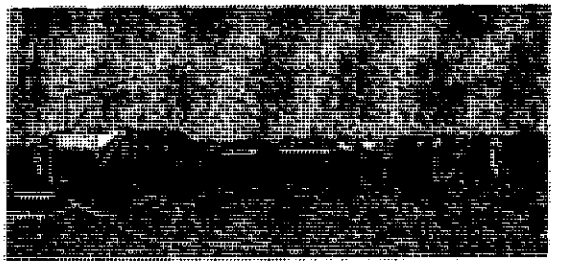

Figure 18. USDA/ARS portable wind tunnel adapted for inlet testing

Figure 19. Wind tunnel motor and axial vane fan

Figure 20. Tunnel transition to the ground level

Detailed flow profile information in the tunnel is obtained using a Pitot tube sensors arranged in a six by six array, oriented orthogonal to the flow near the tunnel outlet. Guidance on the degree of uniformity of the flow profile can be found in the 40CFR53.42 (US EPA 1999b): "... *The wind speed in the wind tunnel shall be determined during the tests using an appropriate technique capable of a precision of 5 percent or better (e.g., hot-wire anemometry). The mean wind speed in the test section of the wind tunnel during the tests shall be within 10 percent of the value specified in table D-2. The wind speed measured at any test point in the test section shall not differ by more than 10 percent from the mean wind speed in the test section....*". Even though these tests were not intended to generate data for an EPA certification, they were used as guidance.

Test aerosols were delivered to the tunnel upstream of the fan with offset-feed auger box (see Fig 21). The aerosol injection was done from six drop-tubes spread across the wind tunnel inlet (see Fig 19) to help in deagglomeration of the test particles, and to obtain uniform aerosol mixing in the air stream. Uniformity of the air velocity profile and aerosol concentration profile were good as shown in Fig. 22 and 23. The velocity profile was obtained at six heights and six locations across the tunnel at the test section. Aerosol profiles were taken in the center of the tunnel test section at 30, 60 and 90 cm above floor.

Figure 21. Offeset-feed auger box

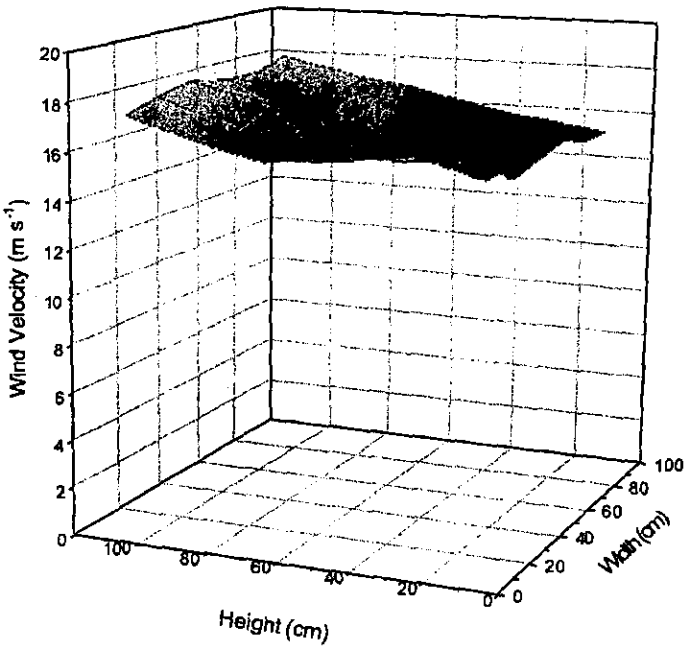

Figure 22. Velocity profile in the wind tunnel for u=17 m s^{-1}

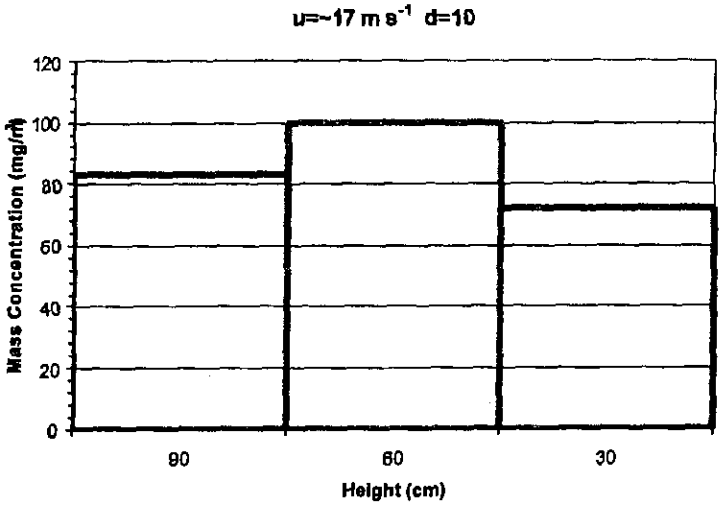

Figure 23. Center-line vertical aerosol concentration profile of 10 μm particles and at a wind speed of ~17 m s^{-1}

For the experiments the outlet of the tunnel was modified by building 3 m x 3 m extension to accommodate large samplers and to avoid excessive blockage. The design of the extension is shown schematically and as built in Fig. 24.

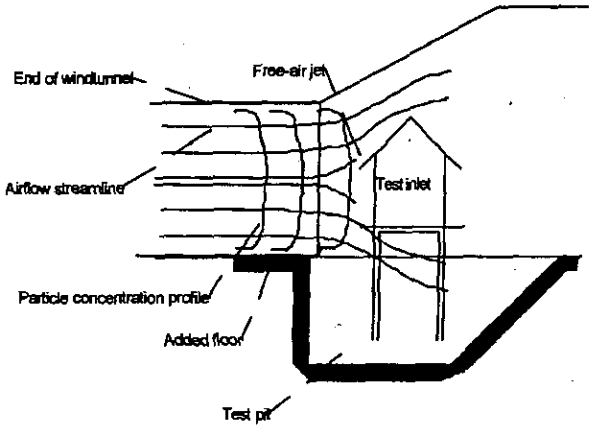

Figure 24. Tunnel extension for testing large inlets

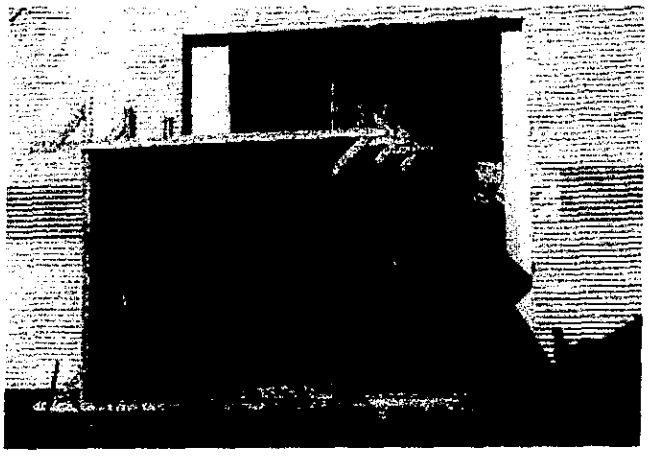

Test aerosols

To obtain values of sampler efficiency as a function of different size aerosol particles and wind speed conditions, large quantities of mono-disperse test particles were needed. Environmental impact considerations (the wind tunnel exhaust to the open environment without filtration) restricted the type of test aerosols for used in this evaluation to nontoxic, natural particles. As contaminated soil particles are of primary concern for the LANL, we decided to obtain test particles in the form of ground and size classified soils. A commercial particulate vendor[7] was identified and contracted to prepare 200 lb each of narrowly distributed (approximately 5-, 10-, and 30- μm) red kaolin clay soil particles. The system used for test particle preparation is shown in Fig. 25. Soil samples were grounded using the RSG "Ultra Fine Grinding" Mill (seen on the left) and classified with ASC air classifiers. The UFG mill introduced by RSG in 1999 is used to grind mineral samples as small as 2-μm particle diameter. To classify soil particles according to their aerodynamic sizes the RSG used their patented Advance Classification System (ACS).

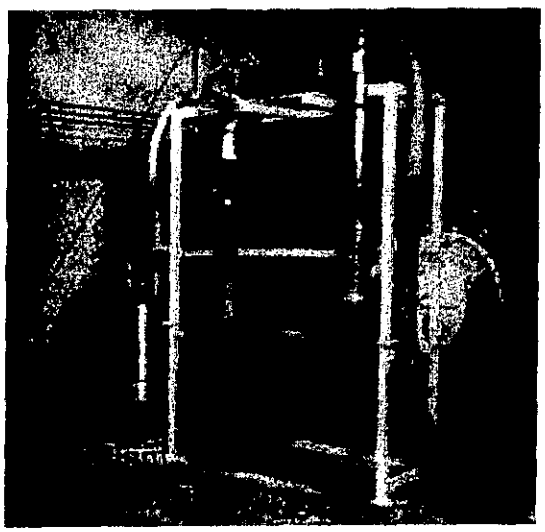

Figure 25. The RSG, Inc. system (UFG mill and ACS-005 air classifier) used in soil test particle preparation (courtesy of RSG. Inc)

The RSG, Inc. performed size analysis on each soil sample with their Microtrac X-100 system that uses tri-laser diffraction analysis[8]. The results of the analysis for 5-, 10-, and 30-μm soil particles are presented in Fig. 26.

[7] RSG, Inc.119 Crews Lane, Sylacauga, AL 35150
[8] Microtrac Inc. at 148 Keystone Drive, Montgomeryville, PA 18939

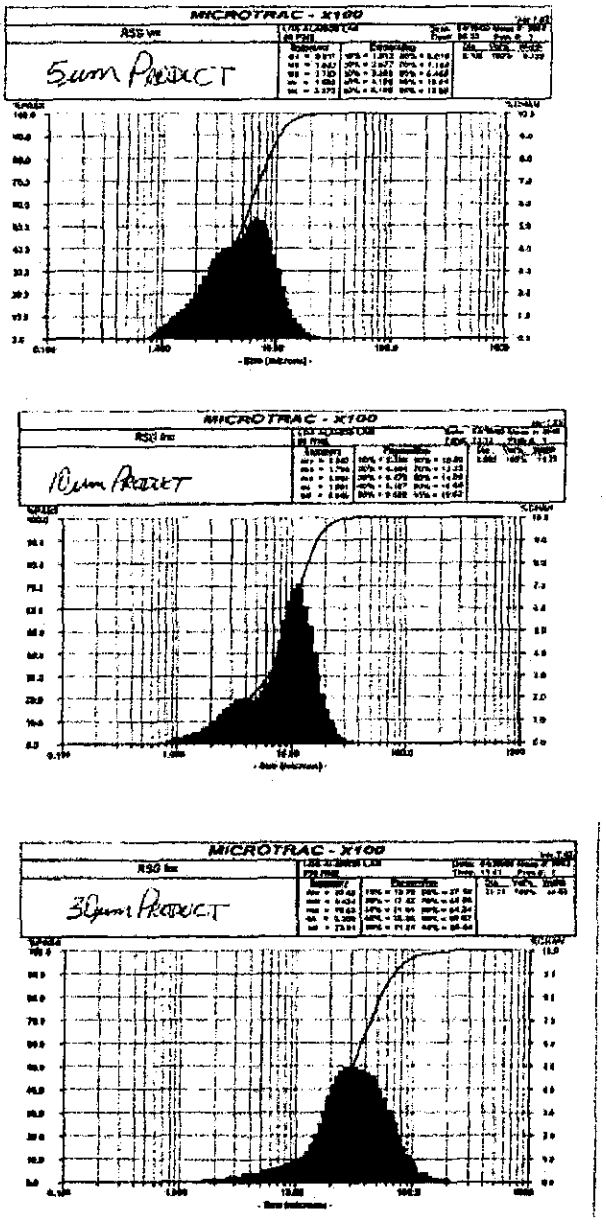

Figure 26. Results of Microtrac analysis of grinded soils samples used for inlet testing

Independent verification of the test soil particles size distribution was performed by Lovelace Respiratory Research Institute (LRRI) using API Aerosizer[9]. The Aerosizer is equipped with a dual laser beam optical sensor system for time-of-flight measurements and integral air flow control systems. Results of the analysis are presented in Fig. 27.

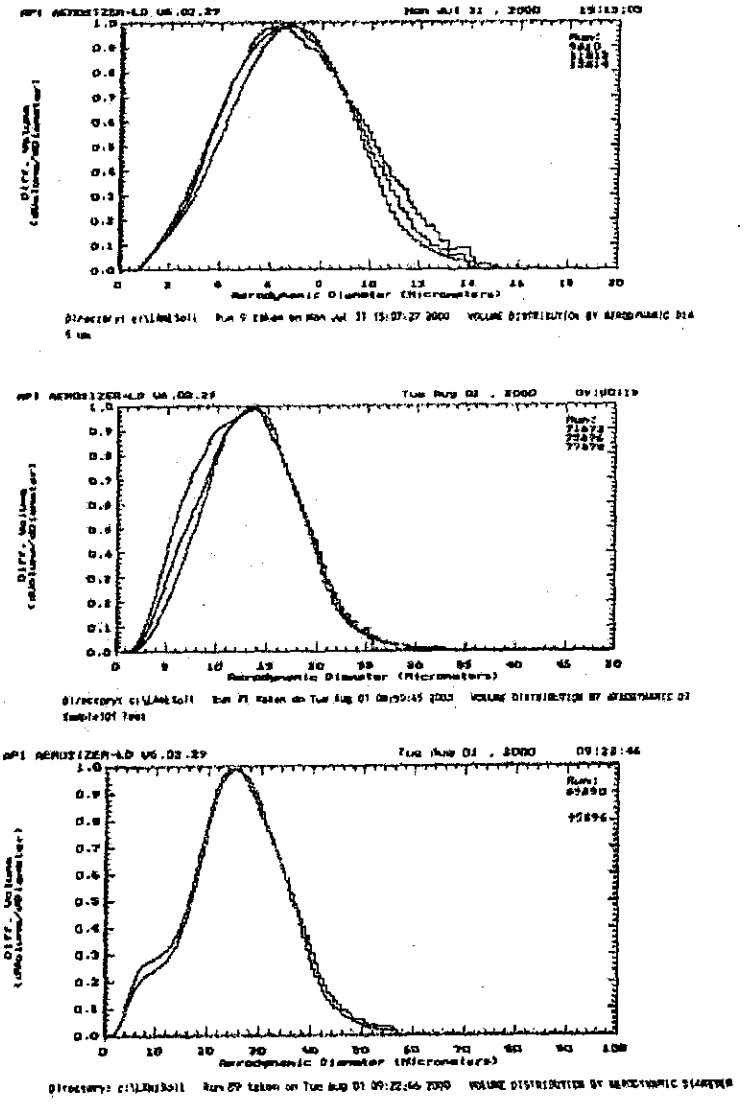

Figure. 27. Size distributions for 5, 10-, and 30-μm test soil particles measured with API Aerosizer.

[9] TSI Incorporated Particle Instruments Division/Amherst 7 Pomeroy Lane, Amherst, MA 01002-2905

Numerical results of the test soil particles aerosizing are presented in Table 2.

Table 2. Results of test soil particle analysis using API Aerosizer

Nominal Diameter (μm)	Volume Median Aerodynamic Diameter (μm)	GSD (μm)	Mean Diameter (μm)	Mean GSD (μm)
5	6.49	1.51		
	6.49	1.50		
	6.57	1.54		
			6.52	1.51
10	12.94	1.46		
	11.97	1.54		
	12.55	1.51		
			12.49	1.50
30	24.03	1.56		
	24.41	1.56		
	23.46	1.59		
			23.97	1.57

Comparing the results of the size distribution analysis carried with the Microtrac and API Aerosizer, some differences are noticeable, especially for larger particles. For the nominal size of 10-μm diameter, the Microtrac analysis yielded a diameter 26% smaller than the API Aerosizer results. For the nominal size of 30-μm, the Microtrac overestimated the size by 36%. These differences could be attributed to different measuring techniques: light scattering versus time-of-flight, and are indication of difficulties in aerosol size distribution measurements. The light scatter techniques used in the Microtrac instrument represents more closely the physical diameter (PD) of the aerosol particles, whereas the API Aerosizer measures aerodynamic diameter (AD). These two are related via Equation 2:

$$\frac{AD}{PD} = \sqrt{\frac{\rho_p}{\rho_w}} \qquad (2)$$

where ?$_p$ is the density of test particles (soil, 2.3 g cm^{-3}) and ?$_w$ is the density of water I g cm^{-3}.

Shrouded Probe – Reference Sampler

In order to determine the effectiveness of each inlet tested in the aerosol wind tunnel it was necessary to obtain an unbiased reference sample of the test aerosols. It was essential that this sample be collected rapidly and accurately regardless of the particle size being generated and of the wind velocity in the wind tunnel. The shrouded probe (McFarland *et al.*, 1989) provides precisely the sampling performance for these tests. The shrouded probe is designed specifically to address some of the problems associated with representative sampling in air streams of varied velocity and direction (Fig. 11). The shrouded probe exhibits near-constant sampling efficiency over a wide range of wind speeds and for particle AD range spanning <1 μm to 20 μm (Huebert *et al.*, 1990). Internal wall losses are very low, which eliminates the need to recover significant portions of the sample after each run. The shrouded probe operates at a single design sample flow rate, unlike isokinetic probes, and therefore there is no need for control and monitoring of sampling rate.

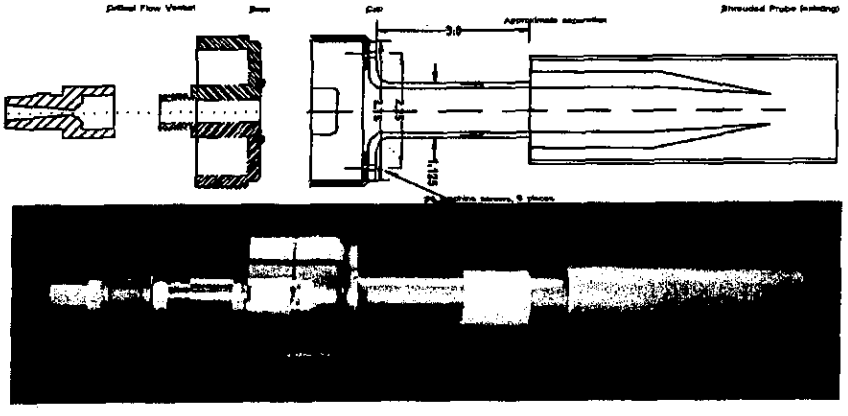

Figure 11. Cross-section and physical realization of a shrouded probe (McFarland *et al.* 1989) connected to quick-change filter cartridge (center) and critical orifice (left).

Shrouded probes were extensively tested (McFarland *et al.*, 1989; Huebert *et al.*, 1990) for their performance under extreme conditions showing excellent sampling efficiency. For this project five special shrouded probe-quick-change filter cartridge-critical orifice assemblies were constructed and used to collect reference (free air stream) samples in the wind tunnel experiment. The built-in critical flow venturi sets the nominal flow rate to 57 L min^{-1}.

IV. Results

Field Test Intercomparisons (Relative)

The comparison of relative performance of different inlets under ambient conditions at TA-54 site is presented in Table 3. The table contains weekly averages of aerosol particle mass concentration and wind speed, as collected in tested inlets and by a propeller anemometer on a tower at 12 m. The test were carried out between March 2-May 5, 2000.

Table 3. Summary of inlet performance field test. Each test involved simultaneous sampling for approximately 170 h under ambient aerosol conditions.

Test No	Inlet	Mass Concentration ($\mu g\ m^{-3}$)	Average Wind Speed ($m\ s^{-1}$)	Soil moisture (%)
1	UM IPM 102-mm Inverted AIRNET	9.8 8.2 5.1	2.6	7.2
2	UM IPM 102-mm Inverted AIRNET	10.3 4.3 3.7	2.5	8.2
3	UM IPM 102-mm Inverted AIRNET	43.5 20.8 15.4	3.3	10.2
4	UM IPM 47-mm Inverted AIRNET	10.6 7.7 5.3	2.5	15.6
5	UM IPM 47-mm Inverted AIRNET	5.1 6.4 4.1	2.8	15.8
6	UM IPM 47-mm Inverted AIRNET	16.8 12.6 10.2	3.2	13.6
7	UM IPM G-A inlet AIRNET	16.3 2.4 10.0	3.8	10.7
8	UM IPM G-A inlet AIRNET	15.9 2.5 11.0	3.3	7.8
9	UM IPM G-A inlet AIRNET	16.7 3.2 9.8	3.1	8.1

Graphical comparison of the relative inlet performance under different inlets configurations is presented in Fig. 28 in terms of weekly averages of mass concentrations. Performance was represented by the total mass of ambient aerosols collected, regardless of size.

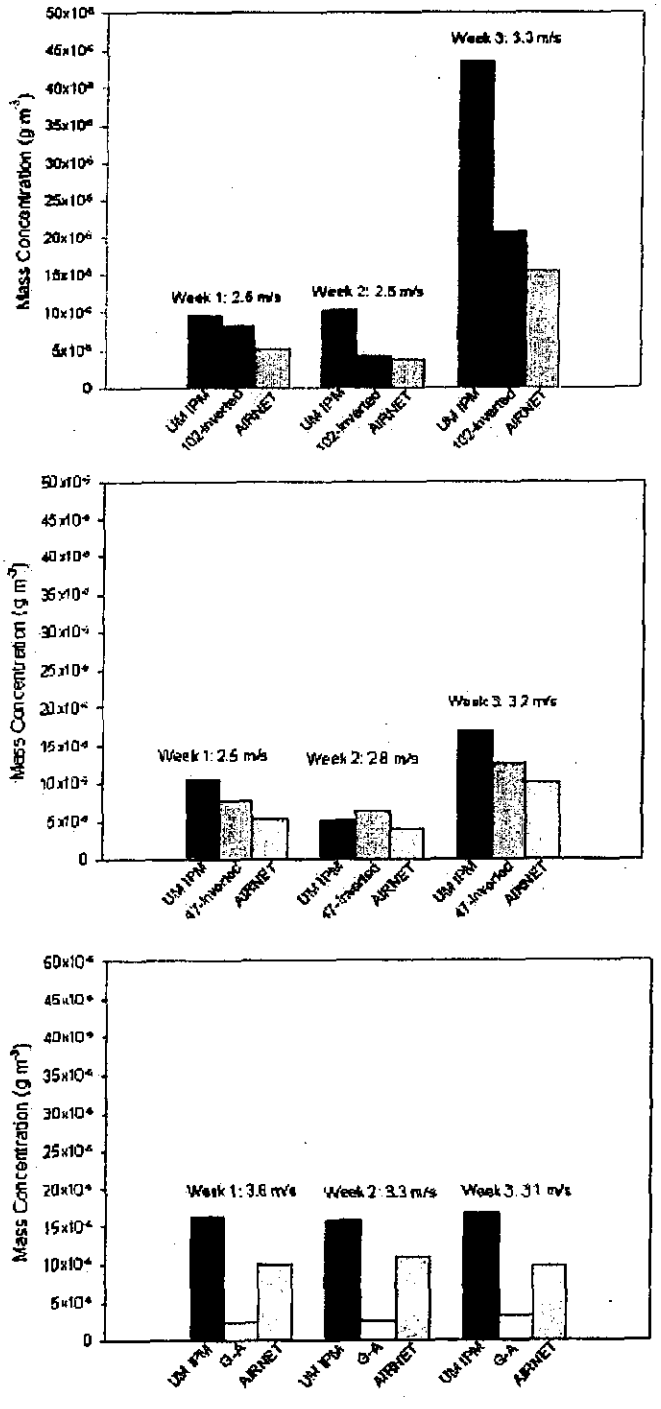

Figure 28. Comparison of performance of individual inlets under ambient aerosol conditions. Weekly averages of wind speed are listed above the bars.

Wind tunnel tests

The wind tunnel tests were made between June 19 - 23, 2000. Three selected inlets: AIRNET, UM IPM, and ECAM were tested for their collection efficiency with 5-, 10- and 30-μm test soil particles and three wind speeds of approximately 12-, 15-, and 17-m s^{-1}.

Each test consisted of 3 or 5 min runs. Test particles were collected on a filter and at an air flow-rate specific for the tested inlet. Test particles were collected simultaneously with a shrouded probe placed in the flow for use as the reference (free stream) aerosol particle concentration. Each run was repeated 2-3 times to enable statistical analysis of the outcome results.

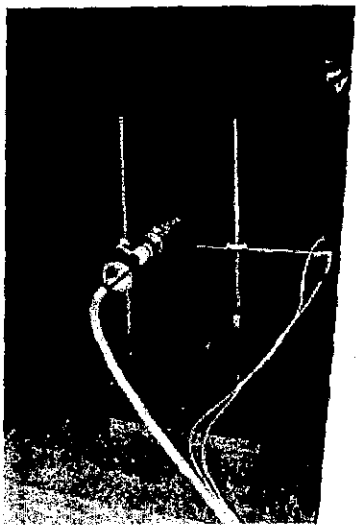

Figure 29. Shrouded probe (left) and Pitot tube (right) used to collect reference values

The reference probe was position 60 cm above the wind tunnel floor and inside the original wind tunnel, along with the Pitot tube used for air velocity measurements. The reference sampler and Pitot tube is shown in Fig. 29. The Pitot tube output was interfaced with a 21X Campbell Scientific datalogger providing 1-min air velocity averages. The datalogger software allowed for on-line monitoring of air velocity, to detect and correct any problems with the Pitot tube clogging.

Before a test, the numbered and pre-weighted filters were loaded into the sampler under test and into shrouded probe cartridge. The pre-test weighing was done just before the test on ANSI traceable Mettler Precision Balance AE100 (latest calibration June 2000). The same balance was used to obtain the post-test mass of the filter. The balance was located in an adjacent building and filters were transported to minimize losses of collected soil particles. Filters were later stored for further analysis if necessary, e.g. for uniformity of filter coverage.

The samplers (AIRNET, ECAM, UM IPM) were positioned in the extension section of the wind tunnel, 60 cm from the original end of the tunnel in the free jet regime. The AIRNET, ECAM, and UM IPM samplers undergoing testing are illustrated in Fig 30, 31, and 32.

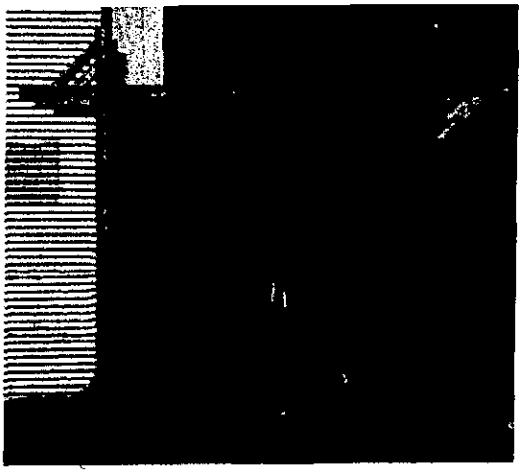

Figure 30. Test of the AIRNET sampler in the wind tunnel

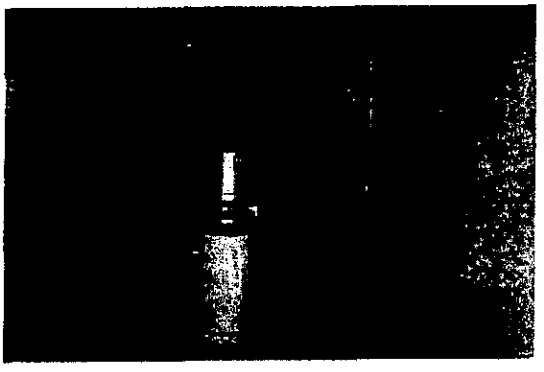

Figure 31. Test of the ECAM sampler in the wind tunnel

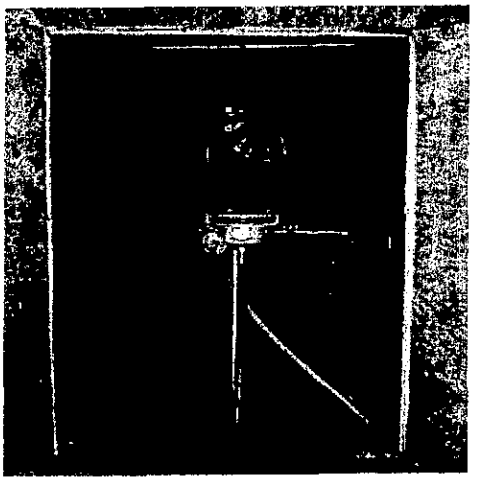

Figure 32. Test of the UM IPM sampler in the wind tunnel

RESULTS AND DISCUSSION

The aerosol inlet performance was evaluated under ambient aerosol conditions at LANL, as well as under the controlled conditions of the high-velocity wind tunnel in ARS, Pullman. This approach was suggested in the EPA draft document (EPA 1999c) stating that "*...Mark et al. (1992) reviewed the attributes of wind tunnel testing, and noted that tests using controlled conditions are a necessity to determine whether an aerosol sampler meets a basic set of established performance specifications. Hollander (1990) suggested that sampler performance criteria should be evaluated in controlled outdoor tests, given the inability of wind tunnels to accurately mimic the influences of outdoor meteorological conditions on sampling...*"

During the ambient tests the aerosol size distribution was not monitored, so only the relative performance of the inlets one to another can be evaluated. Results of ambient conditions experiments presented in Table 3 and Fig. 27 show that under low wind conditions (up to 3.8 m s^{-1} weekly average) the UM IPM inlet using 113 L min^{-1} flow-rate captured the largest mass, with the open face filter the second largest, and the AIRNET station the third largest mass. Similar patterns were repeated for all weekly tests. The PM_{10} G-A inlet, which is a size selective inlet with 50% cut off point for 10-μm particles, restricted penetration of larger particles and thus collected significantly less mass. The AIRNET station performance as an aerosol inlet (as defined here) was slightly below that of the inverted open-face inlets. However, they are still being used as low cost solution, for example in the WIPP Environmental Monitoring Project (Carlsbad Environmental Monitoring & Research Center 2000). The UM IPM inlet, specifically designed to overcome the deficiency of the inverted open-face inlets, has shown performance above other inlets.

The relative performance difference between inlets varied depending on ambient atmospheric conditions. From Table 3 it can be seen that UM IPM inlet measured aerosol concentrations up to 3 times higher than the AIRNET or the inverted filter holder inlet. However, the relatively low wind conditions encountered in these tests are only a limited sample of wind speeds experienced in the LANL environment. There are situations, when environmental sampling has to be done under higher wind velocities,

like those experienced during recent Cerro Grande and Hanford fires, when high winds resuspended contaminated soils.

The controlled test, performed in the high velocity wind tunnel with test particles of selected sizes overcomes the limitations of highly variable, uncontrolled ambient testing with uncharacterized aerosols. The 5-, and 10-μm diameter particles represented the respirable fraction and 30-μm the resuspendable fraction. The results of the wind tunnel experiments are summarized in the Tables 4, 5, and 6 and presented in forms of sampler efficiency curves for three inlets in Figs. 33, 34, and 35. The sampler efficiency was derived as an average of the ratios between the aerosol particle mass concentration measured by the tested inlet (sampled mass concentration) to the reference mass concentration measured by the shrouded probe. The error bars on the graphs represent ±1 standard deviation (SD).

Table 4. Results of wind tunnel experiments for the ECAM sampler

Wind Speed ($m\ s^{-1}$)	Nominal Particle Diameter (μm)	Reference Mass Concentration ($mg\ m^{-3}$)	Sampled Mass Concentration ($mg\ m^{-3}$)	Ratio (%)	SD
12.5	5	97.2	23.1	23.8	1.2
	10	58.3	8.3	14.2	1.9
	30	34.7	1.8	5.2	4.9
14.7	5	116.6	23.2	19.9	1.4
	10	67.3	13.4	19.9	2.4
	30	37.4	2.2	5.9	1.7
16.6	5	117.6	19.1	16.2	0.5
	10	174.0	22.5	12.9	1.5
	30	68.0	1.0	1.5	1.6

Table 5. Results of wind tunnel experiments for the UM IPM sampler

Wind Speed ($m\ s^{-1}$)	Nominal Particle Diameter (μm)	Reference Mass Concentration ($mg\ m^{-3}$)	Sampled Mass Concentration ($mg\ m^{-3}$)	Ratio (%)	SD
12.5	5	91.5	110.6	120.9	21.6
	10	86.0	53.9	62.7	15.3
	30	39.8	20.4	51.3	1.8
14.7	5	89.3	104.4	116.9	18.7
	10	83.3	41.3	49.6	14,4
	30	35.6	18.7	52.5	13.4
16.6	5	124.3	166.2	133.7	7.5
	10	88.9	25.1	28.2	0.7
	30	62.1	28.6	46.1	6.3

Table 6. Results of wind tunnel experiments for the AIRNET sampler

Wind Speed ($m\ s^{-1}$)	Nominal Particle Diameter (μm)	Reference Mass Concentration ($mg\ m^{-3}$)	Sampled Mass Concentration ($mg\ m^{-3}$)	Ratio (%)	SD
12.5	5	118.8	92.3	77.7	5.2
	10	69.4	57.2	82.4	4.5
	30	42.0	70.0	166.7	22.7
14.7	5	104.8	90.1	86.0	8.2
	10	63.1	39.2	62.1	12.6
	30	36.4	85.9	236.0	49.6
16.6	5	51.2	62.0	121.1	34.5
	10	54.3	39.3	72.4	2.1
	30	22.6	45.6	201.8	14.0

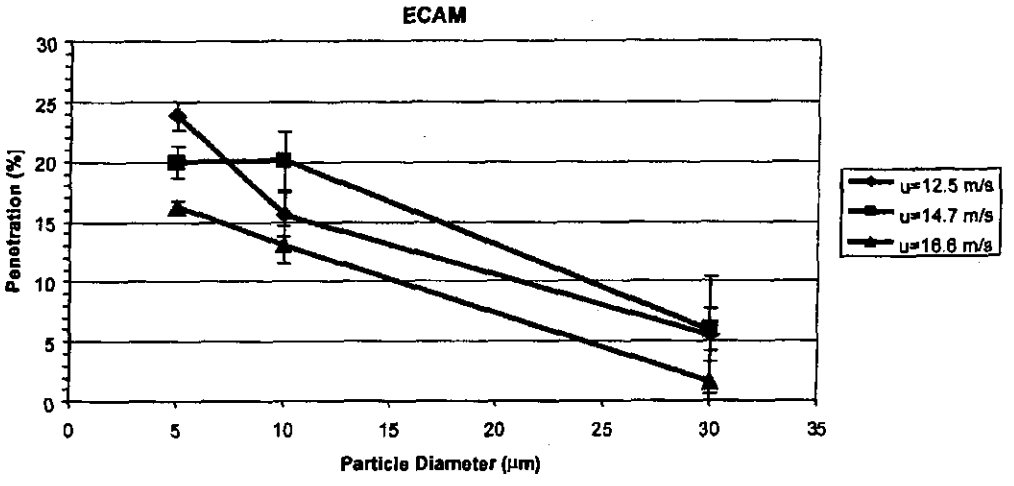

Figure 33. Penetration curves for the ECAM sampler for three wind speeds u=~12, ~15, and ~17 m s^{-1}.

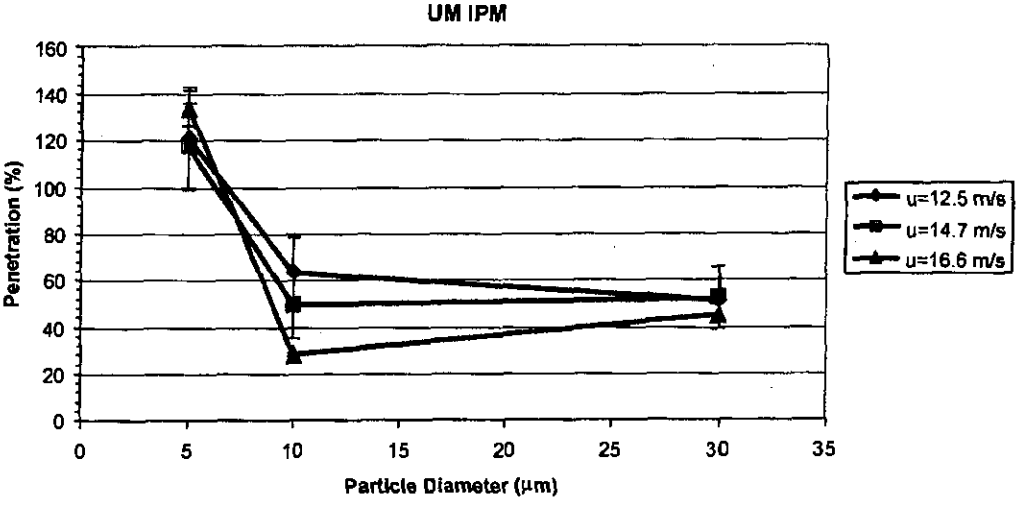

Figure 34. Penetration curve for the UM IPM sampler for three wind speeds u=~12, ~15, and ~17 m s^{-1}

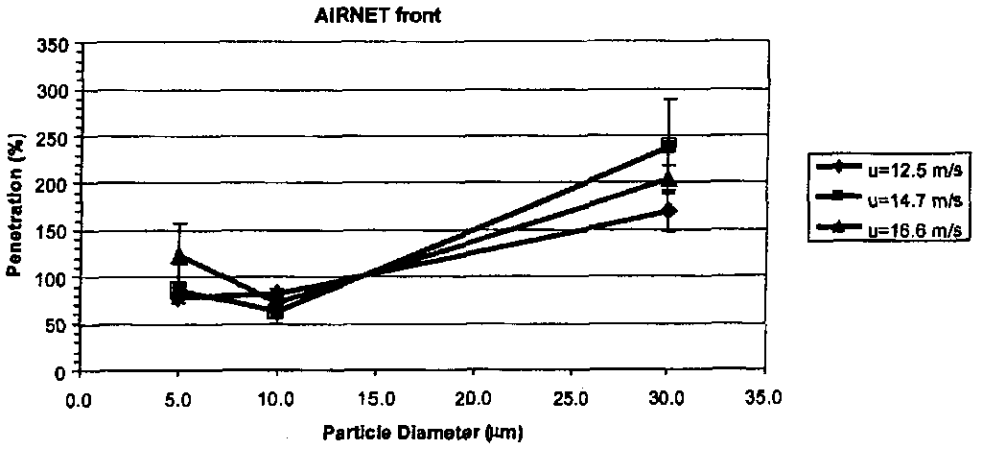

Figure 35. Penetration curve for the AIRNET sampler with the internal filter holder facing the flow stream for three wind speeds u=~12, ~15, and ~17 m s^{-1}

Several observations can be made based on the data presented in the foregoing penetration curves. First, with regard to the ECAM data, it is clear that the test design did not perform as respected for a design goal of a D_{50} cut-point of 10 µm. A possible explanation for this unexpected outcome is that the addition of the experimental dust trap cone changed the cyclone properties such that the cut-point was moved back to less than 5 µm AD. The shape and position of this cone are clearly sensitive design parameters. Further investigation of the critical design parameters of this element of the cyclone are planned for future work on this inlet. A an earlier study with slightly different version of the ECAM inlet (Murray Moore personal communication, June 2000) at lower wind velocity of 6.7 m s^{-1} showed that this inlet has regular penetration curve with around 60% penetration for 10-µm particles. With the version of inlet used in this study it was found that for wind speeds above 10 m s^{-1} the penetration drops to around 20%. For this high wind speeds there was still finite probability for 30-µm particles (penetration values around 5%) to penetrate the ECAM inlet.

The UM IPM sampler has been tested by its designers Liu and Pui (1981) for 8.5-, 11.0- and 13.4-µm diameter at low wind speeds. In their paper the penetration efficiency was over 100% for particles of 8.5-, 11.0- and 13.4-µm diameter at wind speed of 0.6 m s^{-1}, and dropped to 90% for 8.5 and 11.0-µm particles and to 80% for 13.5-µm at wind

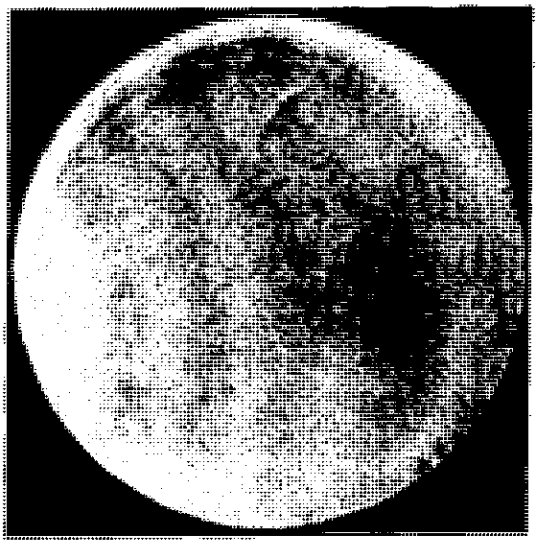

Figure 36. 102-mm filter used in one of the tests showing non-uniform coverage

speed of 2.8 m s^{-1}. No higher wind velocity was tested. Our high velocity tests have shown similar inlet behavior for all tested wind speeds with sharp drop in penetration from 5- to 10-μm diameter particles from 120-130% to 30-60% and then constant for 30-μm diameter particles. These values are below theoretical predictions of the ideal "hole-in-an-infinite-wall" inlet by Zebel (1978). Zebel's predicted aspiration efficiency of circular inlet of 9.2 cm diameter for particles 15-μm aerodynamic diameter was 100% at low wind speed, decreasing to 90% at a wind speed of 6.9 m s^{-1} and 80% at 15.8 m s^{-1}. In our case inlet diameter was 11.6 cm and for particles10-μm AD at wind speeds of 12.5- 14.7- and 16.6 m s^{-1} aspiration efficiency was about 63%, 49% and 28%, respectively. Similar observation of decrease in aspiration efficiency for larger particles (13.4-μm) and higher wind speeds was made by the designers of the original IPM inlet (Liu and Pui, 1981). They observed as well a decrease in aspiration efficiency of their inlet larger than that predicted by Zebel's (1978) theory. Their suggested explanation of the discrepancy was that the actual flow field at the inlet is more complicated than that assumed by Zebel. Our experiments, using solid particles (in contrast to Liu and Pui, 1981 who use liquid particles), have shown another property of the UM IPM inlet shown in Fig. 36. The deposition pattern of a 10-μm AD test aerosol on the 102-mm filter is showing strong directional dependence with higher loading on the downwind side (top of the picture) of the inlet. This was also observed on some field samples.

The louvers of the AIRNET sampling station housing an open face filter act as air inlets to the interior space. The ambient low wind velocity conditions of the field test created sampling conditions inside the housing very similar to those outside. The similar performance of AIRNET and inverted open face filter sampler is therefore not

unexpected. However, under high wind conditions in the wind tunnel, the AIRNET sampler exhibited about 96% efficiency for 5-μm particles and about 60% efficiency for the respirable fraction represented by 10-μm particles, but overestimation of concentration for 30-μm particles for all wind speeds tested. The overestimation ranged from 170% for ~12 m s^{-1}, 237% for ~15 m s^{-1} and 204% for ~17 m s^{-1} wind speeds. The explanation of this phenomenon could be that the AIRNET housing inlet is sampling subisokinetically and therefore large particles are impacted through the louvers into the AIRNET housing with higher efficiency than smaller size particles. Therefore, the open face filter sampler inside is sampling from atmosphere containing a higher concentration of large particles than outside the housing. This hypothesis is supported by results from penetration tests carried out with the open face filter located inside AIRNET housing facing the air flow, being parallel to it and opposing it. The results of such tests are presented in Fig. 37 and 38.

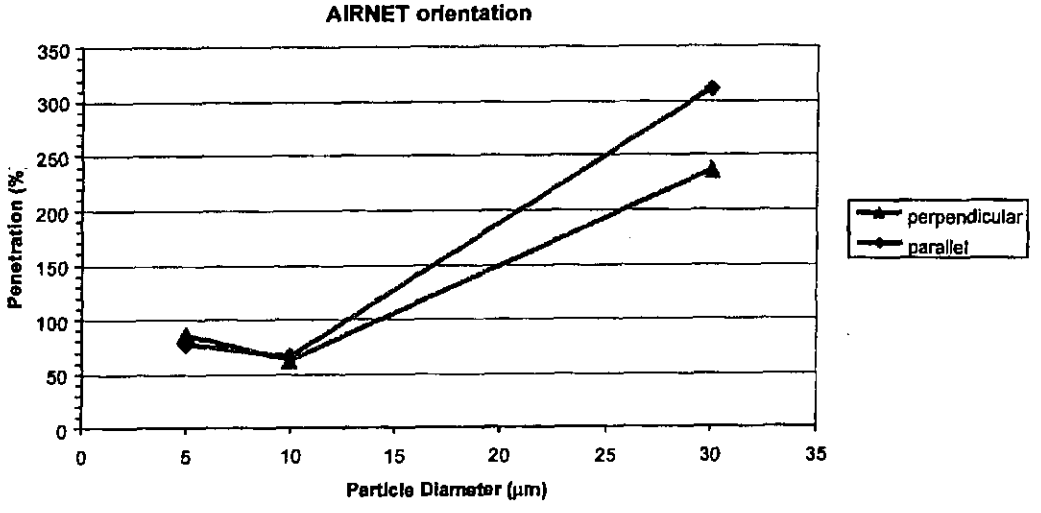

Figure 37. Comparison of penetration vs particle diameter for the AIRNET sampler with the internal filter holder perpendicular to and parallel to the flow stream for wind speeds of ~15 m s^{-1}

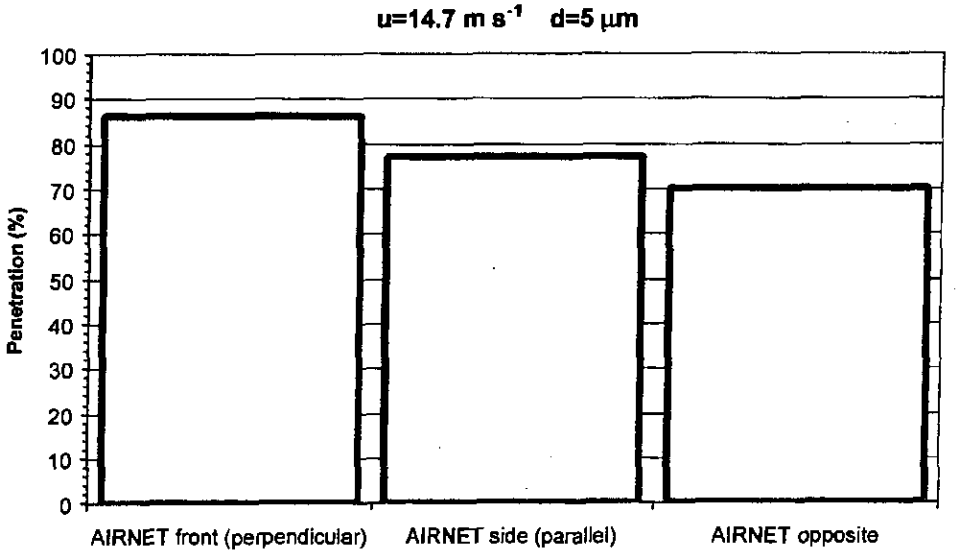

Figure 38. Penetration efficiency of 5-µm particles for different orientation of the AIRNET housing with respect to the wind tunnel flow.

There was a 21% decrease in penetration of 5-µm diameter particles into the filter of the AIRNET sampler when the internal filter holder was facing the flow versus the situation where the sampler was rotated 180 degrees.

CONCLUSIONS

A number of different types of ambient sampler inlets were tested in this project, each with a different intended role and application. All the inlets must operate in ambient environmental conditions that are sometimes unfavorable to good sample collection. As a result, certain design compromises have been made to accommodate the intended use under adverse conditions. The simplest inlet of all is a simple filter holder. But when it is operated in an inverted condition to protect the filter from rain and gravitational settling of large particles onto the exposed filter, performance is affected, with smaller ambient mass concentrations estimated in the LANL field trials compared with a protected, upright filter holder as in the UM IPM sampler design (Figure 27).

Higher ambient wind velocities, which while not common, do occur and are associated with critical resuspension and transport processes, required a different test

approach which was provided in this study by a high velocity wind tunnel. Both the effects of increasing wind speed and increasing particle size were evaluated. The results show that while wind speed increases do have a significant effect on collection efficiency, the largest effect was that due to increasing particle size. The UM IPM sampler is supra-efficient for particles in the 5 μm size range (penetration > 100%), but then for particles between 10 and 30 μm diameter, the efficiency drops to between 20% and 40%, depending on wind velocity. It would appear that a significant fraction of particles above a critical size simply move through the capture zone of the inlet with sufficient inertia that they are able to cross the curving flow streamlines induced by the sample flow into the filter and avoid capture. This is a well-known phenomenon that leads to sub-isokinetic sampling in the case of sample extraction probes facing into a flow field with a *lower* inlet velocity than the free-stream velocity. Under such conditions, inertia tends to carry more large particles into the inlet than would be expected from the free-stream concentration. Here, since the inertial trajectories are parallel and away from the filter, the effect is to actually cause *fewer* of the larger size particles to be captured. It may be that the addition of a deflection cone on the upper plate, as has been used in some other designs, would remedy this problem by causing the parallel flow lines to diverge toward the filter slightly, and thus change the inertial trajectory toward the collection surface (Fig. 39).

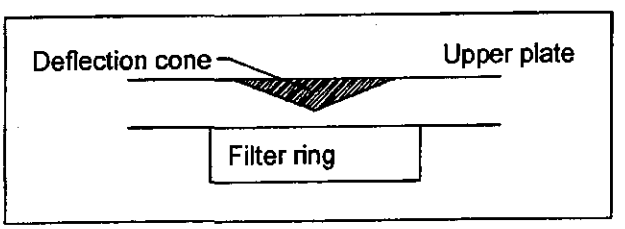

Figure 39. Modification of the UM design to improve high wind velocity collection efficiency for large particles

With regard to the ECAM sampler, as has been previously noted, the design of the large particle trap needs further design work, or perhaps only better placement in the cyclone relative to the outlet tube, to move the cut point up to the design target of 10 μm AD.

As with all of the samplers tested, the AIRNET sampler is particle size and wind speed sensitive. In the wind tunnel experiments, it collected virtually all of the small particles (~96% average efficiency for 5-μm particles), more than 50% of the 10-μm particles (which is comparable to EPA equivalent PM_{10} sampler), while oversampling for large particles. Therefore, particulate matter mass concentrations would be conservatively estimated at least for the higher wind speeds (>10 m s^{-1}) that occurred during the experiment.

Results obtained during this 1-year project suggest the need for further, more detailed studies if the full knowledge of the aerosol inlets used in the LANL is to be accumulated. The extreme condition may be experience during accidents with transportation of nuclear materials or natural disaster like fires. The results of environmental surveillance, even if it is carried on longer time scales (weeks) can be distorted by short-term extreme conditions (high winds) if the response of the sampler is unknown.

ACKNOWLEDGEMENTS

The authors would like to acknowledge the ESH Division TDEA Committee that provided funding for this project and number of people who help us during the study: Jeff Baars, Jake Martinez, Bill Olsen ESH-17, Bob Barry USDA/ARS Pullman. Special thanks for Yung-Sung Cheng from Lovelace Respiratory Research Institute for performing size distribution measurements of test soil particles.

References

Bird, A.N., Jr., D.V. Brady, and J.D. McCain (1973). Evaluation of sampling systems for use of the M8 alarm aboard ships. Report SRI-EAS-73-064. Southern Research Institute, Birmingham, AL.

Carlsbad Environmental Monitoring & Research Center (2000). WIPP Environmental Monitoring Project. Retrieved from the World Wide Web: http://www.cemrc.org/overview/wipp.html.

Holländer, W. (1990) Proposed Performance Criteria for Samplers of Total Suspended Particulate Matter. Atmos. Environ. Part A 24: 173-177.

Huebert, B.J., G. Lee, and W.L. Warren (1990). Airborne aerosol inlet passing efficiency measurements. J. Geophys. Res. 95: 16369-16381.

Liu, B.Y.H., and D.Y.H. Piu (1981). Aerosol Sampling Inlets and Inhalable Particles. Atmospheric Environ. 15: 589-500.

Mark, D., C.P. Lyons, S.L. Upton, and D.J. Hall (1992). A Review of the Rationale of Current Methods for Determining the Performance of Aerosol Samplers. J. Aerosol Sci. 23: S611-S614.

McFarland, A.R., and C.A. Ortiz (1982). A 10 μm Cutpoint Ambient Aerosol Sampling Inlet. Atmospheric Environ. 16(12): 2959-2965.

McFarland, A. R., C.A. Ortiz (1984). Characterization Of Sierra-Andersen Model 321a μm Size Selective Inlet For Hi-Vol Samplers. College Station, TX: Texas A&M University, Department of Civil Engineering, Air Quality Laboratory; report no. 4716/01/02/84/ARM.

McFarland, A.R., C.A. Ortiz, M.E. Moore, R.E. Deotte, and S. Somasundaram (1989). A Shrouded Aerosol Sampling Probe. Environ. Sci. Technol. 23: 1487-1492.

Pietersma, D., L.D. Stetler, and K.E. Saxton (1996). Design and Aerodynamics of a Portable Wind Tunnel for Soil Erosion and Fugitive Dust Research. Transactions of the ASAE 39(6): 2075-2083.

U.S. Environmental Protection Agency (1990). EPA Quality Assurance Manual, April 11, 1990 Section 2.20.0 "Reference Method for Determination of Particulate Matter as PM10 (Dichotomous Method)".

U.S. Environmental Protection Agency (1999a). National Primary And Secondary Ambient Air Quality Standards. 40 CFR Part 50.7.

U.S. Environmental Protection Agency (1999b). Ambient Air Monitoring Reference And Equivalent Methods. 40 CFR Part 53.

U.S. Environmental Protection Agency (2000). Sampling and Analysis Methods for Particulate Matter and Acid Deposition. Draft: 4.14: 4-38. Retrieved June 29, 2000 from the World Wide Web: http://www.epa.gov/nceawww1/pdfs/partmatt/vol1/0671ch04.pdf

Zebel G. (1978). Some problems in the sampling of aerosols. In Recent Developments in Aerosol Science (Edited by D.T. Shaw) pp. 167-185, John Wiley, New York.